P.99

KANSAS EVAPOTRANSPIRATION LABORATORY

JOHNSON
GRANT-CR
IN-43

(NASA-CR-181282) ASSESSMENT OF THE BIOPHYSICAL CHARACTERISTICS OF RANGELAND COMMUNITY USING SCATTEROMETER AND OPTICAL MEASUREMENTS Final Report (Kansas State Univ.) 99 p Avail: NTIS HC A05/MF A01

N87-28111

Unclas
G3/43 0093245

RESEARCH FOR EFFICIENT WATER USE

Kansas State University, Manhattan

FINAL REPORT

Title

Assessment of the Biophysical Characteristics of Rangeland Community

Using Scatterometer and Optical Measurements

NAG9-156

NAG9-156

By: E. T. Kanemasu

Ghassem Asrar

Ranga Myneni

Robert Martin, Jr.

R. Bruce Burnett

4. Title and Subtitle

Assessment of the Biophysical Characteristics of Rangeland Community Using Scatterometer and Optical Measurements

5. Report Date

August 1, 1987

6. Performing Organization Code

7. Author(s)

Kanemasu, E.T. et al.

8. Performing Organization Report No.

9. Performing Organization Name and Address

Evapotranspiration Laboratory
Kansas State University

10. Work Unit No.

11. Contract or Grant No.

NAG9- 156

13. Type of Report and Period Covered

FINAL REPORT

12. Sponsoring Agency Name and Address

NASA/JSC

14. Sponsoring Agency Code

15. Supplementary Notes

16. Abstract

NAG9-156

This report contains the research activity conducted in NAG9-156. The first 3 chapters deal with modeling the radiation regime of plant canopies in the visible and near infrared region. The last chapter treats the microwave research on the Konza Prairie.

17. Key Words (Suggested by Author(s))

Leaf area index, light interception
scattering, modeling

18. Distribution Statement

19. Security Classif. (of this report)

20. Security Classif. (of this page)

21. No. of Pages

22. Price*

*For sale by the National Technical Information Service, Springfield, Virginia 22161

Form 624 (Rev Nov 75)

ATTACHMENT 2

NASA

Table of Contents

Summary

The first chapter describes the use of a single scattering theory for assessing light (PAR) scattering in a plant canopy.

Knowledge of the distribution of solar radiant energy in vegetated canopies facilitates computation of canopy photosynthetic rates and/or reflectance/transmittance. The classical turbid medium theory is extended to describe single scatter of parallel direct and anially symmetric diffuse flux inputs in a family of vegetative canopies where the spatial dispersion of the leaves follows the binomial distributions. The penetration functions for upward and downward scattered flux densities are formulated in terms of the interception functions of the corresponding flux inputs. The pattern of upward and downward single scattered horizontal flux generation and the dependence of the boundary valued fluxes (reflectance/transmittance) on leaf area index, sun position, and leaf angle distribution are presented. Finally, we show that the inversion problem is reduced to finding the roots of a polynomial, relating leaf are index, extinction coefficients, and the albedo. The relationship between canopy reflectance of usable radiation and leaf area indek is nonlinear, the degree of which is determined by the leaf spatial dispersion and angular characteristics.

The second chapter describes a method for treating multiple scattering in a plant canopy. he method of Successive Orders of Scattering Approximations (SOSA) involves computation of photons scattered once, twice, three times, etc., with the total intensity obtained as the

sum over all orders. The method SOSA is briefly presented. The implemented formulation was tested for energy conservatively scattering medium. The scattered fluxes for each order of scattering are presented to help understand the process of multiple scattering in plant canopies. The method was tested against measured values of canopy reflectance for a soybean canopy and also against the predictions of other established formulations published in the literature. Finally, some theoretical relationships between spectral indices, LAI and absorbed radiant energy are presented. The predicted spectral reflectance factors were in good agreement with the measured values and the predictions of other established methods published in the literature. However, SOSA slightly overestimated reflectance in the visible part of the solar spectrum. The relationships between computed values of Normalized Difference, LAI and absorbed radiant energy were nonlinear, the degree of which increased with oblique view zenith angles.

The third chapter uses the method of successive orders of scattering approximation to estimate canopy reflectance factors. Canopy reflectance factors predicted by SOSA were in good agreement with the measured values and with the predictions of other established formulations published in the literature. However, SOSA slightly overestimated canopy reflectance factors in the visible region of the solar spectrum. Some possible reasons were discussed. Sensitivity analysis of SOSA revealed that the formulation is highly sensitive to detail in leaf angle distribution input. The profile of ascending and descending fluxes showed how these fluxes are generated and propagated through the canopy. Finally, the profile of net normalized radiance inside the canopy was found to be dependent on canopy leaf area index, view zenith angle for a given wavelength.

The fourth chapter discusses C-band scatterometer measurements made of a tallgrass prairie in an attempt to determine the degree of correlation between (1) the backscattering coefficient and different expressions of soil moisture and (2) the backscattering coefficient and various canopy parameters. The findings of this study support those made in previous studies in terms of the optimum polarization and view angle selection for soil moisture work. There were two findings which were unexpected. The first was a moderately strong correlation and partial correlation between σ^{o} and leaf water potential, which indicates some capability of C-band measurements in detecting extremes in the water status of prairie vegetation under shallow soil conditions. The second was the finding that site differences (primarily differences in vegetation) due to burn treatments appeared to be sufficient to cause significant differences in the sensitivity of σ^{o} to soil moisture. The site differences could not be removed by any known expression of soil moisture. These two findings were unexpected since previous radar studies had reported minimal vegetation effects when using a frequency and view angles such as those in this study.

Chapter 1.0

Single Scattering of Parallel Direct and Axially Symmetric Diffuse Solar Radiation in Vegetative Canopies

REMOTE SENSING OF ENVIRONMENT 20:165–182 (1986)

Single Scattering of Parallel Direct and Axially Symmetric Diffuse Solar Radiation in Vegetative Canopies*

R. B. MYNENI, R. B. BURNETT, G. ASRAR, AND E. T. KANEMASU

Evapotranspiration Laboratory, Department of Agronomy, Waters Annex, Kansas State University, Manhattan, Kansas 66506

Knowledge of the distribution of solar radiant energy in vegetated canopies facilitates computation of canopy photosynthetic rates and/or reflectance/ transmittance. The classical turbid medium theory is extended to describe single scatter of parallel direct and axially symmetric diffuse flux inputs in a family of vegetative canopies where the spatial dispersion of the leaves follows the binomial distributions. The penetration functions for upward and downward scattered flux densities are formulated in terms of the interception functions of the corresponding flux inputs. The pattern of upward and downward single scattered horizontal flux generation and the dependence of the boundary valued fluxes (reflectance/transmittance) on leaf area index, sun position, and leaf angle distribution are presented. Finally, we show that the inversion problem is reduced to finding the roots of a polynomial, relating leaf area index, extinction coefficients, and the albedo.

Introduction

An accurate estimation of direct and diffuse radiative flux propagation and generation of complemetary radiative field in vegetative canopies is important for two reasons. First, it permits one to evaluate canopy photosynthesis (De Wit, 1965; Monteith, 1965; Duncan et al., 1967; Gutschick and Wiegel, 1984; among others) and reflectance/transittance (Lemeur, 1971; Suits, 1972). Second, the inversion of these mathematical formulations enables one to estimate phytometric characteristics such as leaf area index (Goel and Strebel, 1983) or intercepted radiation (Asrar et al., 1984) from measurements of canopy reflectance. Various models have been developed and tested over the years. The method of estimating the vertical profile of horizontal flux densities of radiant energy using the equation of transfer for plane parallel media formulated with appropriate geometrical and optical characteristics of scattering elements is a common denominator to most models. The generic problem of radiative transfer in layered media is treated by Chandrasekhar (1950), Hunt (1971), and Liou (1980). Radiative propagation in vegetative canopies is treated exhaustively by Ross (1981) and also by Lemeur (1971; 1973), Lemeur and Blad (1974), and Lemuer and Rosenberg (1979). There are various approximate methods of solving the coordinate-imposed propagation equation (Cooper et al., 1982; Gerstl and Zardecki, 1985). Gutschick and Wiegel (1984) developed a rapidly solvable integral equation for radiative flux interception by a scattering element in a layered media, the convergent numerical solution of which can be line-integrated to obtain a profile of angle-resolved fluxes or their strict plane projections.

In this paper, we extend the theory of Lemeur (1971) to describe single scatter

*Contribution 86-200-J from Agricultural Experiment Station, Kansas State University.

0034-4257/86/$3.50

of parallel direct and axially symmetric diffuse flux inputs in a family of vegetative canopies where the spatial disposition of the leaves follows the binomial distributions. Nilson (1971) proved the theoretical applicability of these distributions and has shown that the ensemble of distributions to characterize diverse leaf spatial dispersions ranging from mosaic fashion regularity to extreme clumping. However, the number of layers, N, is an additional critical parameter, which is theoretically intractable since it is a property of the intergral geometry of the canopy. As $N \rightarrow \infty$, the formulation approaches the treatment for random canopies.

The equations and their solutions for upward and downward horizontal flux densities arising from single scatter and the pattern of generation of such fluxes is presented in detail. Finally, we show that an exact analytical solution exists for the inversion problem. This solution is reduced to finding the roots of a polynomial. This generalization of Lemeur's (1971) work permits one to evaluate monochromatic albedos/transmittances in vegetative canopies of diverse architecture, which in principle can be inverted.

Theory

Derivation of binomial formula

Consider a horizontally extensive vegetated canopy of some finite physical depth z, continuous along the three physical dimensions, filled with small scattering elements. This is an extreme idealization of a real plant stand, which is extensive but horizontally finite. Isolate an elementary volume randomly in this vegetated space and describe the local phytometric characteristics that are pertinent to the treatment of radiative transfer. There are two important considerations in the isolation of such an elementary volume. First, the dimensions of this elementary volume are such that enough leaf area is contained therein, upon which one can derive the local phytometric attributes with sufficient accuracy. Second, the derived phytometric attributes are continuous and, hence, amenable to mathematical representation.

Imply that the leaf area in this elementary volume can be cut into elemental metameric leaf sections with negligible lateral area and no accountable mutual shading between the leaf sections. Since leaves are finite in size and specific in shape, this infinite divisibility involves some approximation. Represent depth in the canopy by f, the accumulated leaf area per unit ground area, measured from the top of the canopy. Hence, all radiative field characterics can be expressed as a function of f, which is in conformity with the standard works (Lemeur and Blad, 1974; Ross, 1981). At the ground surface, $f = F$, the global leaf area index of the vegetative canopy. The divisibility of the leaf area into elemental leaf sections permits one to ascribe the features exhibited by the leaf sections to the phytometric features of the vegetated canopy. Hence, the spatial disposition of the leaves is implied by the positional distribution of the leaf sections. Further consider the vegetative canopy as a multilayered medium constructed from a finite number of plane parallel, horizontal layers. The actual number of layers, (N, $N = F/\Delta f$), is determined by the successive apparition of the leaves on the stem or correspondingly, in the case of a tree, by the successive insertion of branches on the trunk and by the size of the leaves themselves. The parameter N is specific to a canopy and escapes a simple theoretical formulation. The propagation of solar radiation in this layered medium is analogous to piercing the vegetative canopy with long needles of infinitesimally small radius. When one such needle is pierced through the canopy along a prescribed direction (r_s), the divisibility of the canopy is such that only one or no contact of the needle with the leaf sections is probable in any one layer. It is instructive to note that the layering of the canopy insures that the problem of radiative transfer is reduced to studying the probability distribution of an event in a two-class population statistically (contact or no contact), which makes it amenable to solution by the binomial formulae. Let $X(f, r_s)$ be the random variable denoting the number of contacts between the level $z = 0$ and the level $z = f$. The relationship between the plane parallel layers in the canopy is assumed to be one of statistical independence, in the sense that the realization of X in a layer is effectively independent of its realization in another layer.

Consider that over an arbitrary basal area at a depth f, in the elementary volume, a hypothetical cross-wire square grid is overlayed. The volume is now pierced with the needles along a specified direction such that the needles pass through the center of each small square in the grid. Let A denote the probability of one contact in a layer, and let B denote the probability of no contact in a layer ($A + B = 1$). These probabilities are related to the mean number of contacts, $\bar{n}(f, r_s)$, between the depth zone $z = 0$ to $z = f$ (next section). The probability of n contacts in N layers is given by the positive binomial formula

$$P_n = \binom{N}{n} A^n B^{(N-n)}$$
$$= \frac{N(N-1)(N-2)\cdots(N-n+1)}{n(n-1)(n-2)\cdots(2)(1)}$$
$$\times A^n(1-A)^{(N-n)}$$
$$= \frac{N!}{n!(N-1)!} A^n(1-A)^{(N-n)}, \qquad (1)$$

where $n = 0, 1, 2, \ldots, N$. Hence, the probability of no contact in N layers is

$$P_0 = (1-A)^N. \qquad (2)$$

If the spatial dispersion of the elemental leaf sections is such that more than one contact of the needle with the sections is possible, then the probability distribution of radiation interception in these types of vegetative canopies can be described by the so-called negative binomial distribution. The probability of j contacts in any layer is given by

$$P_j = (A)^j(1+A)^{-j-1},$$

and the probability of n contacts in N layers is given by

$$P_n = \frac{(N+n-1)!}{n!(N-1)!} A^n(1+A)^{-N-n}, \qquad (3)$$

where $n = 0, 1, 2, \ldots,$ because of the probability of multiple contacts. The probability of no contact in N layers is given by

$$P_0 = (1+A)^{-N}. \qquad (4)$$

Note that as $N \rightarrow \infty$, the binomial distributions tend to the Poisson distribution:

$$P_n = \bar{n}^n n! [\exp(-\bar{n})], \tag{5}$$

$$P_0 = \exp(-\bar{n}), \tag{6}$$

for $n = 0, 1, 2, \cdots$.

Derivation of the probability of interception

The probability of interception of arbitrarily pierced needles into the canopy along a direction r_s is physically equivalent to the ratio of the area occluded by the elemental leaf sections along the length of the needles to the total area covered by the needles. It is also equivalent to the total projected area of the elemental leaf sections contained in the depth zone of study on a plane perpendicular to the direction of needle insertion. It should be intuitively obvious that, on an average, there would be as many contacts as the total projected area if a sufficient number of thin needles have been pierced. Hence, the mean number of contacts $\bar{n}(f, r_s)$ between the zone boundaries is equal to the total projected area along the direction of insertion:

$$\bar{n}(f, r_s) = \int_0^f \frac{G(f, r_s)}{\cos\theta_s}\, df, \tag{7}$$

where $G(f, r_s)$ is the area projected by unit leaf area index at depth f on a plane perpendicular to the direction of insertion. If G is independent of f, then $\bar{n}(f, r_s)$ is a linear function of f,

$$\bar{n}(f, r_s) = \frac{G(r_s)\,\Delta f}{\cos\theta_s}, \tag{8}$$

and the probability of contact in any one layer in the vegetative canopy is given by

$$A = \frac{G(r_s)\,\Delta f}{\cos\theta_s} = k\,\Delta f. \tag{9}$$

The function $G(f, r_s)$ depends on the distribution function of leaf area orientation $[g(f, r_1)]$ and on the direction of needle insertion. The distribution function of leaf area orientation determines the fraction of total leaf area oriented in the vegetative canopy at depth f, so that the normals to the upper face of the elemental leaf sections are within a unit solid angle $(d\Omega_1)$ around the direction r_1 and

$$\int_{2\pi} g(f, r_1)\, d\Omega_1 = \int_0^{2\pi} d\phi_1 \int_0^{\pi/2} g(f, r_1) \sin\theta_1\, d\theta_1 = 1. \tag{10}$$

For purposes of analysis, the hemisphere containing the normals may be divided into K equal sectors along the θ_1 coordinate and into L sectors along the ϕ_1 coordinate. Equation (10) may then be written as

$$\begin{aligned} &\int_0^{2\pi} d\phi_1 \int_0^{\pi/2} g(f, r_1) \sin\theta_1\, d\theta_1 \\ &\quad = \sum_{i=1}^{K} \int_{(\pi/(2K))(i-1)}^{(\pi/(2K))i} \sin\theta_1\, d\theta_1 \\ &\quad \times \sum_{j=1}^{L} \int_{(2\pi/L)(j-1)}^{(2\pi/L)j} g(f, r_1)\, d\phi_1 \\ &\quad = \sum_{i=1}^{K} \sum_{j=1}^{L} g_{ij} = 1, \end{aligned} \tag{11}$$

where g_{ij} is the fraction of total leaf area oriented in the solid angle Ω_{ij} between the boundaries

$$\theta_i = (\pi/(2K))(i-1) \text{ to } (\pi/(2K))i,$$
$$\phi_j = (2\pi/L)(j-1) \text{ to } (2\pi/L)j. \quad (12)$$

The $G(f, r_s)$ function may be defined as (Ross, 1981)

$$G(f, r_s) = \int_0^{2\pi} d\phi_1 \int_0^{\pi/2} g(f, r_1) \times |\cos r_s{}^\wedge r_1| \sin\theta_1 \, d\theta_1 \quad (13)$$

and may be further expanded as

$$\sum_{i=1}^{K} \int_{(\pi/(2K))(i-1)}^{(\pi/(2K))\,i} \sin\theta_1 \, d\theta_1 \times \sum_{j=1}^{L} \int_{(2\pi/L)(j-1)}^{(2\pi/L)j} g(f, r_1) |\cos r_s{}^\wedge \bar{r}_1| \, d\phi_1, \quad (14)$$

where $\bar{r}_1$ (the effective leaf normal) is given by the coordinates $(\bar{\theta}_{ij}, \bar{\phi}_{ij})$ of the mean normal in the solid angle Ω_{ij} bounded by the corresponding sector boundaries. The angle between the effective leaf normal and the direction of needle insertion can be expressed using the cosinous law in spherical coordinates as

$$|\cos r_s{}^\wedge \bar{r}_1| = \left| \mu_s \mu_1 + \sqrt{(1-\mu_1^2)} \times \sqrt{(1-\mu_s^2)} \cos(\phi_s - \phi_1) \right|, \quad (15)$$

where $\mu_s = \cos\theta_s$ and $\mu_1 = \cos\theta_1$. There is sufficient experimental evidence to assume that the elemental leaf sections show no preference in their azimuthal orientation in a majority of crop species (Nichiprovich, 1961; Ross and Nilson, 1976; Blad and Baker, 1973; Lemeur, 1973; among others). Several theoretical leaf inclination models such as horizontal, planophile, and erectophile can be used to evaluate the $G(f, r_s)$ function. For further treatment, the reader is referred to the works of Nilson (1971) and Ross (1981).

Derivation of the penetration function for upward and downward scattered horizontal flux densities

The probability that an arbitrary needle pierced into the canopy along a set direction will reach a depth f without making a contact with the elemental leaf sections is

$$P_0 = I^p(f),$$

where $I^p(f)$ is the penetration function, which is simply the zero term of the underlying distribution describing the spatial disposition of the canopy elements (Nilson, 1971). Hence,

$$I_1^p(f) = \exp(-kf),$$
$$I_2^p(f) = \left(1 - \frac{kf}{N}\right)^n, \quad (16)$$
$$I_3^p(f) = \left(1 + \frac{kf}{N}\right)^{-n},$$

where the subscripts 1, 2, and 3 represent Poisson and positive and negative binomial distributions, respectively. The probability that several needles pierced into the canopy from all possible directions in the hemisphere will reach a depth f without making a contact with the canopy elements is given by

$$H^p(f) = \int_0^{2\pi} \int_0^{\pi/2} I^p(f) \sin\theta \, d\theta \, d\phi. \quad (17)$$

For the purposes of analysis, the double integral may be simplified by introducing discrete sectors on the hemisphere (Lemeur, 1971). For conformity with Lemeur's (1971) work, the hemisphere is divided into 12 parallel sectors along the θ coordinate. By assuming total azimuthal independence, integration of Eq. (17) yields

$$H^p(f) = \sum_{i=1}^{12} I^{p^i}(f) E_i, \tag{18}$$

where

$$E_i = 2\cos\theta_i'(\cos\theta_i - \cos\theta_{(i+1)})$$

is the projection of the ith sector of the hemisphere onto the horizontal and θ_i' is the coordinate of the midparallel of the ith sector. For the three types of leaf dispersions, $H^p(f)$ can now be formulated as

$$H_1^p(f) = \sum_{i=1}^{12} E_i \exp(-k_i' f),$$

$$H_2^p(f) = \sum_{i=1}^{12} E_i\left(1 - k_i'\frac{f}{N}\right)^N, \tag{19}$$

$$H_3^p(f) = \sum_{i=1}^{12} E_i\left(1 + k_i'\frac{f}{N}\right)^{-N}.$$

Specifically, I^p and H^p are the penetration functions for direct and diffuse incoming radiative flux densities, respectively. The negative derivative of these penetration functions gives the mean normalized flux density impinging on the variably inclined and dispersed leaf sections (Saeki, 1963; Cowan, 1966; Lemeur, 1971):

$$I^i(f) = -\frac{dI^p(f)}{df},$$

$$H^i(f) = -\frac{dH^p(f)}{df},$$

where I^i and H^i are the interception functions for direct and diffuse radiation fields, respectively. For the various spatial dispersions under study, they are

$$I_1^i(f) = k\exp(-kf),$$

$$I_2^i(f) = k(1 - kf/N)^{N-1},$$

$$I_3^i(f) = k(1 + kf/N)^{-N-1},$$

$$H_1^i(f) = \sum_{i=1}^{12} k_i' E_i[\exp(-k_i' f)], \tag{20}$$

$$H_2^i(f) = \sum_{i=1}^{12} k_i' E_i(1 - k_i' f/N)^{N-1},$$

$$H_3^i(f) = \sum_{i=1}^{12} k_i' E_i(1 + k_i' f/N)^{-N-1}.$$

Scattered radiation in the canopy is generated by reflection and transmission of intercepted radiation by the leaf sections. The leaves may be assumed to be perfect Lambertian diffusers, and the upper and lower faces of the leaf sections scatter similarly. Though scattering from individual leaf sections is isotropic, the scattered flux emanating from a layer is generally distributed according to the view angle. This is apparent when one considers that the length of the needle required per unit vertical depth at oblique insertions is more, and that the gaps are fewer. The penetration functions for upward $[S_p^{\uparrow}(\mathrm{Fr})]$ and downward $[S_{\downarrow}^{p}(\mathrm{Fr})]$ horizontal flux densities due to scattering by leaf sections has been shown by Cowan (1966) and Lemeur (1971) to be related to the interception functions of direct and diffuse radiation fields:

$$S_p^{\uparrow}(\mathrm{Fr}) = \frac{\omega(\lambda)}{2\pi} \int_{F_r}^{F} I^i(f) H^i(f - \mathrm{Fr})\, df, \tag{21}$$

$$S_{\downarrow}^{p}(\mathrm{Fr}) = \frac{\omega(\lambda)}{2\pi} \int_0^{F_r} I^i(f) H^i(\mathrm{Fr} - f)\, df, \tag{22}$$

where Fr is the reference depth in the vegetated canopy and a variable in f and ω is the scattering coefficient for wavelength λ. In case of canopies where the spatial dispersion is random, the solution is straightforward, after inserting the appropriate interception functions:

$$S_{p1}^{\uparrow}(\mathrm{Fr}) = \frac{\omega}{2\pi} \sum_{i=1}^{12} kk_i' E_i \exp(k_i'\mathrm{Fr}) \times (-k - k_i')^{-1} \times \left[\exp(-kf - k_i' f)\right]\Big|_{f=\mathrm{Fr}}^{f=F}, \tag{23}$$

$$S_{\downarrow}^{p1}(\mathrm{Fr}) = \frac{\omega}{2\pi} \sum_{i=1}^{12} kk_i' E_i \exp(-k_i'\mathrm{Fr}) \times (-k - k_i')^{-1} \times \left[\exp(-kf - k_i' f)\right]\Big|_{f=0}^{f=\mathrm{Fr}}. \tag{24}$$

The wavelength subscript is dropped, since the equations describe single scatter only; and the analysis is done for the integrated wavelength interval 0.40–0.70 μm (PAR). In canopies where the spatial dispersion is either described by the positive or negative binomial distribution, the solution to Eqs. (21) and (22) is considerably more complicated. If Fr is set to zero, the solution of Eq. (21) yields the albedo in the corresponding wavelength. In the case of positive binomial distribution, this yields

$$S_{p2}^{\uparrow}(\mathrm{Fr}) = \frac{\omega}{2\pi} \sum_{i=1}^{12} kk_i' E_i \times \int_0^F \left(1 - \frac{kf}{N}\right)^{N-1} \times \left(1 - \frac{k_i' f}{N}\right)^{-N-1} df. \tag{25}$$

The solution now depends on the value of N, the number of layers. If $b = -k/N$ and $c = -k_i'/N$, a generalized solution may be written as

$$\begin{aligned} S_{p2}^{\uparrow}(\mathrm{Fr}) = \frac{\omega}{2\pi} \sum_{i=1}^{12} kk_i' E_i & \times \left[\sum_{j=1}^{N} \pm \frac{b^{(j-2)}}{c^{(j-1)}} \times \frac{(j-1)!(j-1)!}{(2j-2)!} \times \left(1 - \frac{kf}{N}\right)^{(N-j+1)} \times \left(1 - \frac{k_i' f}{N}\right)^{(N+j-2)} \right] \\ & \pm \frac{b^{(N-1)}}{c^{(N-1)}} \frac{(N-1)!(N-1)!}{(2N-2)!} \times (2N-1)^{-1} \times \left(1 - \frac{k_i' F}{N}\right)^{(2N-1)}. \end{aligned} \tag{26}$$

For even values of N, the positive sign is taken in the term within the second summation and the negative sign in the last term. For odd values of N, the signs are reversed. This solution, for the purposes of our analysis, is difficult to implement. The parameter N is a whole number and hence certain combinations of F and Δf cannot be studied. It is extremely laborious to evaluate for a prescribed value of Δf and F. Consider that, for $F = 5.0$ and $\Delta f = 0.1$, there are 49 subterms inside the second summation operator! Further, it is very easy to generate meaningless results if one fixes the value of N and varies F in steps, since the solution is polynomial in the latter. The results have physical significance only in some intervals. Hence, we replaced N with the relation $(F/\Delta f)$ and resorted to numerical solution (200 steps), since there is no analytical solution except when $(F/\Delta f)$ is a whole number.

Consider that Eq. (26) is polynomial in F. The aim of an inversion problem is to find the value of F from a measured value of the albedo. One way to do this is to crudely evaluate Eq. (26) for a range of F values and pick the value that satisfies the equality sign. A much simpler method is to bring the right side of the equation to the left side and set the resulting polynomial to zero. Now, the roots of this polynomial can be evaluated using any standard numerical technique. However, the difficulty lies in inputing the extinction coefficients. Perhaps, it is possible to empirically evaluate for a given plant canopy the extinction coefficients (Asrar et al., 1984) and then solve the equation. In any case, this is an interesting problem and worth investigating further. This is the first time an exact analytical solution is available for the inversion problem, and the advantages are obvious.

Results and Discussion

The interception functions for direct and diffuse radiation in the three model leaf dispersion canopies are plotted against downward accumulated leaf area index (LAI) in Figs. 1(a) and (b), respectively. The Poisson model divides the functional space, with the binomial distributions on either side approaching it, as $\Delta f \rightarrow 0$. The positive binomial model exhibits a steep slope compared to the negative binomial model above an LAI of ca. 3. However, below this depth, the position of the binomial models relative to the Poisson model is reversed. The rate of radiation interception is rapid in the upper layers of the canopy, and virtually very little radiation penetrates to the lower layers and is intercepted. The general behavior of the positive binomial model is exaggerated with higher values of Δf, since this implies a higher probability of making a contact in any one layer. Hence, Δf may be seen in this model as an indicator of the regularity of leaf dispersion in the vegetated space (Nilson, 1971). On the other hand, in case of the negative binomial model, higher values of Δf decrease the probability of the needle making a contact; and hence, in these canopies, Δf is an indicator of leaf clumping in space.

The penetration functions for upward $(S_p^{\uparrow}(\mathrm{Fr}))$ and downward $(S_{\downarrow}^{p}(\mathrm{Fr}))$ scattered horizontal flux densities of photosynethtically active radiation (PAR) are plotted against Fr, in Fig. 2(a) and (b), respectively. The leaf area index of the canopy was 5; the elevation of the sun was 60; and the leaf orientation distribution was assumed to be random. The upward scattered flux is mostly generated

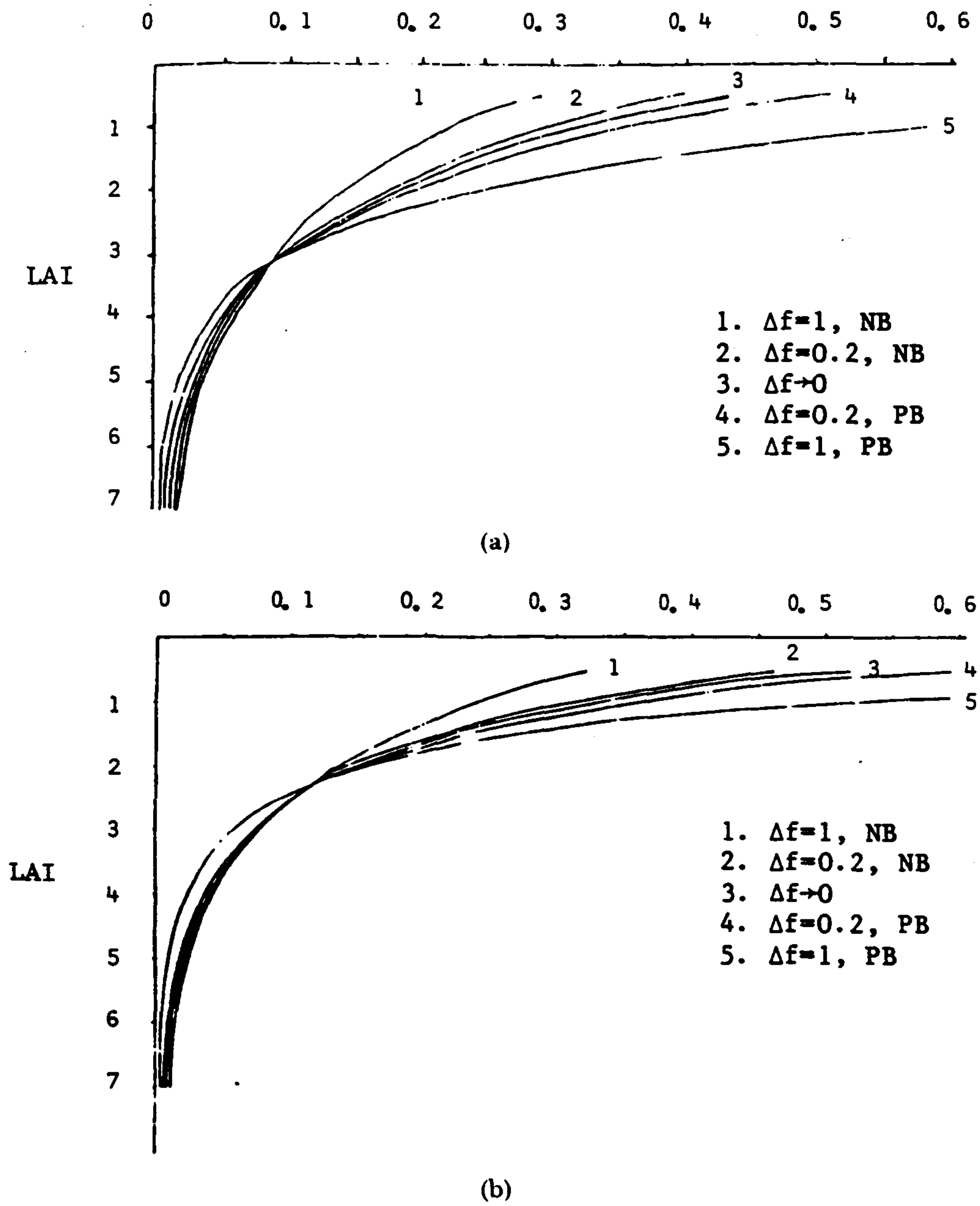

FIGURE 1. The relationship of the interception functions of direct (a) and diffuse (b) radiation with leaf area index in a uniformly inclined canopy. PB and NB correspond to canopies whose spatial dispersion of the leaves follows the positive and negative binomial distributions, respectively.

in the upper layers of the canopy, since most of the incoming radiation is intercepted in these layers. The rate of such flux generation is a function of leaf dispersion, with regular dispersion of leaves generating higher flux densities [Fig. 2(a)]. At the upper boundary of the canopy ($Fr = 0$), the value of $S_p^{\uparrow}(0)$ is also the albedo of the canopy. As illustrated in the figure, the albedo or the emergent flux from the canopy is strongly influenced by the leaf spatial dispersion.

The dependence of the penetration function for downward scattered horizontal flux density on the reference depth is remarkably different than that of the corresponding upward flux [Fig. 2(b)]. In canopies where leaves exhibit strong reg-

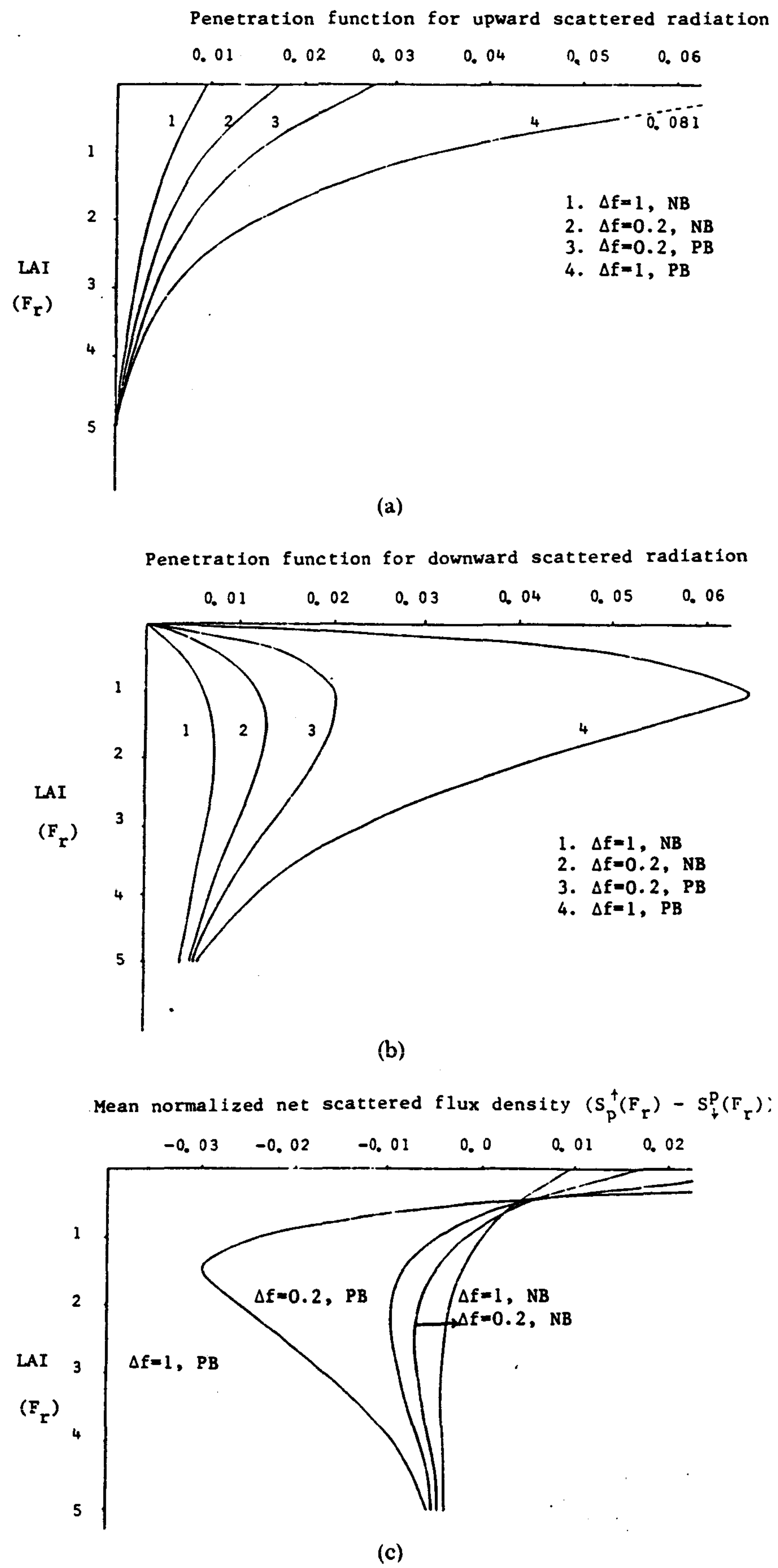

FIGURE 2. The relationship of the penetration functions of upward (a) and downward (b) scattered flux densities with reference leaf area index. Similar relationship for mean normalized net scattered flux density is plotted in (c). The leaf area index of the canopy is 5; the leaf angle distribution is uniform; and the elevation of the sun in 60°. PB and NB are as in Fig. 1.

ularity of leaf dispersion, ($\Delta f = 1$, positive binomial distribution), there is a sharp peak at a reference depth of ca. 1, which gradually falls with increasing Fr. As the ability of the canopy to intercept and scatter radiation decreases (less regularity or more clumping), this peak is flattened and stretched down the canopy.

The difference between the penetration functions for upward and downward scattered flux densities is the mean normalized net horizontal scattered flux density (S_n(Fr)) and is plotted in Fig. 2(c) against reference depth. There is more radiant energy scattered downwards than upwards, except in the upper layers of the canopy. Therefore, the variation of S_n(Fr) with depth is similar to that of $S^p_\downarrow(F_r)$ [Fig. 2(c)]. Since more radiation is scattered downwards than upwards, the net result is not only an increased radiation in the layers below, but also an increased intercepted radiation in these layers, where the probability of intercepting unimpeded incoming radiant energy is less. This can also be ascertained by taking the slope of the penetration function for downward scattered flux, the overall result being a much more uniform pattern of radiant energy interception than is apparent.

An important case in point is the generation of upward and downward scattered flux densities relative to the scattering leaf area inside the vegetated canopy. By gradually moving the reference depth upwards in the canopy, the upward scattered flux increases and reaches a maximal value at FR = 0, the albedo or the emergent flux from the canopy, [Fig. 2(a)]. This corresponds, conceptually, to adding leaf area to the vegetated space at the upper boundary in conformity with the stipulated phytometric characteristics of the canopy. This is equivalent to increasing the scattering capability of the vegetated space and, hence, increasing in its upward scattered flux density. Therefore, as FR $\rightarrow$ 0, $S_p^\uparrow$(Fr) $\rightarrow$ albedo. However, as the reference depth is moved upwards in the canopy, the downward scattering area is decreased; but the downward scattered flux density is increased [Fig. 2(b)]. For a canopy with a prescribed set of phytometric characteristics, there seems to be a certain value of leaf area index at which the downward scattered flux is maximized. Appending further leaf area to this canopy will decrease the downward scattered radiation, since there is now an increased probability of capturing this energy by the additional leaf area.

The generation of upward and downward scattered flux densities inside the canopy gives us an insight into how the albedo [$S_p^\uparrow(0)$] and the effective transmittance [$S^p_\downarrow(F)$] of the canopy vary with its absolute leaf area. The albedo of the canopy increases with increasing leaf area index, only up to a certain magnitude beyond which additional leaf area does not result in increased interception of radiant energy. Naturally, the manner in which the invested leaf area is distributed in space determines where this plateau can occur [Fig. 3(a)]. It is intuitively obvious that more leaf area can be invested if the arrangement of such leaf area in space is clumped than when it is arranged in a mosaic fashion. However, the ability to intercept and scatter radiant energy will correspondingly be reduced. On the other hand, the effective transmittance of the canopy increases rapidly with leaf area index, reaches a maximal value, and

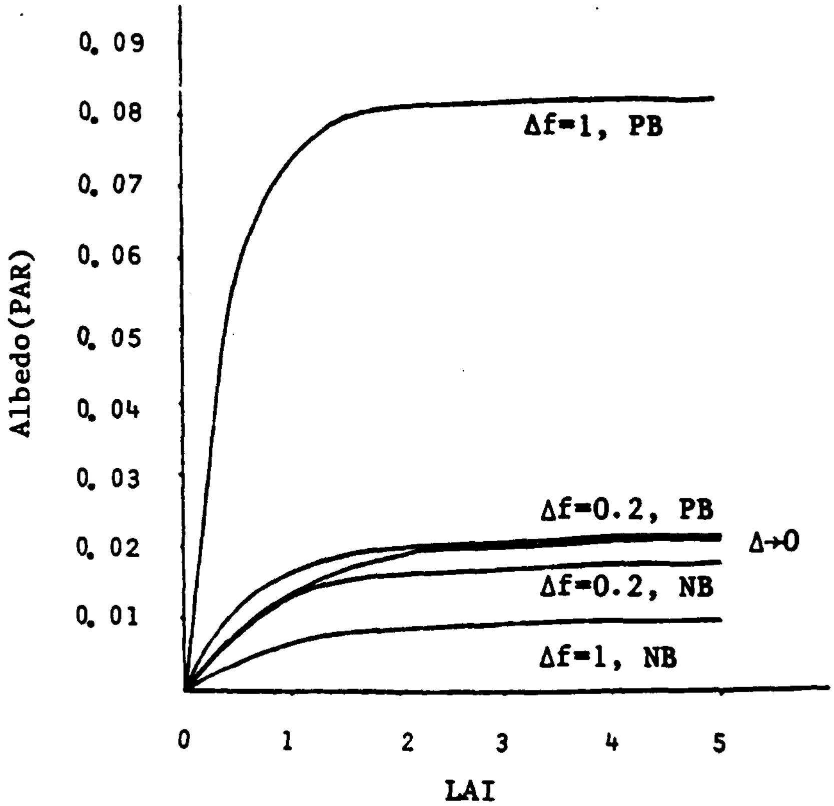

(a)

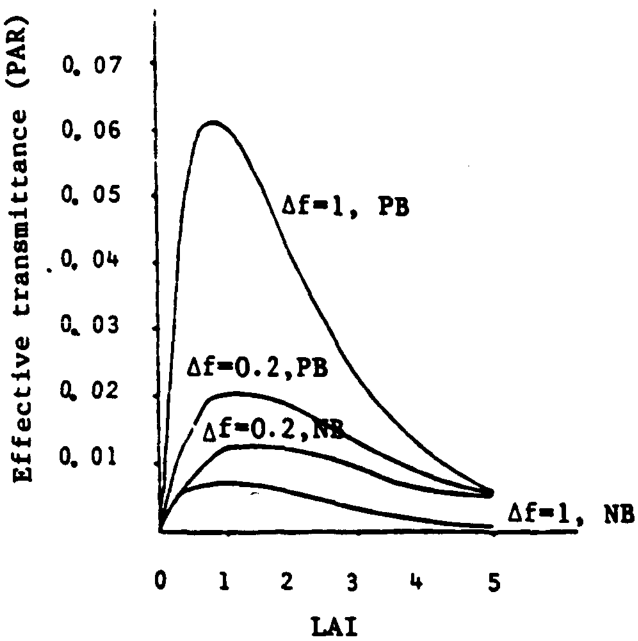

(b)

FIGURE 3. The relationship of albedo (a) and effective transmittance (b) in the PAR region with canopy leaf area index. The leaf angle distribution is uniform, and the elevation of the sun is 60°. PB and NB as in Fig. 1.

then decreases with further increase in leaf area, since the ability to intercept this scattered energy is higher [Fig. 3(b)].

The emergent flux from the canopy has been used in remote sensing endeavors as a predictor of canopy leaf area index and other phytometric attributes. Empirical relationships show that the leaf area index of the canopy and transformations of monochromatic emergent fluxes are linearly related. As illustrated here and in other earlier works (Lemeur, 1971; Ross, 1981), the variables in case are nonlinearly related and the relationship levels off after a certain value of LAI, depending on the canopy. Specifically, the leaf dispersion and orientation determine the plateau and the degree of nonlinearity of this relationship. Strictly speaking, LAI is not directly related to the emergent flux of the canopy. It is the fraction of total leaf area projected onto the direction of incoming radiation, and the proportion of such projected leaf area observed by the radiometer determines the emergent flux from the canopy. One can easily conceive, for a given leaf area, different geometrical arrangements of leaves that could result in a range of reflectances from a single view angle. However, if the view angle and the canopy's internal geometric features are invariant with time (crop growth), then the empirical experimental relationship is valid, since there is a 1:1 relationship between the canopy LAI and the projected leaf areas.

The albedo and the effective transmittance of the canopy are plotted against solar elevation in Figs. 4(a) and (b), respectively. The albedo and the effective transmittance are considerably higher for oblique ray incidences, since the pathlength of the rays inside the canopy is higher, thereby increasing the probability of interception and scattering by the leaf elements. This behavior is pronounced in a more regularly dispersed canopy. The albedo and the effective transmittance of a severely clumped canopy is, however, almost invariant with solar elevation as the gap proportion is high. The mean normalized net scattered flux density in the canopy at different sun elevations is given in Fig. 4(c). For low sun elevations,

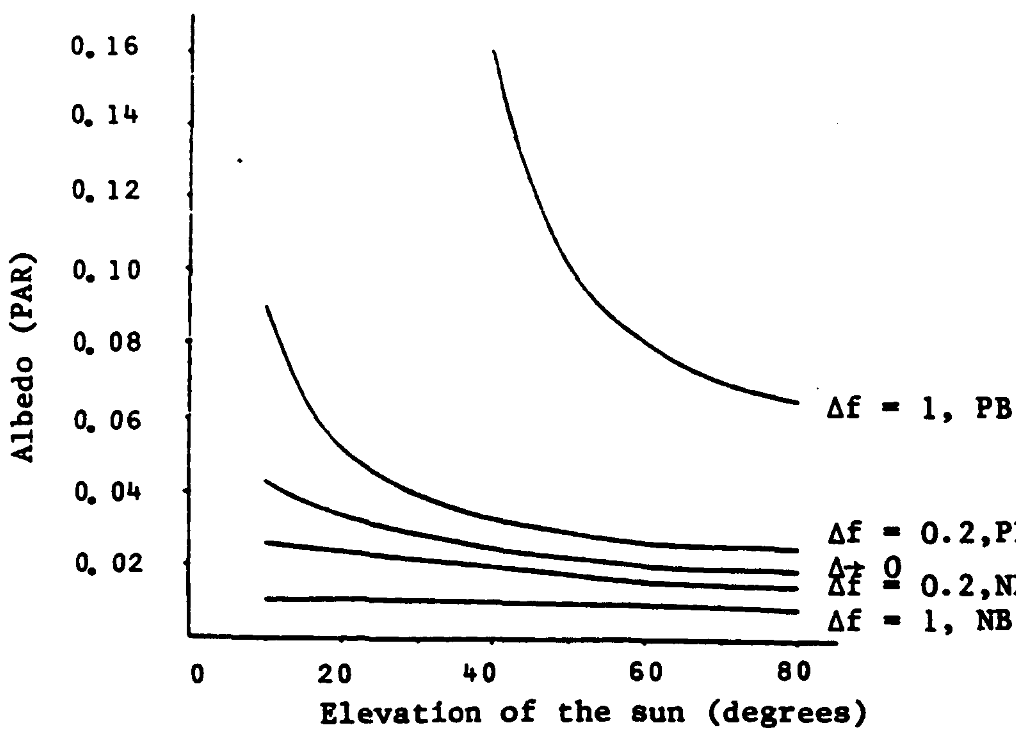

(a)

FIGURE 4. The relation ship between albedo (a), effective transmittance (b), and mean normalized net scattered flux (c) with sun elevation. The leaf area index of the canopy is 5, and the leaf angle distribution is uniform. PB and NB as in Fig. 1. In (c), the canopy leaf spatial dispersion follows the positive binomial distribution, where $\Delta f = 0.2$.

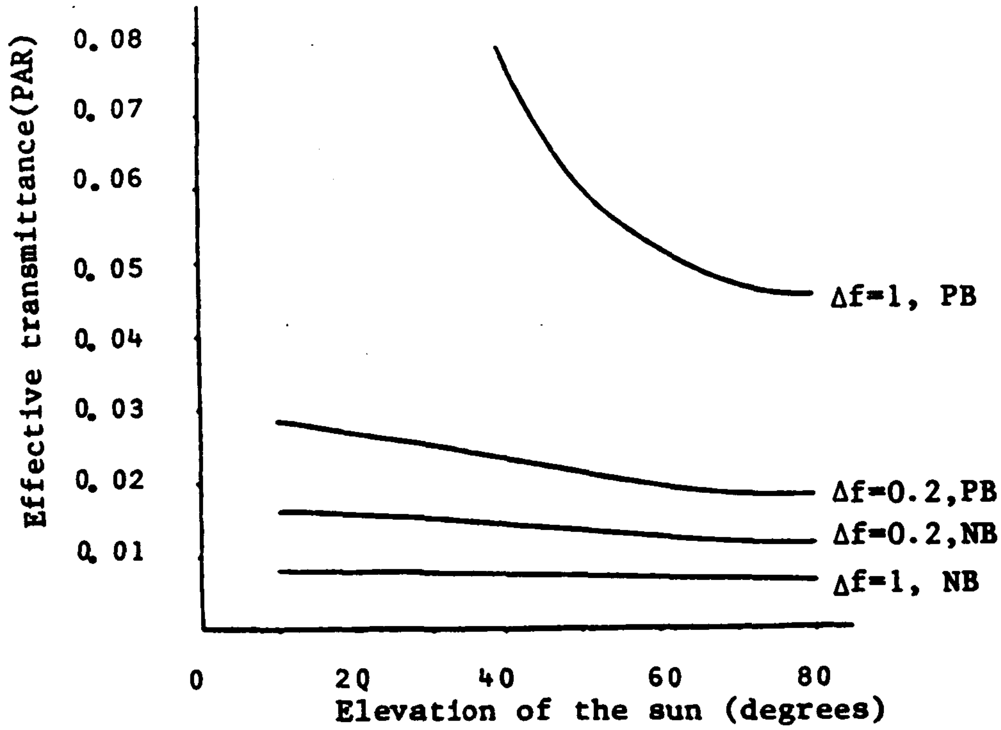

(b)

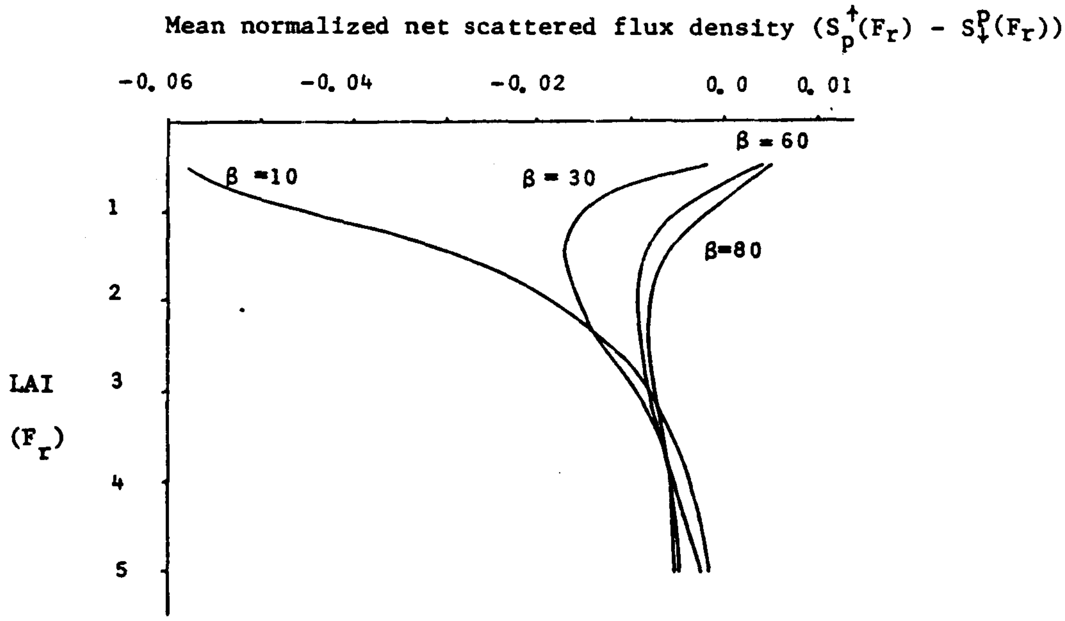

(c)

FIGURE 4. (continued)

more radiation is scattered downwards than upwards. It is interesting to note how much of the flux that emerges from the canopy at the top is generated in the upper layers of the canopy.

The albedo and the effective transmittance are plotted against canopy LAI for horizontal, planophile, and erectophile leaf orientation distributions in Figs. 5(a) and (b), respectively. The combination of horizontal and regular dispersion of leaves results in a higher probability of radiation interception and scattering. However, the LAI at which the relationship flattens is less compared to erectophile and/or clumped canopies. It is also apparent that

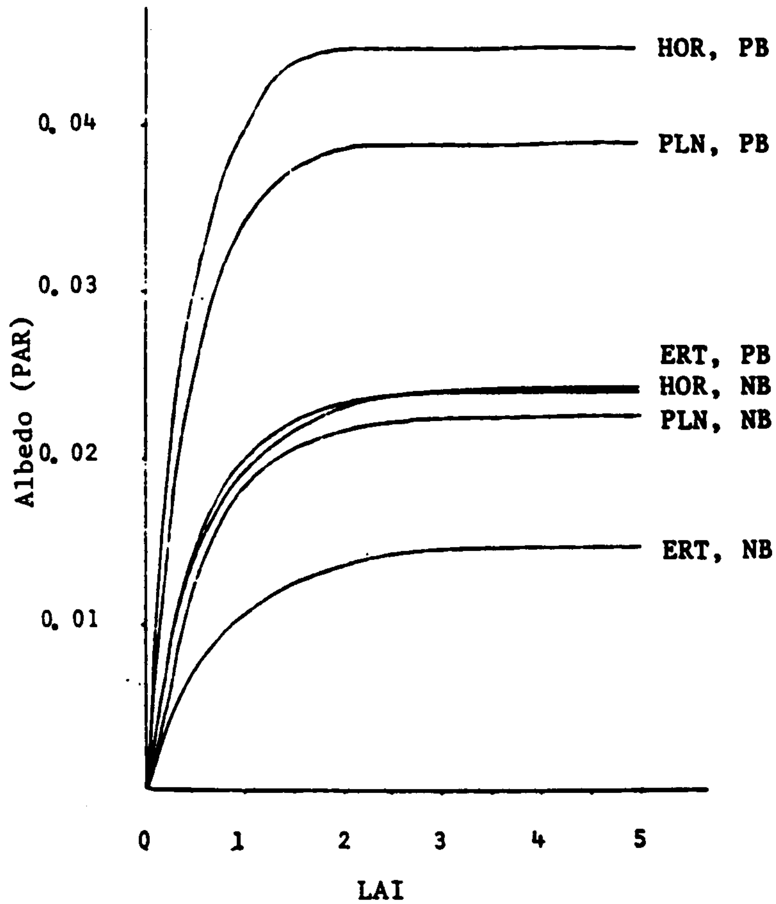

(a)

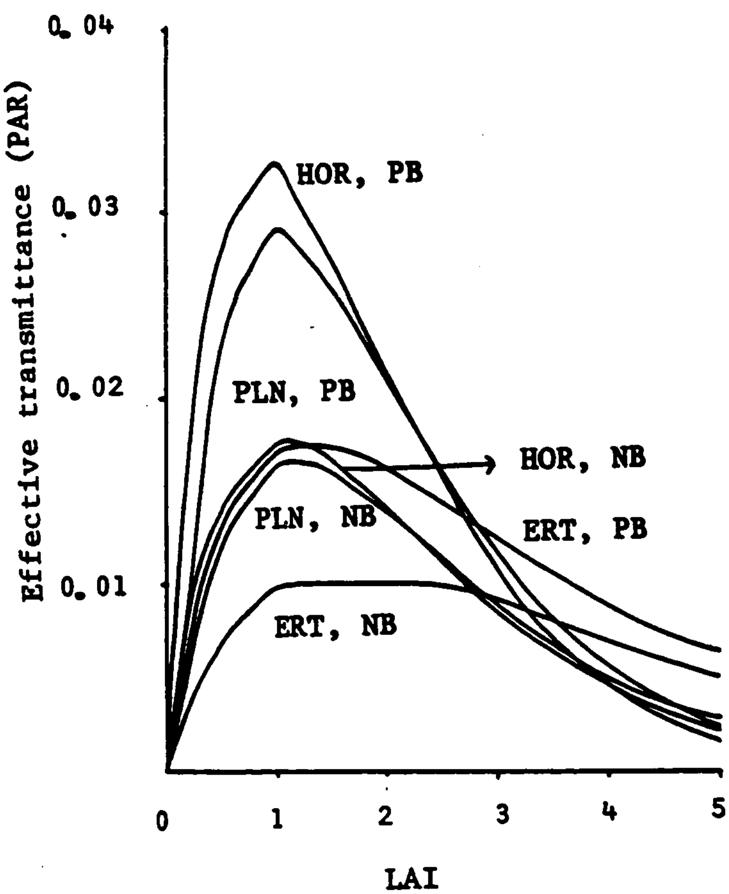

(b)

FIGURE 5. The relationship between albedo (a), effective transmittance (b), and mean normalized net scattered flux (c) with canopy leaf area index. HOR, PLN, and ERT refer to horizontal, planophile, and erectophile leaf angle distributions, respectively. The elevation of the sun is 60°, and PB and NB are as in Fig. 1.

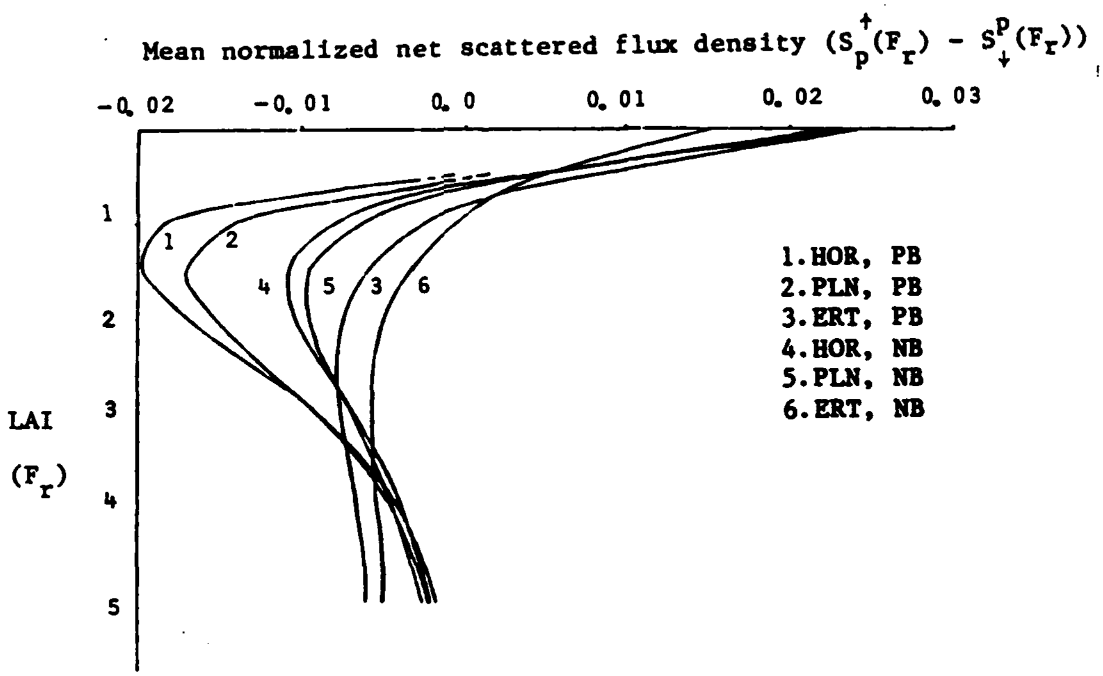

FIGURE 5. (continued)

much more radiation is scattered downwards than upwards in the former canopies [Fig. 5(c)]. As is illustrated in these figures, the nonlinearity of the relationship between LAI and albedo is generally determined by the leaf spatial dispersion and orientation functions. Hence, it can be concluded that these phytometric characteristics primarily. determine the radiant energy field characteristics in vegetated spaces.

The foregoing discussion illustrates the versatility of the statistical formulation presented here. The parameter Δf (or N) permits the applicability of the formulation to a wide range of simulations of functional behavior. If multiple scattering is included, then the formulation allows one to evaluate monochromatic albedos, the inversion of which can be used for remote sensing purposes. However, one has to first empirically evaluate the value of Δf from the experimental data. It is this aspect of the formulation that lends its versatility. The effective transmittance of a canopy can also be used for remote sensing purposes in canopies where it is difficult to measure emergent flux above the canopy, viz., forest canopies. However, the problem is more complicated, since, in addition to downward scattered flux, one also measures unimpeded direct and diffuse fluxes. From data on canopy permeability on perfectly overcast days, perhaps it is possible to find empirically a value of Δf and then numerically invert the formulation for leaf area index. This is a challenging problem, but is of practical importance.

Conclusions

The formulation presented here can be used to describe single scatter of radiant energy in diverse vegetative canopies. The relationship between canopy reflectance (PAR) and leaf area index is nonlinear, the degree of which is determined by the leaf spatial dispersion and angular characteristics. In the range of canopies studied here, more radiant energy is scattered downwards than upwards and the emergent flux at the top is mostly generated in the upper layers of the canopy. The results clearly illustrate the versatility of the formulation. However, one has to evaluate the value of N, perhaps empirically, before the formulation is used in a specific case.

Professor Dr. R. Lemeur taught modeling radiative transfer to R. B. M., and his help is gratefully acknowledged. We also thank Mrs. P. Chapman and Miss A. Bervoets for help in preparing the manuscript. The authors also wish to thank Dr. D. Baldocchi and two anonymous reviewers for their helpful comments.

References

Asrar, G., Fuchs, M., Kanemasu, E. T., and Hatfield, J. L. (1984), Estimating absorbed photosynthetic radiation and leaf area index from spectral reflectance in wheat, *Agron J.* 16:300–306.

Blad, B. L., and Baker, G. G. (1972), Orientation and distribution of leaves within soybean canopies, *Agron J.* 64:26–29.

Chandrasekhar, S. (1950), *Radiative Transfer*, Dover, New York.

Cooper, K., Smith, J. A., and Pitts, D. (1982), Reflectance of a vegetation canopy using the adding method, *Appl. Opt.* 22:4112–4118.

Cowan, I. R. (1966), The interception and absorption of radiation in plant stand, *J. Appl. Ecol.* 5:367–379.

De Wit, C. T. (1965), Photosynthesis of leaf canopies, Agric. Res. Rep. No. 663, Center for Agric. Publ. and Doc., Wageningen, Netherlands.

Duncan W. G., Loomis, R. S., Williams, W. A., and Hanau, R. (1967), A model for simulating photosynthesis in plant communities, *Hilgardia* 4:181–205.

Gerstl, S. A. W., and Zardecki, A. (1985), Coupled atmosphere/canopy model for remote sensing of plant reflectance features, *Appl. Opt.* 24:94–103.

Goel, N. S., and Strebel, D. E. (1983), Inversion of vegetation canopy reflectance models for estimating agronomic variables. I. Problem definition and initial results using the Suits model, *Remote Sens. Environ.* 13:487–507.

Gutschick, V. P., and Wiegel, F. W. (1984), Radiation transfer in vegetative canopies and other layered media: rapidly solvable exact integral equation not requiring Fourier resolution, *J. Quant. Spectrosc. Radiat. Transfer* 31:71–82.

Hunt, G. E. (1971), A review of computational techniques for analyzing the transfer of radiation through a model cloudy atmosphere, *J. Quant. Spectrosc. Radiat. Transfer* 11:655–690.

Lemeur, R. (1971), Mathematical model for the study of parallel, isotropic and scattered radiation in theoretical and real canopies, Ph.D. thesis, Chair of Plant Ecology, University of Ghent.

Lemeur, R. (1973), A method for simulating the direct solar radiation regime in sunflower, Jerusalem artichoke, corn and soybean canopies using actual stand structure data, *Agric. Meteorol.* 12:229–247.

Lemeur, R., and Blad, B. L. (1974), A critical review of light models for estimating the shortwave radiation regime of plant canopies, *Agric. Meteorol.* 14:255–286.

Lemeur, R., and Rosenberg, N. J. (1979), In *Comparison of forest water and energy exchange models* (S. Halldin, Ed.), Int. Soc. Ecol. Modelling, Copenhagen, pp. 77–100.

Liou, K. N. (1980), *An Introduction to Atmospheric Radiation*, Academic, New York.

Monteith, J. L. (1965), Light distribution and photosynthesis in field crops, *Ann. Bot.* 29:17–37.

Nichiprovich, A. A. (1961). Properties of plant crops as an optical system. *Sov. Plant Physiol.* 8:428–435.

Nilson, T. (1971), A theoretical analysis of the frequency of gaps in plant stands, *Agric. Meteorol.* :25–38.

Ross, J. (1981), In *The Radiation Regime and Architecture of Plant Stands* (H. Lieth, Ed.), Dr. W. Junk Publishers.

Ross, J. K., and Nilson, T. (1976), In *Photosynthesis of Productive Systems.* (A. A. Nichiprovich, Ed.), transl. by Israel Prof. Sci. Transl., Jerusalem, pp. 86–89.

Saeki, I. (1963), In *Environmental Control of Plant Growth* (L. T. Evans, Ed.), Academic, New York and London, pp. 79–84.

Suits, G. H. (1972), The calculation of the directional reflectance of a vegetative canopy, *Remote Sens. Environ.* 2:117–125.

Received 9 December 1985; revised 27 May 1986.

Chapter 2.0

Light Scattering in Plant Canopies: The Method of Successive Orders of Scattering Approximations (SOSA)

Agricultural and Forest Meteorology, 39 (1987) 1–12
Elsevier Science Publishers B.V., Amsterdam — Printed in The Netherlands

LIGHT SCATTERING IN PLANT CANOPIES: THE METHOD OF SUCCESSIVE ORDERS OF SCATTERING APPROXIMATIONS (SOSA)*

R.B. MYNENI, G. ASRAR and E.T. KANEMASU

Evapotranspiration Laboratory, Department of Agronomy, Waters Annex, Kansas State University, Manhattan, KS 66506 (U.S.A.)

(Received 16 April 1986)

ABSTRACT

Myneni, R.B., Asrar, G. and Kanemasu, E.T., 1987. Light scattering in plant canopies: the method of Successive Orders of Scattering Approximations (SOSA). Agric. For. Meteorol., 39: 1–12.

The method of Successive Orders of Scattering Approximations (SOSA) involves computation of photons scattered once, twice, three times, etc., with the total intensity obtained as the sum over all orders. The method SOSA is briefly presented. The implemented formulation was tested for energy conservation in a conservatively scattering medium. The scattered fluxes for each order of scattering are presented to help understand the process of multiple scattering in plant canopies. The method was tested against measured values of canopy reflectance for a soybean canopy and also against the predictions of other established formulations published in the literature. Finally, some theoretical relationships between spectral indices, LAI and absorbed radiant energy are presented.

INTRODUCTION

The problem of radiative transfer has been pursued by investigators in such diverse disciplines as astrophysics, atmospheric physics, biology, chemistry, engineering design, laser interaction, metallurgy, nuclear engineering, remote sensing, etc. Most of the fundamental treatment can be found in the classical works of Chandrasekhar (1950), Sobolev (1974) and Van de Hulst (1980). The generic problem of radiative transfer and solution techniques in layered media were reviewed by Hunt (1971) and Hansen and Travis (1974).

Recent technological advances in remotely measuring sensors, in spatial and spectral resolution, and a desire for greater measuremental accuracy have all resulted in a heightened awareness of the need to understand radiative transfer in vegetative media. The methods commonly used in astrophysics and atmospheric physics have been employed to increase our understanding of radiant energy propagation in plant canopies (Ross, 1981). The desire to compute the radiant energy distribution in plant canopies is primarily twofold.

*Contribution 86-275-J from the Agricultural Experiment Station, Kansas State University, U.S.A.

0168-1923/87/$03.50

First, to compute canopy photosynthetic rates (De Wit, 1965; Duncan et al., 1967; amongst others) and canopy reflectance (Suits, 1972). Second, the inversion of these mathematical formulations enables us to estimate canopy variables such as leaf area index and/or radiative field characteristics such as absorbed radiant energy from remote measurements of canopy reflectance (Goel and Strebel, 1983; Asrar et al., 1984; amongst others). The n-flux methods have been quite popular because of their simplicity and have been extensively used to model canopy reflectance (Allen and Richardson, 1968; Allen et al., 1970; Suits, 1972; Bunnik, 1978; Verhoef, 1984; amongst others). It should, however, be noted that the differential equations describing the flux propagation are heuristic and in non-random canopies it is not possible to compute photon dispositions that obey the conservation principle (see Gutschick and Weigel, 1984). On the other hand, there have been some rigorous methods that have been used to model canopy reflectance. One such approach is the adding-doubling method of Van de Hulst (1980) which Cooper et al., used to model the canopy reflectance of a soybean canopy. Gerstl and Zardecki (1985a,b) solved the integro-differential transfer equation using the Discrete-ordinate finite-element technique for a coupled media of atmosphere and plant canopy. Gutschick and Weigel (1984) developed a rapidly solvable exact integral equation for radiative flux interception by a scattering element in a layered media, the convergent numerical solution of which can be line-integrated to obtain a profile of angle-resolved fluxes. These rigorous methods are quite complicated and tedious. They generally require a large computer. The method of successively estimating each order of scattering is one of the oldest and simplest of all the solutions to the multiple scattering problem. The method is mathematically simple and can be solved on a mini-computer within a reasonable CPU time. In the following sections, we briefly present the theory, some intermediate results, compare model predictions with measured field data and finally present some theoretical relationships between predicted spectral indices and leaf area index. Extensive results using this method have been published elsewhere (Myneni et al., 1986).

THEORY

We assume that:

(1) The plant canopy is a plane parallel, horizontally homogeneous, and extensive turbid medium of arbitrary finite physical depth, z, continuous along the three coordinates.

(2) There are no embedded sources of radiation inside the plant canopy.

(3) Leaves or their parts are the only canopy elements to interact with solar radiation.

(4) The individual leaves or their parts scatter radiation isotropically.

(5) Scattering involving quantum transitions is not considered.

(6) Processes at different wavelengths are independent.

(7) There is no polarization of light.

(8) Radiation is incident from any direction on top/bottom in infinitely wide homogeneous beams, so that the intensity does not depend on x and y coordinates.

We consider the transport equation

$$\mu \frac{dI(\tau, \Omega)}{d\tau} = I(\tau, \Omega) - \frac{\omega}{4\pi} \int_{4\pi} I(\tau, \Omega') \, P(\Omega, \Omega') \, d\Omega' - \frac{\omega}{4\pi} P(\Omega, -\Omega_0) E_0 \exp(-\tau/\mu_0) \tag{1}$$

where, θ = polar zenith angle; $\mu = \cos\theta$ ($-\mu$ denotes descending flux and μ for ascending flux); Ω = direction (θ, ϕ); $d\Omega$ = solid angle = $\sin\theta \, d\theta \, d\phi$; I = Intensity (quantal units $L^{-2}T^{-1}st^{-1}$); E_0 = incident collimated flux density (quantal units $L^{-2}T^{-1}$); Ω_0 = direction of collimated flux incident at the top = θ_0, ϕ_0; ω = albedo of single scattering; $P(\Omega, \Omega')$ = phase function that introduces the appropriate stream from direction Ω' into direction Ω; τ = optical depth defined by the relation;

$$\tau = n' G(\Omega) \int_0^z dz' \tag{2}$$

The $G(\Omega)$ function may be defined as (Ross, 1981),

$$G(\Omega) = \int_0^{2\pi} \int_0^1 g_L(\Omega_L) \, |\Omega \cdot \Omega_L| \, d\mu_L d\phi_L \tag{3}$$

where $g_L(\Omega_L)$ is the leaf normal orientation distribution that determines the fraction of total leaf area oriented in the canopy, so that the normals to the upper face of the leaves are within a unit solid angle around the direction located by Ω_L and normalizes to

$$\int_{\frac{\pi}{2}} g_L(\Omega_L) \, d\Omega_L = 1 \tag{4}$$

Note that we define $g_L(\Omega_L)$ as the fraction of total leaf area whose normals fall within a unit solid angle around the direction Ω_L, and hence, we do not have the 2π factor as found in the works of Ross (1981). The dot product in eq. 3 can be expanded as,

$$|\Omega \cdot \Omega_L| = |\mu\mu_L + (1 - \mu^2)^{1/2} (1 - \mu_L^2)^{1/2} \cos(\phi - \phi_L)| \tag{5}$$

Assuming azimuthal independence, the measured leaf inclination distribution can be used to estimate the G function (eq. 3) by evaluating the integral numerically.

Consider that the plant canopy is subject to the following inputs at the top,

$$\begin{aligned} I(0, \Omega) &= 1 \\ E_0 &= 1 \end{aligned} \tag{6}$$

The collimated flux density is relative to a horizontal plane. If the exitant intensity from the vegetative canopy is assumed to consist exclusively of energy derived from single scattering of collimated flux, then the source function is simply,

$$J(\tau, \Omega) = \frac{\omega}{4\pi} P(\Omega, -\Omega_0) E_0 \exp(-\tau/\mu_0) \tag{7}$$

Now, for a finite thickness of the plant canopy, bounded on the two sides (perpendicular to the plane of stratification) at $\tau = 0$ and at $\tau = \tau_1$, the ascending and descending fluxes at an intermediate optical depth τ are

$$\begin{aligned} I(\tau, \Omega) &= I(\tau_1, \Omega) \exp(-(\tau_1 - \tau)/\mu) + \\ &\quad + \frac{\omega}{4\pi} P(\Omega, -\Omega_0)\, E_0 \int_{\tau}^{\tau_1} \exp\left[-\left(\frac{(\tau' - \tau)}{\mu} + \frac{\tau'}{\mu_0}\right)\right] \frac{d\tau'}{\mu} \end{aligned} \tag{8}$$

$$\begin{aligned} I(\tau, -\Omega) &= I(0, -\Omega) \exp(-\tau/\mu) + \\ &\quad + \frac{\omega}{4\pi} P(-\Omega, -\Omega_0)\, E_0 \int_{0}^{\tau} \exp\left[-\left(\frac{(\tau - \tau')}{\mu} + \frac{\tau'}{\mu_0}\right)\right] \frac{d\tau'}{\mu} \end{aligned} \tag{9}$$

For each higher order of scattering, the source functions and the intensities may be evaluated successively by means of recursion principles. These relations may be generalized as,

$$\left.\begin{aligned} J_{m+1}(\tau, \Omega) &= \frac{\omega}{4\pi} \int_0^{2\pi} \int_{-1}^{1} P(\Omega, \Omega') I_m(\tau, \Omega') d\mu' \, d\phi' \\ I_m(\tau, \Omega) &= \int_{\tau}^{\tau_1} J_m(\tau', \Omega) \exp[-(\tau' - \tau)/\mu] \frac{d\tau'}{\mu} \\ I_m(\tau, -\Omega) &= \int_{0}^{\tau} J_m(\tau', -\Omega) \exp[-(\tau - \tau')/\mu] \frac{d\tau'}{\mu} \end{aligned}\right| \tag{10}$$

where $m > 1$.

The total intensity at level τ is obtained from the summation over all orders of scattering,

$$\left.\begin{aligned} I(\tau, \Omega) &= \sum_{m=1}^{\infty} I_m(\tau, \Omega) \\ I(\tau, -\Omega) &= \sum_{m=1}^{\infty} I_m(\tau, -\Omega) \end{aligned}\right| \tag{11}$$

and may be normalized with incident input after angle integration to yield reflectance and transmittance,

$$R(0) = \frac{2\pi}{(\pi + 1)} \int_0^1 I(0, \Omega)\, \mu \, d\mu$$

$$T(\tau_1) = \frac{2\pi}{(\pi + 1)} \int_0^1 I(\tau_1, -\Omega)\, \mu \, d\mu \qquad (12)$$

Note that since the transport equation does not describe the penetration of collimated flux through gaps in the canopy, this flux contribution has to be added to the descending fluxes in the first leg of the computations.

More details on the actual computational procedure are discussed elsewhere (Myneni et al., 1986).

RESULTS AND DISCUSSION

Ranson and Beihl (1982) reported a comprehensive modelling data set collected on a soybean canopy. The measured leaf angle distribution was used to compute the G function. The leaf distribution in space was assumed to be random and azimuthal dependence was neglected. In order to see if the implemented formulation was obeying the principle of energy conservation, we set the single scattering albedos of the leaves to unity. The soil boundary was assumed to be a perfect Lambertian diffuser, with conservative reflecting properties (100%). The normalized upward and downward horizontal flux densities for successive orders of scattering are plotted in Figs. 1 and 2, respectively. After about six orders of scattering, there is almost 100% of input everywhere in the canopy. This is not surprising considering the optical depth of the medium. Hence, we concluded that the computed photon dispositions actually

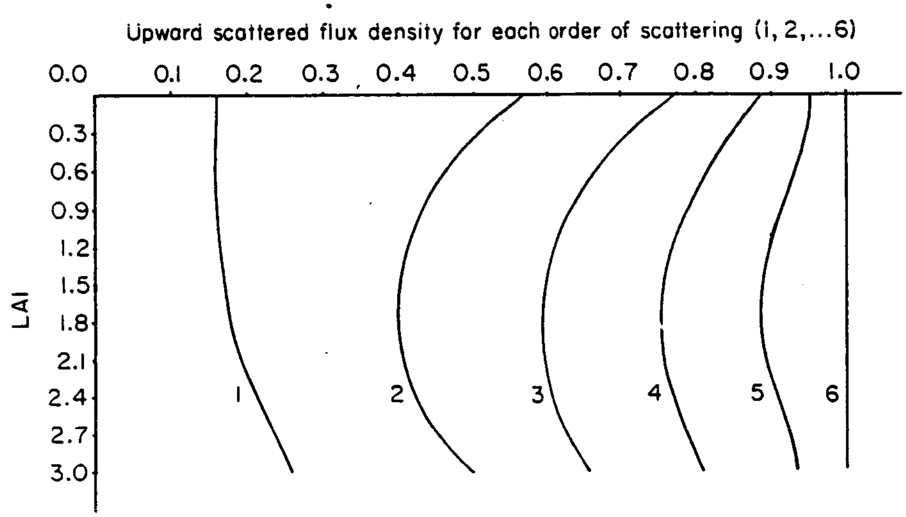

Fig. 1. Profile of normalized ascending scattered flux density for each successive order of scattering in a soybean + soil media with conservative scattering properties.

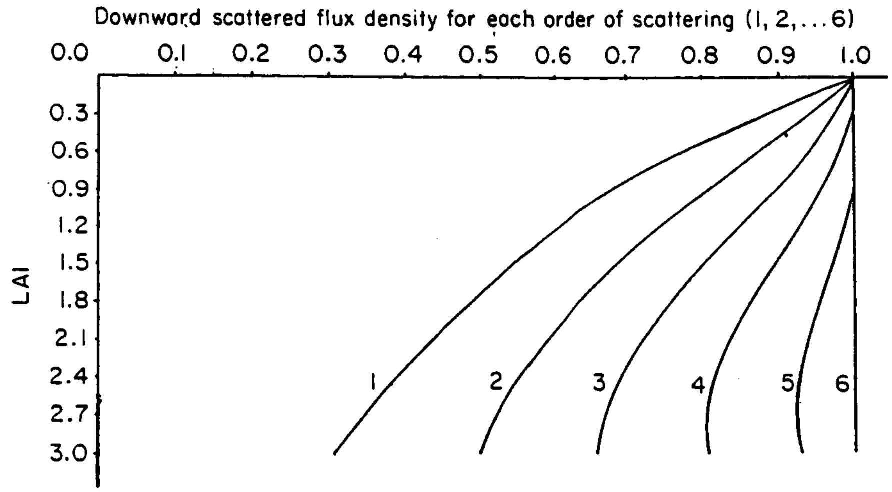

Fig. 2. Profile of normalized descending scattered flux density for each order of scattering in a soybean + soil media with conservative scattering properties.

obey the principle of energy conservation and all further analysis was carried up to six orders of scattering only.

Ranson and Beihl (1982) also reported leaf reflectance and transmittance in the Exotech Model 100 wavelength bands 2 (0.6 to 0.7 μm) and 4 (0.8 to 1.1 μm), computed from measured values with a DK-2 spectrophotometer by considering the responsivity of the radiometer, referenced to a barium sulphate calibration panel used in the field. We inserted these coefficients in the formulation of SOSA and the results from a first leg of computations are presented in Fig. 3. Curves 2 and 3 represent downward penetration of axially symmetric diffuse, and collimated input fluxes, respectively. The normalized downward and upward scattered flux densities derived from single scattering of collimated flux in wavelength band 2 (curves 1 and 4, respectively) and 4 (curves 6 and 7) are also given in Fig. 3. These profiles are symmetrical and differ only in their relation to depth in the canopy. This may be expected if one considers the integral equation that describes these fluxes. Curves 5 and 8 denote upward

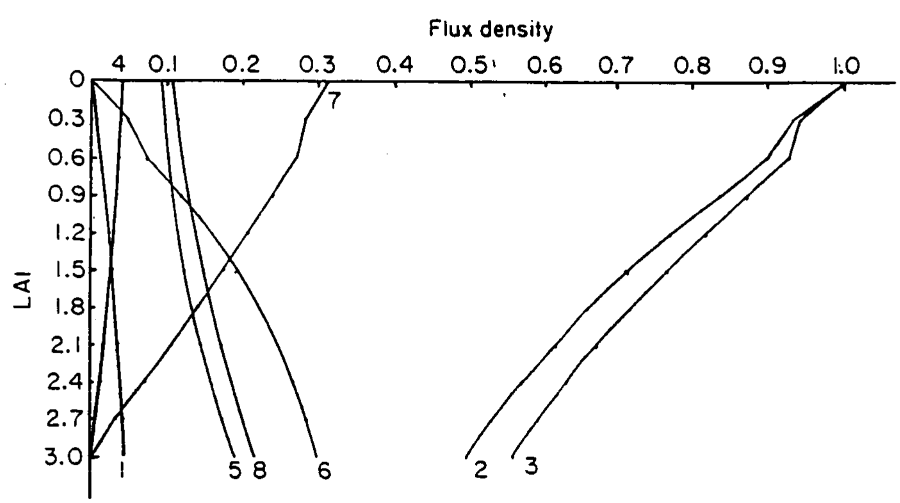

Fig. 3. Profile of normalized flux densities from a first leg of computations using SOSA.

penetration of flux density reflected from the soil in the two wavelength bands. These fluxes decrease with increasing depth due to increased probability of interception by the leaves. These profiles, as opposed to the ones presented in Figs. 1 and 2, are not smooth since we implemented a layer-specific leaf angle distribution that was reported by Ranson and Beihl (1982).

The absolute values of the downward and upward scattered flux densities for higher orders of scattering in wavelength band 4 are plotted in Figs. 4 and 5, respectively. The curves in Figs. 4 and 5 for any arbitrary order of scattering are not necessarily symmetrical, since the source functions for the ascending and descending fluxes are not numerically equivalent. The upward penetration of flux reflected from the soil is plotted in Fig. 6, for different orders of scattering. As is apparent from Figs. 4, 5 and 6, the absolute values of all the flux densities are approaching zero with increase in order of scattering (i.e., the sum of successive orders is approaching a constant value). The results presented here help in the conceptualization of the process of multiple scattering in plant canopies.

Plant canopy phytometric, leaf optical properties and canopy multispectral reflectance were measured on a soybean crop, with a green leaf area index of 2.87. This data set was collected at the Laboratory for Applications of Remote Sensing (LARS) and is described in detail by Ranson and Beihl (1982). They also reported leaf reflectance and transmittance in the four Exotech Model 100 radiometer wavelength bands, which were computed values based on the responsivity of the radiometer and the barium sulphate calibration panel used in the field. Leaf reflectance and transmittance was summed to obtain the leaf albedo of single scattering and was used to run the formulation. Extensive validation of SOSA is presented elsewhere (Myneni et al., 1986). However, we will present here one case of validation. Cooper et al. (1982) computed the spectral reflectance factors of the same soybean canopy using the adding method (AM) and Suits' (1972) method (SM). The results of Cooper et al. (1982), along with the spectral reflectance factors in the two Exotech wavelength

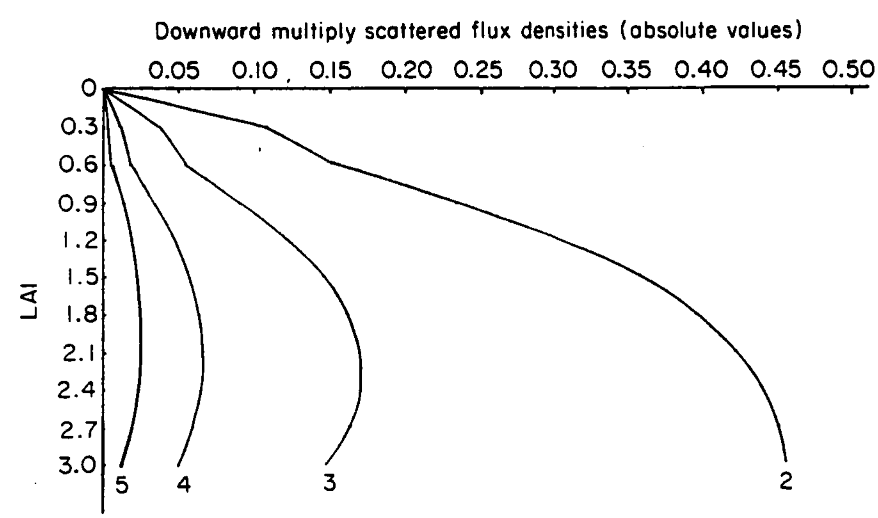

Fig. 4. Profile of descending flux densities for each higher order of scattering in a soybean canopy.

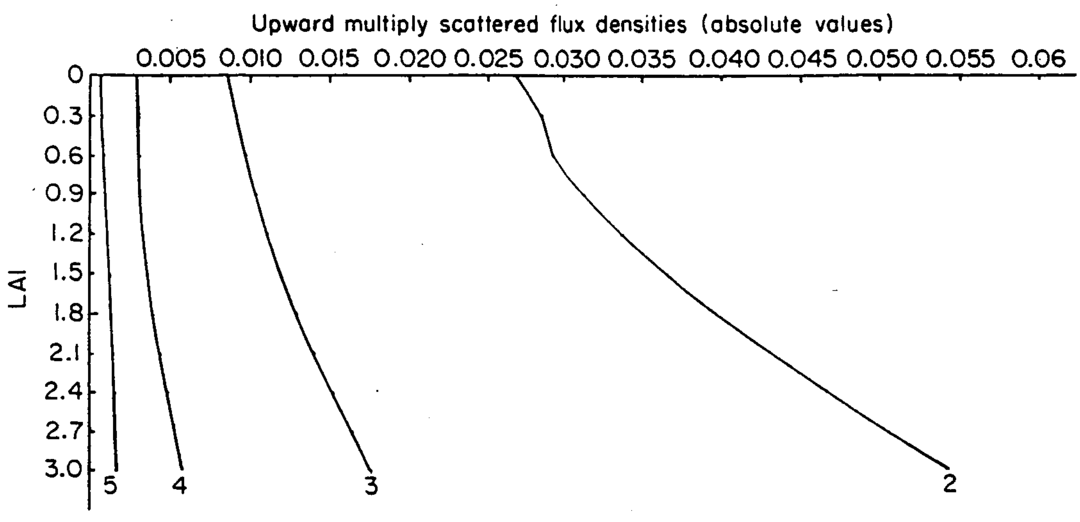

Fig. 5. Profile of ascending flux densities for each higher order of scattering in a soybean canopy.

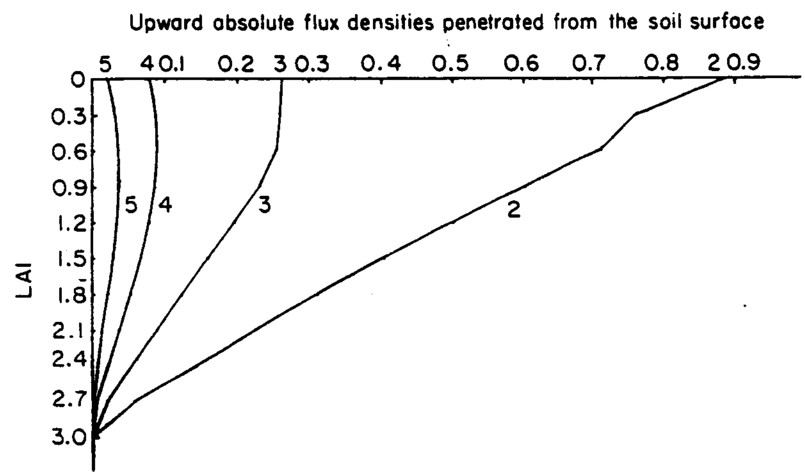

Fig. 6. Profile of ascending flux densities derived from reflectance of the soil background, for each higher order of scattering.

bands 1 and 3 (0.5 to 0.6 μm, and 0.7 to 0.8 μm, respectively) computed by the method of SOSA are presented in Fig. 7. The leaf scattering coefficients in these wavelength bands reported by Ranson and Beihl (1982) were used in the formulation of SOSA to obtain these results. The predictions of SOSA were slight overestimates in wavelength band 1, but the absolute values of the reflectance is small and it is impossible to obtain an exact numerical correspondence. In the near infrared wavelength band, the predictions of SOSA were in good agreement with the measured values.

Spectral indices like Normalized Difference (*ND*) are derived to maximize the contrast between the canopy and soil reflectances. Such contrast is provided by the differential scattering behavior of the canopy and the soil in the near infrared and red wavelengths of the spectrum. Leaf scattering in the near infrared is high. Refractive index discontinuities at the cell wall/air space interface are mainly responsible for infrared scattering. On the other hand, leaf scattering at red wavelengths is minimal due to strong absorption by the leaf

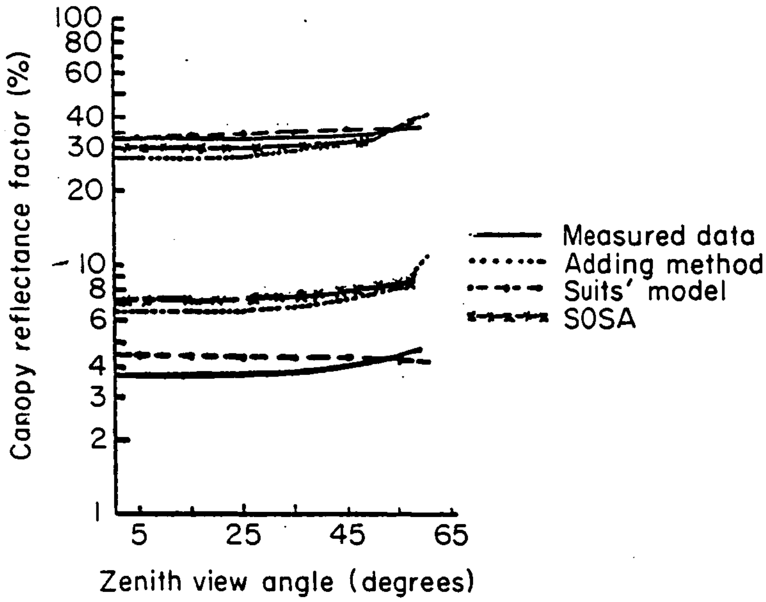

Fig. 7. Soybean canopy reflectance factors with view zenith angle for a solar zenith angle of 35°. The results correspond to Exotech Model 100 wavelength bands 1 and 3. The results of the adding method are of Cooper et al. (1982).

pigments. The soil background, however, does not exhibit this preferential scattering behavior.

The leaf area index of the soybean canopy was decremented from 3 to 0.5, in steps of 0.5 and the canopy + soil background reflectances in the two Exotech wavelength bands 2 (0.6 to 0.7 μm) and 4 (0.8 to 1.1 μm) were computed using the method of SOSA. A plot of computed *ND* with *LAI* is given in Fig. 8. The *ND*

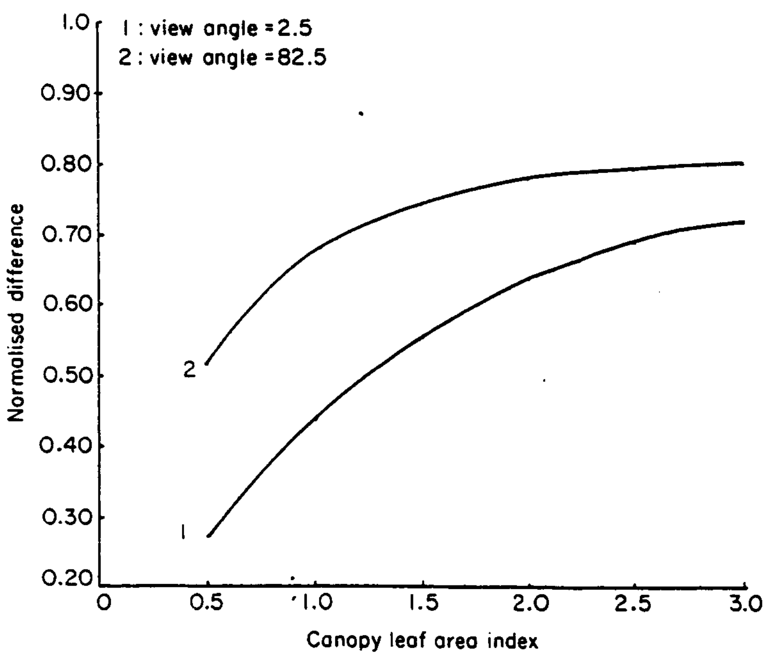

Fig. 8. Normalized difference with canopy leaf area index for two view zenith angles.

was computed from reflectance factors measured at two zenith view angles (2.5° and 82.5°). The relationship is nonlinear, the degree of which increases with oblique view angles. For a highly oblique view angle (82.5°), ND was almost invariant with *LAI*, after a canopy *LAI* of 2.0. This is also intuitively obvious when we consider the probability of mean free path of the rays for oblique ray transits.

The difference of directional fluxes at the upper ($LAI = 0$) and lower ($LAI = F$, canopy total *LAI*) boundaries of the vegetative canopy for both ascending and descending propagation directions was summed to yield absorbed radiant energy at a specific wavelength and was normalized with incident input. These data correspond to Exotech wavelength band 2 and are plotted in Fig. 9, with *ND* for the two view zenith angles. The relationship between *ND* and absorbed energy is slightly nonlinear for a view zenith angle of 2.5° and is highly nonlinear for an oblique view zenith angle (82.5°). Hence, care must be exercised when one tries to estimate *LAI* or absorbed energy using spectral indices. These relations are also substantiated from experimental data by Asrar et al. (1984).

CONCLUSIONS

The method of Successive Orders of Scattering Approximations (SOSA) involves computations of photons scattered once, twice, three times, etc., with the total intensity obtained as sum over all orders of scattering. In a conservatively scattering medium, the computed photon dispositions were consistent with the principles of energy conservation. The various constitutive flux

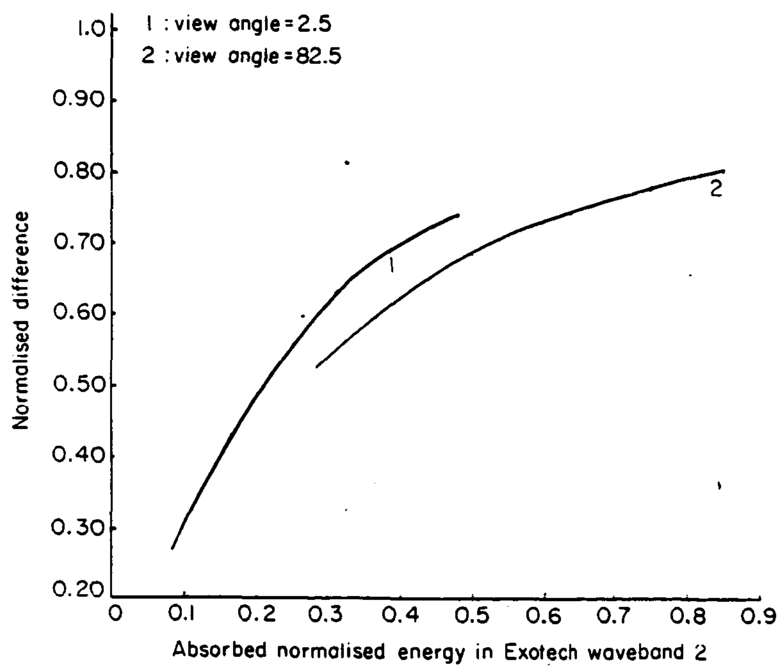

Fig. 9. Normalized difference with absorbed radiant energy in Exotech Model 100 wavelength band 2 for two view zenith angles.

profiles approached absolute values of zero at sixth order of scattering. The predicted spectral reflectance factors were in good agreement with the measured values and the predictions of other established methods published in the literature. However, SOSA slightly overestimated reflectance in the visible part of the solar spectrum. The relationships between computed values of Normalized Difference, *LAI* and absorbed radiant energy were nonlinear, the degree of which increased with oblique view zenith angles.

ACKNOWLEDGEMENTS

The authors wish to thank Dr. Ranson and Dr. Beihl for providing the validation data set. Dr. Gerstl provided valuable comments on a preprint of this manuscript. We are also thankful to Dr. Baldocchi for his extensive peer review of this manuscript. Mrs Chapman, Bervoets-Myneni and Miss Sump helped with the preparation of this manuscript.

REFERENCES

Allen, W.A. and Richardson, A.J., 1968. Interaction of light with a plant canopy. J. Opt. Soc. Am., 58: 1023.

Allen, W.A., Gayle, T.V. and Richardson, A.J., 1970. Plant canopy irradiance specified by the Duntley equations. J. Opt. Soc. Am., 60: 372–376.

Asrar, G., Fuchs, M., Kanemasu, E.T. and Hatfield, J.L., 1984. Estimating absorbed photosynthetic radiation and leaf area index from spectral reflectances in wheat. Agron. J., 76: 300–306.

Bunnik, N.J.J., 1978. The multispectral reflectance of shortwave radiation by agricultural crops in relation with their morphological and optical properties. Mededelingen Landbouwhogeschool, Wageningen, The Netherlands.

Chandrasekhar, S., 1950. Radiative Transfer. Dover, New York.

Cooper, K., Smith, J.A. and Pitts, D., 1982. Reflectance of a vegetative canopy using the adding method. Appl. Opt., 21: 4112–4118.

De Wit, C.T., 1965. Photosynthesis of leaf canopies. Agric. Res. Rep. No. 663, Center for Agric. Publ. and Doc., Wageningen, The Netherlands.

Duncan, W.G., Loomis, R.S., Williams, W.A. and Hanau, R., 1967. A model for simulating photosynthesis in plant communities. Hilgardia, 4: 181–205.

Gerstl, S.A.W. and Zardecki, A., 1985a. Discrete-ordinates finite-element method for atmospheric radiative transfer and remote sensing. Appl. Opt., 24: 81–93.

Gerstl, S.A.W. and Zardecki, A., 1985b. Coupled atmosphere/canopy model for remote sensing of plant reflectance features. Appl. Opt., 24: 94–103.

Goel, N.S. and Strebel, D.E., 1983. Inversion of vegetative canopy reflectance models for estimating agronomic variables. I. Problem definition and initial results using the Suits Model. Remote Sens. Environ., 13: 487–507.

Gutschick, V.P. and Weigel, F.W., 1984. Radiation transfer in vegetative canopies and other layered media: rapidly solvable exact integral equation not requiring Fourier resolution. J. Quant. Spectrosc. Radiat. Transfer, 341: 71–82.

Hansen, J.E. and Travis, L.D., 1974. Light scattering in planetary atmospheres. Space Sci. Rev., 16: 527–610.

Hunt, G.E., 1971. A review of the computational techniques for analysing the transfer of radiation through a model cloudy atmosphere. J. Quant. Spectrosc. Radiat. Transfer, 11: 655–690.

Myneni, R.B., Asrar, G. and Kanemasu, E.T., 1986. Theoretical analysis of radiative transfer in a soybean canopy using the method of successive orders of scattering approximations (SOSA). Agric. For. Meteorol., accepted.

Ranson, J. and Beihl, L., 1982. Soybean canopy reflectance modelling data set. Purdue University, LARS, W. Lafayette, IN 47906.

Ross, J., 1981. The Radiation Regime and Architecture of Plant Stands. Dr. W. Junk pub., The Netherlands.

Sobolev, V.V., 1974. Light scattering by planetary atmospheres. Pergamon Press, New York.

Suits, G.H., 1972. The calculation of the directional reflectance of a vegetative canopy. Remote Sens. Environ., 2: 117–125.

Van de Huslt, H.C., 1980. Multiple light scattering. Vols. I & II, Academic Press, London.

Verhoef, W., 1984. Light scattering by leaf layers with application to canopy reflectance modelling: The SAIL model. Remote Sens. Environ., 16: 125–141.

Chapter 3.0

Reflectance of a Soybean Canopy Using the Method of Successive Orders of Scattering Approximations (SOSA)

Agricultural and Forest Meteorology, 40 (1987) 71–87
Elsevier Science Publishers B.V., Amsterdam — Printed in The Netherlands

REFLECTANCE OF A SOYBEAN CANOPY USING THE METHOD OF SUCCESSIVE ORDERS OF SCATTERING APPROXIMATIONS (SOSA)*

R.B. MYNENI, G. ASRAR and E.T. KANEMASU

Evapotranspiration Laboratory, Department of Agronomy, KSU, Manhattan, KS 66506, U.S.A.

(Received June 25, 1986; revision accepted December 11, 1986)

ABSTRACT

Myneni, R.B., Asrar, G. and Kanemasu, E.T., 1987. Reflectance of a soybean canopy using the method of Successive Orders of Scattering Approximations (SOSA). Agric. For. Meteorol., 40: 71–87.

The method of Successive Orders of Scattering Approximations (SOSA) involves the computation of photons scattered once, twice, three times, etc., with the total intensity obtained as the sum over all orders. The source function and the intensities for successive orders can be computed using recursion principles. The predictions of SOSA are in good agreement with the measured canopy reflectance factors and with the predictions of other established formulations published in the literature. The formulation of SOSA is found to be sensitive to detail in leaf angle distribution input. Finally, the profiles of ascending, descending and net normalized radiance are presented to help understand the nature of flux generation and propagation.

INTRODUCTION

The physics of radiative transfer in a medium is best described by the classical electromagnetic wave theory, viz. Maxwell equations (Ishamaru, 1978a and b). If phase information is deemed unimportant, then fates, migrations and interactions of photons in the medium may be considered instead of electromagnetic fields. This results in the theory of radiative transfer that describes the particle nature of the radiation and its transport (Chandrasekhar, 1950).

The desire to compute the radiant energy distribution in vegetative media is primarily two-fold. First, to compute canopy photosynthetic rates (de Wit, 1965; Monteith, 1965; Duncan et al., 1967; Gutschick and Weigel, 1984; amongst others) and canopy reflectance (Suits, 1972). Second, the inversion of these mathematical formulations enables us to estimate canopy phytometric attributes such as leaf area index and/or radiative field characteristics such as

* Contribution 86-274-J from the Agricultural Experiment Station, Kansas State University.

absorbed radiant energy from remote measurements of canopy reflectance (Goel and Strebel, 1983; and Asrar et al., 1984).

The methods used in astrophysics and atmospheric physics have been employed to increase our understanding of radiant energy propagation in vegetative media (Ross, 1981). The quality of computations has greatly increased from the preliminary works of Allen and Richardson (1968) to the present day version of the SAIL model (Verhoef, 1985). It should, however, be noted that the transfer equation of Suits (1972) is entirely heuristic, and as Gutschick and Weigel (1984) pointed out that, for a known degree of isotropy in diffuse flux the implied flux interception is inconsistent, and in non-random canopies it is not possible to enforce energy conservation with the computed photon dispositions. Chen (1984) cast the extended versions of the Kubelka–Munk equations in vector-matrix form, so that the bidirectional canopy reflectance can be computed for canopies with non-horizontal and non-Lambertian leaves. A very powerful Monte Carlo method has been developed by Ross and Marshak (1985), which has a very efficient algorithm for tracing photon fates and is capable of studying anisotropy in scattered fluxes. However, no results have yet been published. Cooper et al. (1982) and Verhoef (1985) used the adding method to solve for canopy reflectance. Gutschick and Weigel (1984) developed a rapidly solvable exact integral equation for radiative flux interception by a scattering element in a layered media, the convergent solution of which can be line integrated to obtain a profile of angle resolved fluxes. Gerstl and Zardecki (1985a and b) used the discrete-ordinates finite-element technique to solve the transport equation in a coupled medium of atmosphere and vegetation.

The method of Successive Orders of Scattering Approximations involves computation of photons scattered once, twice, three times, etc., with the total scattered intensity obtained as the sum over all orders of scattering. It is one of the oldest and simplest methods of approximating a solution to the transport equation (Dave, 1964). The advantages of this method over other methods is discussed elsewhere in this paper, but it suffices here to note that this method offers an intuitive understanding of the process of multiple scattering, which is very desirable because of the complexity of the problem under study.

THEORY

The assumptions are:
(1) The vegetative medium may be idealized as a plane parallel, horizontally homogeneous, and extensive turbid medium of arbitrary finite physical depth, z, continuous along the three physical dimensions. (2) The turbid medium is a radiatively non-participating (i.e. no embedded sources), absorbing and scattering medium. (3) Leaves are the only canopy elements to interact with radiation. (4) The individual leaves or their parts scatter radiation isotropically. (5) Scattering involving quantum transitions is not considered. (6) Processes at different wavelengths are independent. (7) There is a steady state, i.e., independence of time. (8) There is no polarization of light. (9) Radiation is incident from

any direction on top and/or bottom in infinitely wide homogeneous beams, so that the intensity does not depend on x and y coordinates. (10) The density of leaves or their parts is assumed to be a continuous function, $n(z)$. We agree with the arguments of Gutschick and Weigel (1984) regarding over what finite separations leaf sections can be assumed to be randomly distributed and state that the assumption of $n(z)$ as a continuous function to be valid. Without loss of lucidity, the ensuing treatment can be restricted to $n(z) = n' =$ constant, since all distributions scale to the equivalent uniform canopy. Then we may write the familiar relation,

$$F = n' A_L h \tag{1}$$

where A_L is the expectation value of leaf area, h is physical thickness, and F is the accumulated leaf area from the top of the canopy per unit ground area. We consider the propagation equation,

$$\mu \frac{dI(\tau, \Omega)}{d\tau} = I(\tau, \Omega) - \frac{\omega}{4\pi} \int_{4\pi} I(\tau, \Omega')P(\Omega, \Omega')\, d\Omega' - \frac{\omega}{4\pi} P(\Omega, -\Omega_0)\, E_0 \exp(-\tau/\mu_0) \tag{2}$$

where, P = canopy scattering phase function, $\mu = \cos\theta$; θ = polar zenith angle, I = intensity (quantal units $L^{-2}T^{-1}st^{-1}$), Ω = direction (μ, ϕ) = unit vector, $d\Omega$ = solid angle = $\sin\theta\, d\theta\, d\phi$; ϕ = azimuth angle, ω = single scattering albedo (also the scattering coefficient), $\mu_0 E_0$ = incident collimated flux density (quantal units $L^{-2}T^{-1}$) = $\mu_0 \pi I_0$ = unity relative to a horizontal surface (μ_0, ϕ_0), τ = optical depth defined by the relation,

$$\tau = n'G(\Omega') \int_0^z dz' \tag{3}$$

The $G(\Omega')$ function may be defined as (Ross, 1981),

$$G(\Omega') = \int_0^{2\pi} \int_0^1 g_L(\Omega_L) \mid \Omega' \cdot \Omega_L \mid d\mu_L d\phi_L \tag{4}$$

where $g_L(\Omega_L)$ is the leaf normal distribution function that determines the fraction of total leaf area oriented in the canopy, so that the normals to the upper face of the leaves are within a unit solid angle around the direction located by Ω_L, and normalizes to

$$\int_{2\pi} g_L(\Omega_L)\, d\Omega_L = \int_0^{2\pi} \int_0^1 g_L(\Omega_L)\, d\mu_L\, d\phi_L = 1 \tag{5}$$

Note that we define $g_L(\Omega_L)$ as the fraction of total leaf area whose normals fall within a solid angle around the direction Ω_L, hence we do not have the 2π factor as found in the works of Ross (1981). The dot product in eq. 4 may be expanded as,

$$|\Omega' \cdot \Omega_L| = |\mu'\mu_L + (1 - \mu'^2)^{1/2}(1 - \mu_L^2)^{1/2} \cos(\phi' - \phi_L)| \tag{6}$$

As in an earlier analysis (Myneni et al., 1986) the hemisphere containing the leaf normals may be divided into K' equal area sectors along the θ_L coordinate and further into L' sectors along the ϕ_L coordinate. Then eqs. 5 and 4 are reduced to,

$$\int_0^{2\pi}\int_0^1 g_L(\Omega_L)\, d\mu_L\, d\phi_L = \sum_{i=1}^{K'} \int_{(\pi/2K')(i-1)}^{(\pi/2K')i} d\mu_L \sum_{j=1}^{L'} \int_{(2\pi/L')(j-1)}^{(2\pi/L')j} g_L(\Omega_L)\, d\phi_L$$

$$= \sum_{i=1}^{K'} \sum_{j=1}^{L'} g_{L_{ij}} = 1 \tag{7}$$

and

$$G(\Omega') = \sum_{i=1}^{K'} \int_{(\pi/2K')(i-1)}^{(\pi/2K')i} d\mu_L \sum_{j=1}^{L'} \int_{(2\pi/L')(j-1)}^{(2\pi/L')j} g_L(\Omega_L)|\Omega' \cdot \Omega_L|\, d\phi_L \tag{8}$$

where $g_{L_{ij}}$ is the fraction of the total leaf oriented in the solid angle Ω_{Lij} bounded between the boundaries,

$$\left.\begin{aligned} \theta_{Lij} &= \frac{\pi}{2K'}(i-1) \quad \text{to} \quad \frac{\pi}{2K'}i \\ \phi_{Lij} &= \frac{2\pi}{L'}(j-1) \quad \text{to} \quad \frac{2\pi}{L'}j \end{aligned}\right| \tag{9}$$

Finding an exact analytical solution in the most general case to the transfer equation (eq. 2) is no trivial matter and in fact, in only a few specific cases has an analytical solution been found. Hence, various approximations have been developed. The method of Successive Orders of Scattering Approximations (SOSA) is one of the oldest and simplest in concept of all the different solutions to the multiple scattering problem. Various methodologies of SOSA have been developed, but the common denominator is the computation of photons scattered once, twice, three times, etc., with the total scattered intensity obtained as the sum over all orders (Dave, 1964; Irvine, 1965; Hansen and Travis, 1974; amongst others). For cases where a large number of scatterings are possible ($\omega \simeq 1$), it might appear to be tedious to compute each order of scattering, since methods such as the adding and discrete ordinates readily yield the radiant exitant fluxes at the canopy boundaries for sum of all orders. However, there are several reasons why it is valuable to compute each order of scattering. They are:

(a) The concept of this method is very simple. If we know where light originates, we can find where and how it is scattered the first time, then where and how it is scattered the second time, etc. Finally, we can sum all these terms and thus find the total radiation field.

(b) The sum successive orders must converge, for physical reasons, provided the single scattering albedo is $\leqslant 1$. The total energy radiated out cannot surpass the total energy given by the incident light. Furthermore, the scattering processes naturally distribute the radiation smoothly (over depth and direction), so that no local accumulation at any depth (or in any direction) can cause a divergence.

(c) In a Fourier series expansion of the intensity, the high frequency terms arise from photons scattered a small number of times. Thus most of the Fourier terms may be accurately obtained by computing a few orders of scattering.

(d) In the doubling method a significant amount of computing time may be saved by taking an initial optical thickness of ca. 2^{-10} and computing 3 orders of scattering for that layer (Hansen and Travis, 1974).

(e) The results for successive orders provide insight useful for understanding multiple scattering results.

(f) By performing the integrations numerically, this method has the advantage of being applicable to inhomogeneous canopies.

Consider an axially symmetric diffuse input of π units (quantal units $L^{-2}\,T^{-1}$) and 1 unit (similar units) of collimated flux incident on the canopy at the top. The absolute value of the input is irrelevant, since we will normalize all intensities and their plane projections. If the exitant intensity from the vegetative canopy is assumed to consist exclusively of energy derived from single scattering of collimated flux, then the source function is simply,

$$J(\tau, \Omega) = \frac{\omega}{4\pi} P(\Omega, -\Omega_0)\, E_0 \exp(-\tau/\mu_0) \tag{10}$$

For a finite thickness of the vegetative canopy bounded on the two sides (perpendicular to the plane of stratification) at $\tau = 0$ and $\tau = \tau_1$, the ascending and descending directional fluxes are,

$$I(\tau, \Omega) = I(\tau_1, \Omega) \exp(-(\tau_1 - \tau)/\mu) + \frac{\omega}{4\pi} P(\Omega, -\Omega_0)\, E_0 \times \int_{\tau}^{\tau_1} \exp\left[-\left(\frac{(\tau' - \tau)}{\mu} + \frac{\tau'}{\mu_0}\right)\right] \frac{d\tau'}{\mu} \tag{11}$$

$$I(\tau, -\Omega) = I(0, -\Omega) \exp(-\tau/\mu) + \frac{\omega}{4\pi} P(-\Omega, -\Omega_0)\, E_0 \times \int_{0}^{\tau} \exp\left[-\left(\frac{(\tau - \tau')}{\mu} + \frac{\tau'}{\mu_0}\right)\right] \frac{d\tau'}{\mu} \tag{12}$$

Note that the integrated normal components of $I(\tau, -\Omega)$ will be augmented by an incremental contribution due to unimpeded penetration of collimated flux along its direction of propagation. We also have implemented a reflecting boundary at level τ_1, effecting a reversal in the direction of propagation (otherwise, the first term in eq. 11 will be zero!). If, however, as a first assumption, we set the following boundary conditions,

$$
\left.\begin{aligned}
I(0, -\Omega) &= 0 \\
I(\tau_1, \Omega) &= 0
\end{aligned}\right| \quad (13)
$$

then an exact solution may be found for the case of single scattering of collimated flux,

$$
I_1(0, \Omega) = \frac{\omega\mu_0}{4\pi(\mu + \mu_0)} P(\Omega, -\Omega_0)\, E_0 \left[1 - \exp\left[-\tau_1\left(\frac{1}{\mu} + \frac{1}{\mu_0}\right)\right]\right] \quad (14)
$$

$$
I_1(\tau_1, -\Omega) = \frac{\omega\mu_0}{4\pi(\mu - \mu_0)} P(-\Omega, -\Omega_0)\, E_0 \left(\exp\left(-\tau_1/\mu\right) - \exp\left(-\tau_1/\mu_0\right)\right) \quad (15)
$$

and for $\mu = \mu_0$, from l'Hospital's rule we have,

$$
I_1(\tau_1, -\Omega) = \frac{\omega\tau_1}{4\mu_0} P(-\Omega_0', -\Omega_0)\, E_0 \exp\left(-\tau_1/\mu_0\right) \quad (16)
$$

The total intensity at level τ is obtained from the summation over all orders of scattering,

$$
\left.\begin{aligned}
I(\tau, \Omega) &= \sum_{m=1}^{\infty} I_m(\tau, \Omega) \\
I(\tau, -\Omega) &= \sum_{m=1}^{\infty} I_m(\tau, -\Omega)
\end{aligned}\right| \quad (17)
$$

and may be normalized with incident input after angle integration, to yield reflectance and transmittance,

$$
\left.\begin{aligned}
R(0) &= \frac{1}{(\pi + 1)} \int_0^{2\pi}\int_0^1 I(0, \Omega)\, \mu\, d\mu\, d\phi \\
T(\tau_1) &= \frac{1}{(\pi + 1)} \int_0^{2\pi}\int_0^1 I(\tau_1, -\Omega)\, \mu\, d\mu\, d\phi
\end{aligned}\right| \quad (18)
$$

For each higher order of scattering, the source functions and intensities may be evaluated successively by means of recursion principles. The relations may be generalized as,

$$
\left.\begin{aligned}
J_{m+1}(\tau, \Omega) &= \frac{\omega}{4\pi} \int_0^{2\pi}\int_{-1}^{1} P(\Omega, \Omega')\, I_m(\tau, \Omega')\, d\mu'\, d\phi' \\
I_m(\tau, \Omega) &= \int_{\tau}^{\tau_1} J_m(\tau', \Omega) \exp\left[-(\tau' - \tau)/\mu\right] \frac{d\tau'}{\mu} \\
I_m(\tau, -\Omega) &= \int_0^{\tau} J_m(\tau', -\Omega) \exp\left[-(\tau - \tau')/\mu\right] \frac{d\tau'}{\mu}
\end{aligned}\right| \quad (19)
$$

where $m > 1$. Some changes are in order when we implement this solution to evaluate multiple scattering in vegetative media. Since, diffuse flux is also an input (and does not arise only after first order of scattering as in the case of an atmosphere), the descending intensities are augmented by flux contributions due to penetration of input fluxes through gaps in the canopy.

Initially, we choose a finite number of discrete directions (Gaussian quadrature points) for which we approximate the solution of the transport equation. The vegetative canopy's phytometric characteristics, i.e. the leaf angle distribution and leaf spatial disposition (here assumed to be random), are utilized for computing the G function. The canopy is discretized into thin slabs or layers. Assuming that the first order of scattering is due to scattering of collimated flux, eqs. 11 and 12 may be used to evaluate the directional fluxes at all depths of interest. At this stage we also compute the uncollided flux density of collimated and diffuse flux at all layers. The uncollided flux at the soil surface is used to compute the upward fluxes in all directions of interest. Now, a back-sweep may be effected through the canopy. In order to approximate the integral in eq. 19, it is necessary to compute the source function and the intensities at several depths in order to approach the integral values. All computations in this procedure are done using an 8 point Gaussian quadrature. After evaluating each order of scattering, the ratio of successive terms may be tested to see if it approaches a constant value or if a preset tolerance level is achieved or not.

VALIDATION DATA SET

Plant canopy phytometric, leaf optical properties and canopy multispectral reflectance were measured on a soybean crop with a green leaf area index of 2.87 ± 0.44. This data set was collected at the Laboratory for Applications of Remote Sensing (LARS) and is described in detail by Ranson et al. (1982). The leaf optical properties were revised later and the data set was reported by Ranson and Beihl (1982). Briefly, the data set included leaf angle distribution (LAD) for 0.1 m horizontal layers in 10° class intervals (0–90°) for the entire canopy depth, leaf reflectance and transmittance for 0.45 to 1.125 μm in 0.025 μm intervals, measured with a DK-2 spectrophotometer, and soil and plant canopy spectral reflectance factors for a wide range of solar zenith (30–60°) and azimuth angles, at several view angles. They also reported leaf reflectance and transmittance in the four Exotech Model 100 radiometer bands, which were computed values based on the responsivity of the radiometer and the barium sulphate reference panel used in the field. The canopy spectral reflectance measurements were made through the day (28th August, 1980) in the four MSS bands with the radiometer mounted on a boom at a height of 10 m above the ground. The measured reflectance values were given in the form of a spectral reflectance factor, $R_c(\lambda)$,

$$R_c(\lambda) = I_\lambda(\Omega_v)/I'_\lambda(\Omega_v) \tag{20}$$

where Ω_v is the view direction, I_λ is the radiance reflected by the canopy, I'_λ is the radiance reflected from a perfect Lambertian diffuser under similar illumination conditions, and λ is the wavelength (or band) of measurement.

VALIDATION OF SOSA

The leaf albedos of single scattering in the spectral range 0.45 to 1 μm, measured with the DK-2 spectrophotometer (Ranson and Beihl, 1982), were used in the formulation of SOSA to compute the exitant radiances at each discrete value of μ. In order to compute the radiance reflected by a perfect Lambertian diffuser, the canopy cross sections (extinction and scattering) were set to zero and the soil boundary was treated as a perfect Lambertian diffuser with a conservative albedo of single scattering. The spectral reflectance factors were calculated according to eq. 20. The spectral reflectance factors (in %), computed by the method of SOSA for a nadir view direction and for a solar zenith angle of 35°, are plotted in Fig. 1. Cooper et al. (1982) computed the spectral reflectance factors of the same soybean canopy using the Adding Method (AM) and the Suits (1972) Model (SM). The results of Cooper et al. (1982) along with the measured values of Ranson and Beihl (1982) are also plotted in Fig. 1. The predictions of SOSA agree very well with the measured

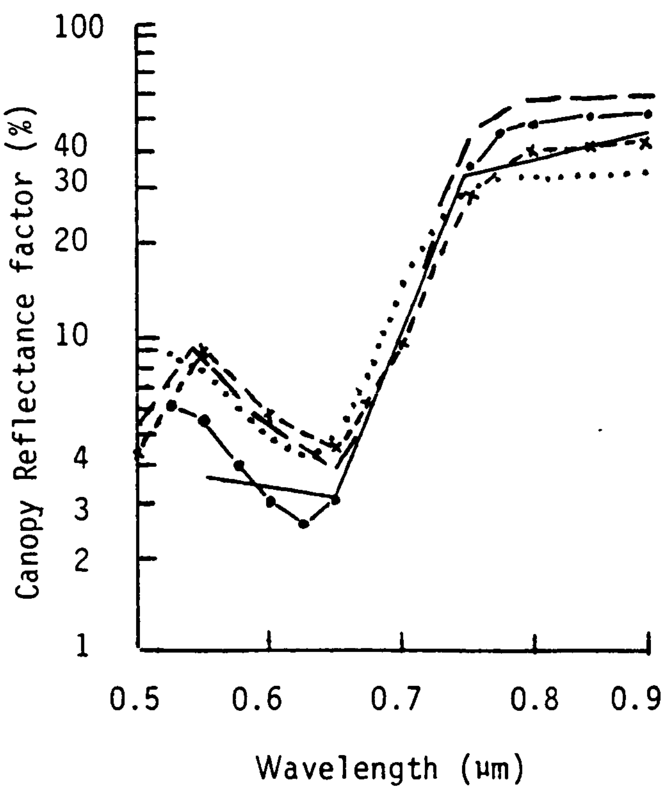

Fig. 1. Soybean canopy reflectance factors with wavelength for a nadir view direction and for a solar zenith angle of 35°. The results of the adding method and the Suits model are from Cooper et al. (1982). --- SOSA sensitivity analysis ; —— measured data; ···· adding method; -·-·- Suits model; ×---× SOSA.

values of Ranson and Beihl (1982) in the near infrared region of the spectrum (0.7 to 0.9 μm). The numerical correspondence between the predictions of SOSA and the measured values is better than the predictions of AM or SM, which over and underestimated the measured values, respectively. In the visible part of the solar spectrum, (0.55 to 0.70 μm), the predictions of SOSA were slight overestimates. However, the absolute values of the reflectance factors in these wavelengths is very small, ca. 2.5 to 6%. More discussion at this juncture is appropriate.

It should be noted that the measured values reported by Ranson and Beihl (1982) are for wavelength bands 0.50 to 0.60 μm and 0.60 to 0.70 μm. There are two ways of computing a comparable reflectance factor using the method of SOSA, or any other method. First, the single scattering albedos of the leaves at several wavelengths in the wavelength band interval may be used to compute spectral reflectance factors and these values may be averaged. Second, the single scattering albedos of the leaves may be converted to a single value, by considering the responsivity of the measuring instrument, and then computing the spectral reflectance factor for the whole band. The spectral reflectance factors (in %) computed using these two methods are given in Table I, along with the measured values for the two above-mentioned wavelength bands. The agreement between the predictions and the measurements is better than that seen in Fig. 1. It may also be noted that higher order scattering is not negligible in some wavelengths (0.55 and 0.70 μm) as is conventionally assumed.

Gerstl and Zardecki (1985b) solved the radiative transfer equation by the discrete-ordinate finite-element method in a coupled system of atmosphere and plant canopy. They reported computed spectral reflectance factors for the same soybean canopy, but based on an earlier version of the data set, (Ranson et al., 1982). They reported spectral reflectance factors for a canopy under a clear

TABLE I

Comparison of predicted canopy reflectance factors with measured values of Ranson and Beihl (1982) in the visible part of the solar spectrum. The reflectance values are for a nadir view angle and for a solar zenith angle of 35°

Wave-length (μm)	Single scattering albedo (%)	Reflectance factors for successive orders of scattering (R_{cn}) 1	2	3	4	5	6	Final R_c	Measured value
0.50	7.50	2.77	4.29	4.33	4.33	4.33	4.33		
0.55	25.10	4.20	9.42	9.81	9.84	9.84	9.84	6.73	
0.60	13.10	3.22	5.90	6.01	6.02	6.02	6.02		3.0–6.0
Exotech band 1	18.10	3.63	7.36	7.56	7.57	7.58	7.58	7.58	
0.60	13.10	3.22	5.90	6.01	6.02	6.02	6.02		
0.65	9.20	2.91	4.78	4.83	4.83	4.83	4.83	7.10	
0.70	26.90	4.35	9.95	10.40	10.44	10.45	10.45		2.5–5.0
Exotech band 2	13.70	3.27	6.08	6.19	6.19	6.19	6.19	6.19	

rural atmosphere with an aerosol optical depth of 0.1 at 0.55 μm, (their Fig. 3). The predictions of Gerstl and Zardecki (1985b), here abbreviated to GZ, and those returned by SOSA are plotted in Fig. 2, for a view zenith angle of 15°, solar zenith angle of 34°, and for a difference in view and solar azimuth angles of 10°. In the visible part of the solar spectrum, the predictions of SOSA were overestimates, relative to the measured values. However, in the near infrared region, the predictions of GZ and SOSA were over and underestimates, respectively. This discrepancy is mainly due to anisotropy in the scattered radiation. Note that the measured values plotted in Fig. 2 are a subset of the measured spectral reflectance factors satisfying the specified difference in azimuthal coordinate between the solar and view directions. Additional computations for various other solar and view directions did show convergence between the predictions of SOSA and of GZ (S.A.W. Gerstl, 1985, personal communication).

In fact, anisotropic scattering is so strong in the reflected radiation, that more information is contained in off-nadir view directions than the nadir view direction. The two phenomena of interest are the hot spot (the Heiligenschein) (Simmer and Gerstl, 1985) and the specular spot (Myneni et al., 1987). Preli-

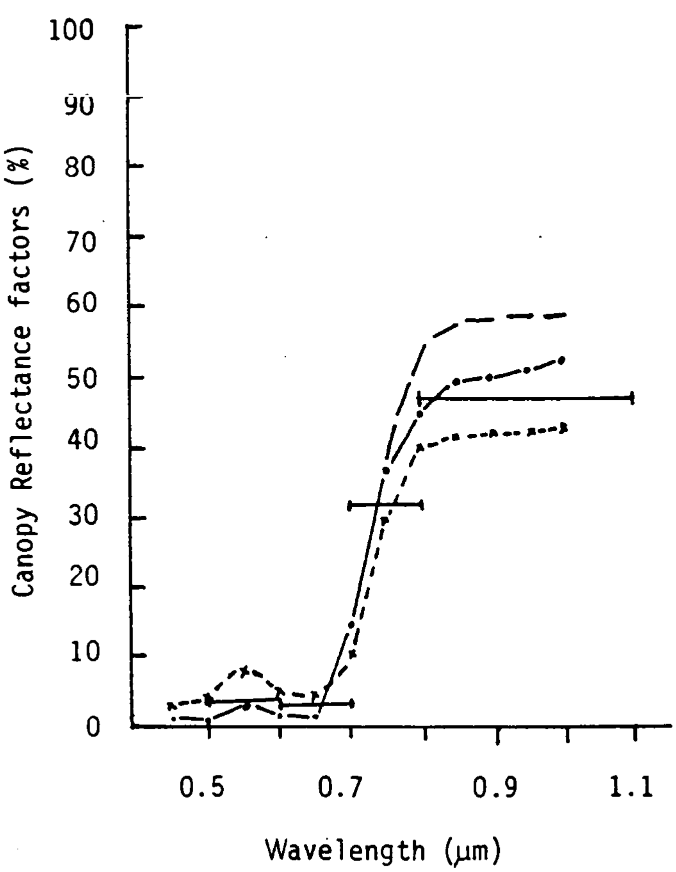

Fig. 2. Soybean canopy reflectance factors with wavelength. The results of the discrete-ordinate finite-element method are of Gerstl and Zardecki (1985). -·-·- Discrete-ordinate finite-element method; ×-×-× SOSA; --- SOSA sensitivity analysis; ├─┤ measured data (θ_s = 34°; θ_v = 15°; $\phi_v - \phi_s$ = 10°).

minary measurements on wheat crop show that when the canopy is viewed at the solar zenith angle in the principal plane, the backscattered radiances (the hot spot) are four times greater than the forward scattered radiances! Most off-nadir measurements in literature have been made in broad angular intervals and hence these peaks are missed. Credit is, however, due to the Estonian workers, who have experimentally documented the existence of the hot spot and the specular spots and have theoretically explained the physics of such peaks (Kuusk et al., 1985; Nilson and Kuusk, 1985). Mal'tseva (1985) presented formulas for determining the centers and isolines of solar glitter and shadowless regions on scanner images produced by ERS satellites. In fact none of the existing formulations in the West correctly model the angular scattering behaviour of the canopies. As Vanderbilt et al. (1985) stated that without accounting for leaf anisotropic behaviour and the specular flux, if a model correctly predicts the angular distribution of scattered radiation, then the model itself is wrong, since they do not model the actual cause-effect relationship. Hence, the future of both theoretical and experimental canopy spectroscopy lies in understanding the angular signatures of the crops, and retrieving the information therein.

SENSITIVITY OF SOSA TO LEAF ANGLE DISTRIBUTION

The results presented in the validation section were obtained by inputing SOSA with layer specific LAD for each of the 10 different layers, that supposedly were to comprise the soybean canopy. The number 10 was, however, quite arbitrary. We chose 10 because information on LAD for these 10 layers was available (Ranson and Beihl, 1982). We summed the leaf areas in all 10 layers for each of the nine leaf angle classes to derive a generalized LAD for the whole canopy. Thus by making LAD invariant with depth, we hoped to find the effect that this generalization might have on the reflectance factors. The reflectance factors are also plotted in Figs. 1 and 2. It is apparent that the predictions of SOSA are overestimates at all wavelengths under study and the spectral reflectance factors in the near infrared region are ca. 60%. This loss of detail in LAD input is manifested as decreased permeability of the vegetation canopy for radiative flux propagation. The downward scattered flux densities normalized to the incident input, for various wavelengths are plotted in Figs. 3 and 4, for a generalized LAD and layer specific LAD, respectively. It is obvious that the canopy constructed for a generalized LAD is less conducive for radiative flux propagation than when layer specific LAD is used. This effect can also be read when we compare the absolute values of flux densities in the two cases at any specific depth. The reason for this rapid extinction of flux is the expanded extinction cross section values (*G*-function). A similar analysis for the ascending flux densities yields similar conclusions (Figs. 5 and 6). These profiles illustrate that by using a generalized LAD for this soybean canopy, the energy distribution in the canopy and the exitant radiances are not comparable to the measured values.

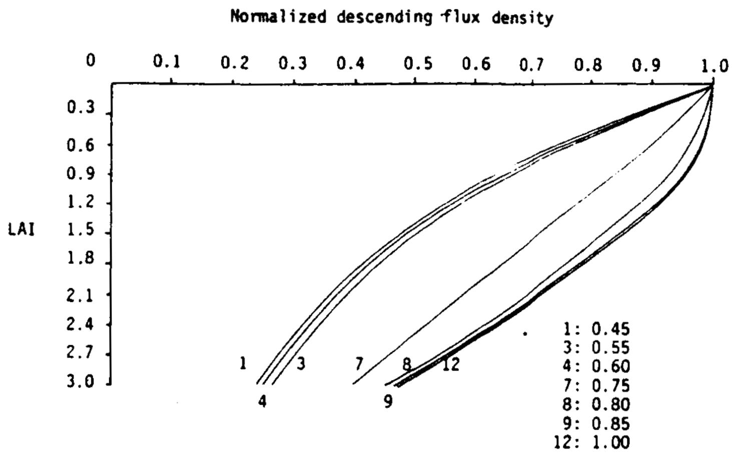

Fig. 3. Profile of normalized descending flux density at different wavelengths in the soybean canopy constructed from a generalized leaf angle distribution.

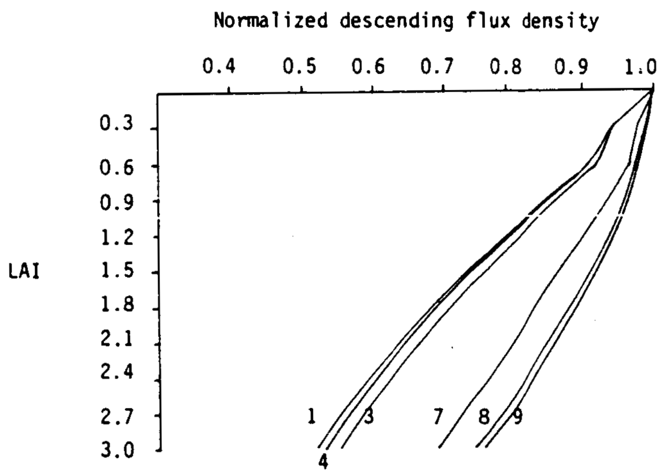

Fig. 4. Profile of normalized descending flux density at different wavelengths in the soybean canopy constructed from a layer specific leaf angle distribution.

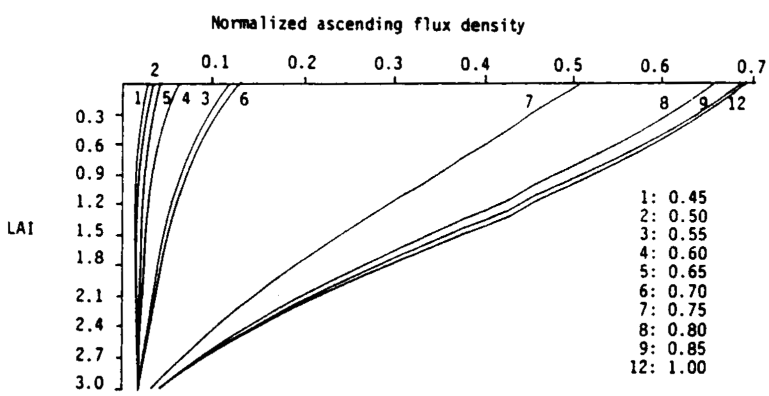

Fig. 5. Profile of normalized ascending flux density at different wavelengths in the soybean canopy constructed from a generalized leaf angle distribution.

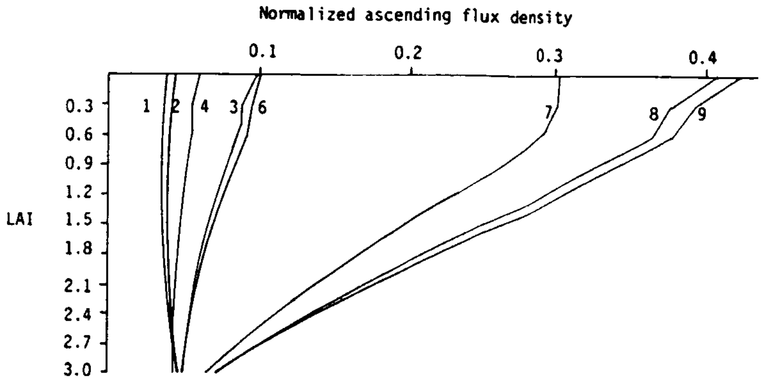

Fig. 6. Profile of normalized ascending flux density at different wavelengths in the soybean canopy constructed from a layer specific leaf angle distribution.

FLUX PROFILES AND LEAF AREA INDEX

The radiant exitant fluxes (either directional or angle integrated) usually measured in the field are the boundary values of a continuous flux profile in the vegetation canopy. The flux profile inside the canopy is of interest, since it enables us to understand how the boundary values are attained and how the flux is generated and propagated. In addition, the flux at any depth in the canopy projected onto the leaf surfaces can be used to estimate photosynthesis.

In general by varying some characteristic of the canopy (here the LAI), the resulting flux profile helps us to understand how that particular attribute of the canopy affects the profile. The descending and ascending flux densities are plotted with canopy depth (in multiples of LAI) in Figs. 7 and 8, respectively, for four soybean canopies with LAI of 0.5, 1, 2, and 3. The LAD is layer specific and the profiles are for Exotech Model 100 band 2. All fluxes are normalized to the incident input flux density. The descending flux density is found to decrease with increase in the depth of the canopy. The rate of attenuation is higher for large values of canopy LAI, resulting in steeper profiles. This is not surprising, since in general, the higher the LAI, the greater is the value of the projected

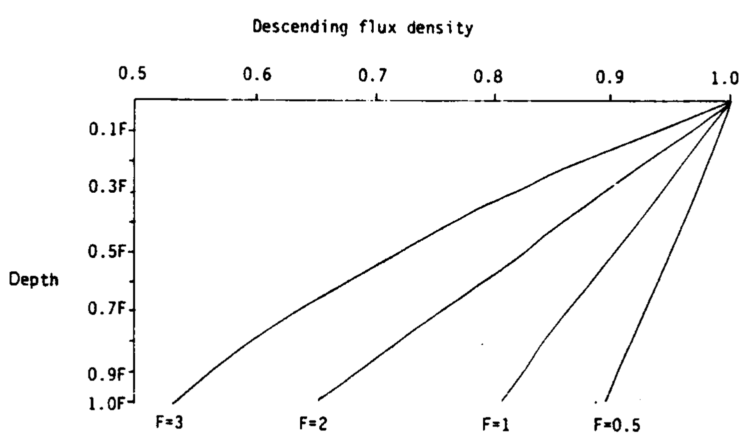

Fig. 7. Profile of normalized descending flux densities in soybean canopies with different leaf area indices.

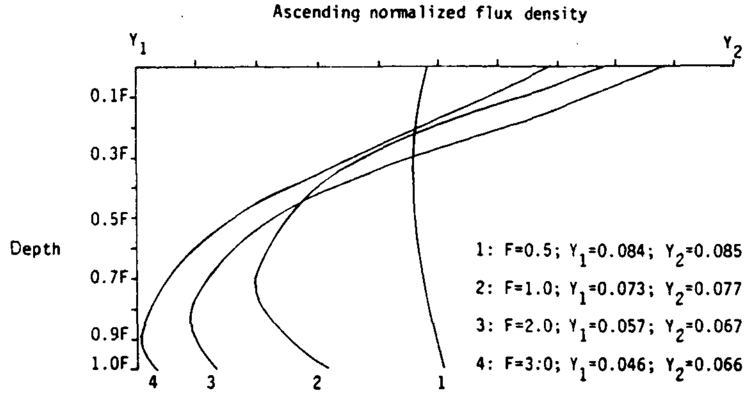

Fig. 8. Profile of normalized ascending flux densities in soybean canopies with different leaf area indices.

leaf area onto the beams, (except, of course, for very large values of LAI). The profile of ascending flux density is, however, remarkably different. At low LAI (0.5), the profile is slightly concave. In the lower part of the canopy, the flux is more attenuated than strengthened by contributions due to multiple scattering. However, in the upper parts of the canopy, the flux is more strengthened than attenuated. This behavior is also apparent from the integral equation describing the propagation of the ascending flux. In general, by moving the reference surface upwards in the canopy, we decrease the projected leaf area to a given direction. This behavior is more pronounced at higher values of LAI, and the point at which the flux strengthening by multiple scattering exceeds flux weakening by extinction shifts deep into the canopy. The value of the ascending flux density at the top of the canopy and the value of the descending flux density at the bottom are, respectively, the hemispherical reflectance and transmittance.

The net normalized radiance (NNR) is plotted in Fig. 9 with depth in the canopy for canopy LAI values of 1 and 3, two view zenith angles (2.5° and 82.5°),

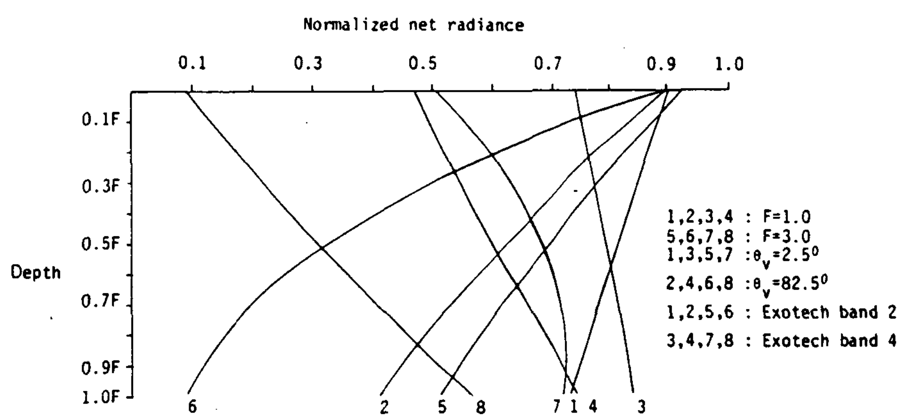

Fig. 9. Profile of normalized net radiance in two soybean canopies (LAI = 1 and 3), in two Exotech Model 100 wavelength bands (2 and 4), and at two view zenith angles (2.5° and 82.5°).

for the Exotech wavelength bands 2 and 4. The NNR decreased with increasing depth in band 2 (curves 1,5,2,6). The rate of fall of NNR, however, is dependent on canopy LAI and view zenith angle. Higher values of LAI and oblique view zenith angles resulted in faster attenuation rates. In this wavelength band, multiple scattering is negligible, and hence, the profiles of NNR are more or less dictated by the profile of descending input fluxes. The profiles for wavelength band 4, however, are very different. In the near infrared, NNR increased with increasing depth in the canopy (curves 3,7,4,8). The rate of this increase is dependent on canopy LAI and view zenith angle. This increase of NNR with depth is grounded in two facts. First, leaf scattering in the near infrared is substantial and second, the rate of extinction of ascending flux with increasing depth is much higher than the rate of extinction of descending flux; the net result being an increased NNR with depth in the canopy. At any view zenith angle and wavelength, the actual values of NNR were higher for a canopy with lower LAI, due to the increased permeability of the sparse canopy, since the incident input was similar in both cases.

CONCLUSIONS

The method of Successive Orders of Scattering Approximations (SOSA) involves computation of photons scattered once, twice, three times, etc., with the total intensity obtained as the sum over all orders. This method was used to compute soybean canopy reflectance factors. Canopy reflectance factors predicted by SOSA were in good agreement with the measured values and with the predictions of other established formulations published in the literature. However, SOSA slightly overestimated canopy reflectance factors in the visible region of the solar spectrum. Some possible reasons were discussed. Sensitivity analysis of SOSA revealed that the formulation is highly sensitive to detail in leaf angle distribution input. The profile of ascending and descending fluxes showed how these fluxes are generated and propagated through the canopy. Finally, the profile of net normalized radiance inside the canopy was found to be dependent on canopy leaf area index and view zenith angle for a given wavelength.

ACKNOWLEDGEMENTS

The authors thank Dr. Ranson and Dr. Beihl for kindly providing the validation data set. Dr. Gerstl and Dr. Simmer provided additional computations of their formulation and a copy of their original figure. We are indebted to Dr. Gerstl for his valuable comments on a preprint of this work. One of the authors (RBM) is grateful to Dr. Travis for a very helpful discussion on the method of SOSA and its hybrid relatives. We also thank Dr. Baldocchi and two anonymous reviewers for their comments and review. Mrs. P. Chapman, Miss G. Sump and Mrs. A. Bervoets helped with the preparation of the manuscript.

REFERENCES

Allen, W.A. and Richardson, A.J., 1968. Interaction of light with a plant canopy. J. Opt. Soc. Am., 58: 1023–1209.

Asrar, G., Fuchs, M., Kanemasu, E.T. and Hatfield, J.L., 1984. Estimating absorbed photosynthetic radiation and leaf area index from spectral reflectance in wheat. Agron. J., 76: 300–306.

Chandrasekhar, S., 1950. Radiative Transfer. Dover, New York.

Chen, J., 1984. Kubelka–Munk equations in vector-matrix form and the solution for bidirectional vegetative canopy reflectance. Appl. Opt., 24: 376–382.

Cooper, K., Smith, J.A. and Pitts, D., 1982. Reflectance of a vegetative canopy using the adding method. Appl. Opt., 21: 4112–4118.

Dave, J.V., 1964. Meaning of successive iteration of the auxilliary equation in the theory of radiative transfer. Astrophys. J., 140: 181–205.

De Wit, C.T., 1965. Photosynthesis of leaf canopy canopies. Agric. Res. Rep. No. 663, Pudoc, Wageningen, The Netherlands.

Duncan, W.G., Loomis, R.S., Williams, W.A. and Hanau, R., 1967. A model for simulating photosynthesis in plant communities. Hilgardia, 4: 181–205.

Gerstl, S.A.W. and Zardecki, A., 1985a. Discrete-ordinates finite-element method for atmospheric radiative transfer and remote sensing. Appl. Opt., 24: 81–93.

Gerstl, S.A.W. and Zardecki, A., 1985b. Coupled atmospheric/canopy model for remote sensing of plant reflectance features. Appl. Opt., 24: 94–103.

Goel, N.S. and Strebel, D.E., 1983. Inversion of vegetation canopy reflectance models for estimating agronomic variables. I. Problem definition and initial results using the Suits model. Remote Sens. Environ., 13: 487–507.

Gutschick, V.P. and Weigel, F.W., 1984. Radiation transfer in vegetative canopies and other layered media: rapidly solvable exact integral equation not requiring Fourier resolution. J. Quant. Spectrosc. Radiat. Transfer, 31: 71–82.

Hansen, J.E. and Travis, L.D., 1974. Light scattering in planetary atmospheres. Space Sci. Rev., 16: 527–610.

Irvine, W.M., 1965. Multiple scattering by large particles. Astrophy. J., 142: 1563–1575.

Ishamaru, A., 1978a. Wave Propagation and Scattering in Random Media. Vol. I. Single scattering and transport theory. Academic Press, New York.

Ishamaru, A., 1978b. Wave Propagation and Scattering in Random Media. Vol. II. Multiple scattering, turbulence, rough surfaces and remote sensing. Academic Press, New York.

Kuusk, A., Anton, J., Nilson, T., Peterson, U., Ross, K., Ross, J. and Savikhin, A., 1985. Reflection indicatrices of vegetation covers. Sov. J. Remote Sens., 4(5): 802–813 (a cover to cover translation).

Mal'tseva, I.G., 1985. Determination of specular spot and hot spot regions in scanner survey from space and optimization of illumination conditions. Sov. J. Remote Sens., 4(2): 327–342. (a cover to cover translation).

Monteith, J.L., 1965. Light distribution and photosynthesis in field crops. Ann. Bot., 17–37.

Myneni, R.B., Burnett, R.B., Asrar, G. and Kanemasu, E.T., 1986. Single scattering of parallel direct and axially symmetric diffuse solar radiation in vegetative canopies. Remote Sens. Environ., 20: 165–182.

Myneni, R.B., Asrar, G., Burnett, R.B. and Kanemasu, E.T., 1987. Radiative transfer in an anisotropically scattering vegetative medium. Agric. For. Meteorol., in press.

Nilson, T. and Kuusk, A., 1985. Approximate analytic relationships for the reflectance of agricultural vegetation canopies. Sov. J. Remote Sens., 4(5): 814–826 (a cover to cover translation).

Ranson, J., and Beihl, L.L., 1982. Soybean canopy reflectance modelling data set. LARS, Purdue Univ., W. Lafayette, IN.

Ranson, J., Vanderbilt, V.C., Beihl, L.L., Robinson, B.F. and Bauer, M.E., 1982. Soybean canopy reflectance as a function of view and illumination geometry. AgRISTARS Tech. Rep. SR-P2-04278 (NAS9-15466).

Ross, J., 1981. The Radiation Regime and Architecture of Plant Stands. W. Junk, The Netherlands.
Ross, J. and Marshak, A., 1985. A Monte Carlo procedure for calculating the scattering of solar radiation by plant canopies. Sov. J. Remote Sens., 4(5): 783–801 (a cover to cover translation).
Simmer, C. and Gerstl, S.A.W., 1985. Remote sensing of angular characteristics of canopy reflectance. IEEE Trans. Geosci. Remote Sens., 23: 648–675.
Suits, G.H., 1972. The calculation of the directional reflectance of a vegetative canopy. Remote Sens. Environ., 2: 117–125.
Vanderbilt, V.C., Grant, L., Beihl, L.L. and Robinson, B.F., 1985. Specular, diffuse, and polarized light scattered by two wheat canopies. Appl. Opt., 24: 2408–2418.
Verhoef, W., 1985. Earth observation modelling based on layer scattering matrices. Remote Sens. Environ., 17: 165–174.

Chapter 4.0

C-Band Scatterometer Measurements of a Tallgrass Prairie

ABSTRACT

C-band scatterometer measurements were made of a tallgrass prairie in an attempt to determine the degree of correlation between (1) the backscattering coefficient and different expressions of soil moisture and (2) the backscattering coefficient and various canopy parameters. The findings of this study support those made in previous studies in terms of the optimum polarization and view angle selection for soil moisture work. There were two findings which were unexpected. The first was a moderately strong correlation and partial correlation between $\sigma°$ and leaf water potential, which indicates some capability of C-band measurements in detecting extremes in the water status of prairie vegetation under shallow soil conditions. The second was the finding that site differences (primarily differences in vegetation) due to burn treatments appeared to be sufficient to cause significant differences in the sensitivity of $\sigma°$ to soil moisture. The site differnces could not be removed by any known expression of soil moisture. These two findings were unexpected since previous radar studies had reported minimal vegetation effects when using a frequency and view angles such as those in this study.

INTRODUCTION

Over the last several years there has been a considerable amount of research dedicated to radar remote sensing in which bare soils [1-7] and traditional agricultural crops [8-15] have served as targets. Grasslands, with only a few exceptions [16, 17], have not received the attention of these other targets. In view of the global importance of grassland areas, this lack of attention is unfortunate.

Grasslands occupy approximately 17% of the earth's land surface [18] and 28% of the United States [19]. Located in remote regions and often covering huge expanses, these areas are better suited to monitoring by remote sensing methods than to more costly and time consuming traditional methods of condition assessment.

The original range of native grasslands in North America has been greatly reduced by farming's need for flat or gently sloping lands with deep, rich soils. As a result, much of the remaining grasslands have been relegated to marginal lands with thin soils, rough topography, and low rainfall. These areas, lacking the water storage capacity of deep soils, are particularly sensitive to periods of low or no rainfall.

Often found in the semi-arid regions of the world, grasslands are occasionally subject to severe drought conditions. In some cases, the detection of dry conditions in a grassland might prove useful in pinpointing potential grassfire areas or better forage areas. In the extreme case, the timely detection of the onset of drought conditions might help reduce the catastrophic consequences which accompany major droughts by providing disaster-relief agencies with more time to prepare.

The following is a discussion of the findings of three summers of C-band, field scatterometer measurements of a tallgrass prairie. It can be viewed as a step in furthering our understanding of what the C-band backscattering coefficient tells us about the various canopy elements and soil parameters of a grassland area.

The objectives of this study were to (1) determine the degree of correlation between soil moisture and the backscattering coefficient and (2) determine the degree of correlation between various grass canopy parameters and the backscattering coefficient for a tallgrass prairie.

MATERIALS AND METHODS

Location and Site Description

This study was conducted during the summers of 1984, 1985 and 1986 on the Konza Prairie Research Natural Area (KPRNA) located near Manhattan, Kansas (39°9'N, 96°40'W). The KPRNA is a 3487 ha tallgrass prairie preserve with a mixed species composition and a silty clay loam (Udic ustoll) as the predominant soil type. In a detailed vegetation study of the KPRNA, approximately 39 species of grass have been identified with big bluestem (*Andropogon gerardi* Vitman), little bluestem (*A. scoparius* Michx.), and Indian grass (*Sorghastrum nutans* (L.) Nash) being the three dominant species [20]. The varied spatial distribution of so many species creates a complex canopy unlike any found in traditional monoculture crops.

The different sites for each year consisted of a burned and an unburned treatment making a total of six treatments (three different sites with two treatments per site) on which microwave, plant parameter and soil measurements were made. Burned and unburned treatments were chosen to provide two different grass canopies. Burning is a common, range management practice used to remove the previous seasons' senescent vegetation. The senescent vegetation lies as a thick mat on the ground reducing the availability of photosynthetically active radiation (PAR) to the new season's growth. Burning during the spring removes this 'litter layer', thus allowing the young vegetation to take full advantage of the PAR during a time when rainfall is usually abundant.

Radar Measurements

The radar used in this study was a C-band scatterometer with a 4.75 GHz center frequency (6.3 cm wavelength) and a 3.4°, 3 dB beamwidth. The sensor was one of three units built by the University of Kansas Remote Sensing Laboratory and is called the microwave scatterometer C-band (MS-C). A boom truck served as a mobile platform for the MS-C providing a minimum slant range of 9 m from the target and a means of extending the scatterometer over the target. Instrument control and data acquisition were accomplished with a Hewlett-Packard HP-41CV handheld computer while an HP digital cassette drive and a thermal printer were used for data storage and inspection, respectively.

Scatterometer measurements were expressed in terms of the backscattering coefficient (σ°) and are reported in units of decibels (dB). Measurements were made using three transmit-receive polarization combinations and three view angles. The nine polarization-view angle combinations used in this study and their measurement labels are listed in Table 1.

When triggered, the HP-41CV collected 30 backscatter measurements from the MS-C over a 30 second time interval. The 30 raw data values, their mean and other information (e.g., slant range, view angle, polarization) were then stored on the digital cassette tape. A summary of the data (e.g., angle of incidence, polarization, mean σ°) was then printed out on the thermal printer. Spatial averaging of the σ° measurement was achieved by driving the truck alongside each of the sites during the 30 second, data collection period.

Soil Measurements

Eight soil samples (0 to 6 cm depth) were taken from within each site concurrently with each set of scatterometer measurements. From the wet and dry weight of these samples, the gravimetric soil water content was determined. Soil bulk densities (0 to 6 cm depth) were determined from eight undisturbed cores taken from each site near the end of the measurement season. Soil properties for each site are listed in Table 2.

The moisture release characteristics of each treatment's soil was determined in the laboratory with a gas pressure, moisture extraction technique using ceramic plates and cellulose acetate membranes [21]. The moisture content of each soil was determined for -32.5, -43.2, -100, -500, -1000 and -1500 KPa soil water potentials (note: -1 bar = -100 KPa). Expressing the soil water potential as a logarithm required the use of the absolute value of the soil water potential rather than the customary negative value. From these data, the logarithmic relationship between soil water potential and volumetric soil moisture can be determined for each soil. This allowed an estimate of the soil water potential given the volumetric moisture content. Figure 1 illustrates the relationship between the soil water potential and volumetric soil moisture (i.e., the moisture release curve) for each soil.

All expressions of soil moisture were derived from one or more of the following: 1) the wet and dry weights of the soil samples, 2) the bulk densities and/or 3) the moisture release curves. The soil moisture expressions tested in this study are listed below.

1) Gravimetric soil moisture, (symbol: m_g), (units: %, g/g or kg/kg)

2) Volumetric soil moisture, (symbol: m_v), (units: %, cm^3/cm^3 or m^3/m^3)

3) Logarithm of soil water potential, (units: none)

4) Percentage of m_v at -32.5 KPa, (similar to the 'percentage of field capacity' used in previous studies), (units: %)

5) Percentage of m_v at -1500 KPa, (similar to the 'percentage of field capacity' used in previous studies), (units: %)

6) Percentage of m_v between -32.5 and -1500 KPa, (often referred to as the percentage of available water), (units: %)

Vegetation Measurements

Agronomic measurements consisted of the wet and dry weights of the green vegetation, the dry weights of the senescent vegetation and green leaf area index (LAI) measurements. A total of nine samples were taken once a week during the microwave measurement period from each site using a 0.1 m^2 frame. From these measurements, the percent moisture content was determined for the green vegetation on both a wet weight and dry weight basis. Canopy height measurements were made once per week in 1985 and 1986 for the green grass and for the litter layer. This measurement allowed the calculation of the moisture content of the vegetation normalized for canopy height [14]. Since agronomic measurements were not always made on the same day as radar measurements, a cubic spline smoothing procedure [22] was used to provide estimates of the vegetation parameters between measurement days. The summary statistics of the agronomic parameters are listed in Table 3.

As part of another experiment, leaf water potential measurements were made (using the pressure bomb method) on these sites during the last two years [23], some of which coincided with our radar measurements. Only seven of these measurements in 1985 and five in 1986 coincided with the radar measurements. This necessitated the combination of the data sets from these two years to determine their correlation with σ°.

RESULTS AND DISCUSSION

Correlations Between $\sigma°$ and Vegetation Parameters

Tables 4 through 9 show the correlation between the vegetation parameters and the backscattering coefficient. These data suggest that the plant parameters are poorly to moderately correlated with $\sigma°$. Not only were the correlations weak, they were inconsistent between years (e.g., positive one year and negative the next).

Both the target and the sensor may have contributed to the weak correlations between $\sigma°$ and the vegetation parameters. The sensor was configured (i.e., 4.75 GHz frequency) to optimize soil moisture sensitivity in part by minimizing sensitivity to vegetation [11, 13]. At this frequency, the thin, narrow leaves and stalks of the grass canopy would be considered 'small' relative to the 6.3 cm wavelength of the microwave radiation. In addition to the canopy elements being small in comparison with the wavelength, the vegetation was relatively sparse. When compared to the corn, milo, soybeans and other crops used in previous studies [11-15], the grass canopies' height, biomass and LAI (Table 3) would appear low, making it likely that a grass canopy is a less attenuating medium than the canopies of these other crops.

Correlations and Partial Correlations Between $\sigma°$ and Leaf Water Potential

Of the five vegetation parameters tested for their correlation with $\sigma°$, leaf water potential appeared to be the strongest.

The correlation coefficients for σ° versus leaf water potential are listed in Table 10. The correlations were particularly high for VV45 on both the burned and unburned treatments.

A partial correlation analysis was performed in an attempt to determine the degree of correlation between σ° and leaf water potential while holding volumetric soil moisture constant. The limitation of this analysis is that the soils were thin (approximately 10 to 30 cm in depth) which resulted in a high degree of dependence of the leaf water potential on the near surface soil moisture. This dependence is particularly strong over the range of soil moisture for which this analysis was run (i.e., 0.07 to 0.28 m^3/m^3 for the burned sites and 0.08 to 0.26 m^3/m^3 for the unburned sites). Over these ranges, small changes in m_v result in large changes in the soil water potential (see Fig. 1) which in turn cause changes in the leaf water potential. On a deeper soil, a plant's access to soil moisture at greater depths would reduce the dependency of leaf water potential on the near surface soil moisture. Under these conditions, the relationship between σ° and leaf water potential might not be as strong as that in the shallow soil case.

Table 10 lists the partial correlation coefficients for the leaf water potential versus σ° at all polarization-view angle combinations given volumetric soil moisture. As expected, the coefficient values decreased for the partial correlation, but the correlation remained high enough for VV45 on both the burned and unburned treatments to suggest that σ° was responding, in part, to the leaf water potential. This finding is consistent with previous findings [14, 15] about $\sigma°$'s greater sensitivity to vegetation at higher angles of incidence (e.g., 45° or greater). HH15 on the burned treatment had almost as strong a partial correlation as VV45, thus indicating that the grass canopy has some effect on $\sigma°$ even at low angles of incidence.

Figure 2 shows the linear relationship between $\sigma°$ and leaf water potential for the burned and unburned treatments for the combined 1985 and 1986 data. The relationship is moderately strong with some scatter in the data. Since the leaf water potential is the average of three to six species, it is possible that this scatter could be due, in a large part, to the variability in the leaf water potential between individual plants or species (see Fig. 3). Whatever the cause of the variability, the implications of this finding remain that it may be possible to detect extremes in the water status of prairie vegetation using C-band scatterometer data taken at high angles of incidence (e.g., 45°).

Correlations Between $\sigma°$ and Expressions of Soil Moisture

As in previous studies, the backscattering coefficient was found to be linearly related and highly correlated with volumetric soil moisture. The linear trend between $\sigma°$ and m_v can be easily seen in Figures 4 through 9. Table 11 lists the correlation coefficients for all polarization-view angle combinations, years and sites for $\sigma°$ versus volumetric soil moisture.

VV15 followed by HH15 had consistently high correlation coefficients (i.e., $r \geq 0.8$) for all treatments. For this reason, VV15 and HH15 were used in all subsequent statistical analysis of the relationship between σ° and soil moisture. This finding also lends additional support to previous studies of the optimal scatterometer configuration for soil moisture remote sensing work.

A variety of soil moisture expressions were tried in an attempt to determine which expressions reduced the site dependence of the relationship between σ° and soil moisture. The degree of site dependence was found to vary with the manner in which soil moisture was expressed.

To test the degree of site dependency, a statistical comparison (i.e., analysis of covariance) of the sensitivity of σ° to soil moisture (i.e., slope values) was made for each expression of soil moisture for HH and VV polarizations at the 15° angle of incidence. Since there were 6 treatments, there were a total of 15 pairwise comparisons to be made of the slopes of the six regression lines for each expression of soil moisture.

One unexpected finding was that when soil moisture was expressed in gravimetric terms, percent of the -32.5 to -1500 KPa m_v difference (i.e., % available water), or as the logarithm of the soil water potential, the slopes of σ° versus soil moisture for each site could be statistically grouped into burned and unburned when using the HH15 configuration. In other words, the sensitivity (slope) of σ° to gravimetric soil moisture, percent of the -32.5 to -1500 KPa m_v difference, and to the logarithm of the soil water potential was the same for all years on the burned site. The same can be said of the unburned site results. The sensitivity of σ° to the above mentioned soil moisture expressions was; however, statistically different (for $\alpha=0.05$) between the burned and unburned sites. Burned site radar data showed a greater sensitivity (higher slopes) to soil moisture than that seen for the unburned site data.

Because of the clear separation of burned and unburned site regression equations when using these three expressions of soil moisture, it may be possible to use two soil moisture prediction equations (one for burned sites and one for unburned sites) on an operational basis by using visible and near-infrared wavelength reflectance data. The capability of distinguishing burned from unburned sites using Thematic Mapper wavebands has already been demonstrated for grasslands using field radiometers [24].

When compared for volumetric or other expressions of soil moisture, the slope comparisons ranged from five to eleven pairs of similar slopes with no useful groupings. None of the soil moisture expressions resulted in a complete removal of site dependency. The regression coefficients and statistics for $\sigma°$ versus each expression of soil moisture are given in Table 12. For the three expressions of soil moisture which exhibit groupings of the sensitivity into burned and unburned classes, the regression coefficients and statistics for $\sigma°$ versus soil moisture for the combined data sets of all three years for these soil moisture expressions are given in Table 13.

The greatest reduction in site dependency was found with expressing soil moisture as a percentage of the -1500 KPa volumetric moisture content in which 11 of the comparisons resulted in similar degrees of sensitivity with 4 remaining different for the

α=0.05 level. To say that all 15 comparisons resulted in all slopes being similar would have required us to compare the slopes at an alpha level of 0.0002. In other words, we can say with 99.98% certainty that at least one of the slopes is different from one of the other slopes. We definitely cannot say that one prediction line is adequate for predicting soil moisture for all six treatments.

Since expressing soil moisture as a percentage of the -32.5 KPa or the -1500 KPa volumetric soil moisture (expressions which have been claimed to greatly reduce site dependence due to textural differences [2, 6, 13, 25]) did not remove the site dependence, this suggests that the site differences were due to differences other than soil texture (e.g., vegetation cover). This conclusion is further supported by the fact that the soil textures for all sites and years were relatively similar (Table 2) while some of the vegetation characteristics were not (Table 3).

This finding was unexpected given that studies prior to this one [5, 11, 13, 15] have indicated that the frequency and view angle used in this study are considered relatively insensitive to vegetation, particularly since the amounts of vegetation encountered in this study would be considered low as compared with traditional agricultural crops.

Of the eight agronomic parameters listed in Table 3, the greatest difference between burned and unburned site vegetation cover is the presence of the senescent vegetation (litter) layer on the unburned sites. While in a dry state, this layer probably has a negligible effect on $\sigma°$ measurements. Moistened from a rain shower or from absorbing the morning dew, this layer may make a significant contribution to the radar backscatter. It should be pointed out that measurements were never made when free water droplets were present on the vegetation surfaces.

CONCLUSIONS

As in previous studies, a high degree of correlation was found between the C-band backscattering coefficient and soil moisture. This strongly indicates the capability of C-band radar as an instrument for estimating soil moisture for grassland areas. The grass canopy parameters, on the other hand, were only moderately correlated with σ°. C-band radar appears to have only a marginal capability for estimating vegetation parameters for grassland areas. In the case of one vegetation parameter, leaf water potential, even a marginal estimation capability may be useful.

Many of the findings described in this study support those made in previous studies in terms of polarization and view angle selection for soil moisture work (i.e., low angles of incidence and HH and VV polarizations work best). There were; however, two findings which were unexpected.

The first was the moderately strong correlation and partial correlation between σ° and leaf water potential. The implication of this finding is that it may be possible to detect extremes in the water status of prairie vegetation using C-band data. Such detection capability might prove useful in detecting those areas most affected by drought conditions in remote regions. It should be stressed; however, that the correlations between σ° and leaf water potential may simply be the result of the leaf water potential's dependence on the near surface soil moisture under shallow soil conditions. Additional study is required to determine if the correlations remain as strong for deep soil conditions.

The second unexpected finding was that the presence of small amounts of vegetation, such as those encountered in this study, appears to be sufficient to cause statistically significant differences in the sensitivity of σ° to soil moisture for different grassland sites. These differences do not appear to be removed by using any known expression of soil moisture or by using HH and VV polarizations at low angles of incidence. HH15 appears to offer the advantage of neatly separating the sensitivities of σ° to some expressions of soil moisture (i.e., gravimetric soil moisture, percent of available water and the logarithm of the soil water potential) into burned and unburned treatments. While VV15 did show groupings and differences in the sensitivity of σ° to soil moisture for different treatments and years, there were no convenient groupings as with HH15. Unfortunately, the three expressions of soil moisture for which this holds true are not necessarily the preferred expressions for all soil moisture work.

The implication of the latter finding is that at least two soil moisture prediction algorithms, one for burned treatments and another for unburned treatments (litter present and litter absent), should be used in any soil moisture estimation program which uses HH15, C-band backscatter data from grassland areas to estimate these three expressions of soil moisture. The decision of which algorithm to use for which sites could be determined by visible and near-infrared reflectance data. An alternative approach to dealing with this site dependent relationship is to investigate the use of a slightly longer wavelength scatterometer system. If indeed the site dependence is due to vegetation differences between burned and unburned treatments, a slightly longer wavelength might remove the vegetation effects while retaining an acceptable degree of sensitivity to soil moisture.

REFERENCES

[1] A. T. Chang, S. G. Atwater, V. V. Salomonson, J. E. Estes, D. S. Simonett, and M. L. Bryan, "L-band radar sensing of soil moisture," IEEE Trans. Geosci. Remote Sensing, vol. GE-18, no. 4, pp. 303-310, Oct. 1980.

[2] M. C. Dobson and F. T. Ulaby, "Microwave backscatter dependence on surface roughness, soil moisture, and soil texture: part III - soil tension," IEEE Trans. Geosci. Remote Sensing, vol. GE-19, no. 1, pp. 51-61, Jan. 1981.

[3] A. M. Sadeghi, G. D. Hancock, W. P. Waite, H. D. Scott, and J. A. Rand, "Microwave measurements of moisture distributions in the upper soil profile," Water Resources Res., vol. 20, no. 7, pp. 927-934, July 1984.

[4] F. T. Ulaby, "Radar measurement of soil moisture content," IEEE Trans. Antennas Propagat., vol. AP-22, no. 2, pp. 257-265, March 1974.

[5] F. T. Ulaby and P. P. Batlivala, "Optimum radar parameters for mapping soil moisture," IEEE Trans. Geosci. Electron., vol. GE-14, no. 2, pp. 81-93, April 1976.

[6] F. T. Ulaby, P. P. Batlivala, and M. C. Dobson, "Microwave backscatter dependence on surface roughness, soil moisture, and soil texture: part I - bare soil," IEEE Trans. Geosci. Electron., vol. GE-16, no. 4, pp. 286-295, Oct. 1978.

[7] W. P. Waite, A. M. Sadeghi, and H. D. Scott, "Microwave bistatic reflectivity dependence on the moisture content and matric potential of bare soil," IEEE Trans. Geosci. Remote Sensing, vol. GE-22, no. 4, pp. 394-405, July 1984.

[8] T. F. Bush and F. T. Ulaby, "Radar return from a continuous vegetation canopy," IEEE Trans. Antennas Propagat., vol. AP-24, no. 3, pp. 269-276, May 1976.

[9] R. Bernard, PH. Martin, J. L. Thony, M. Vauclin, and D. Vidal-Madjar, "C-band radar for determining surface soil moisture," Remote Sensing Environ., vol. 12, pp. 189-200, 1982.

[10] J. F. Paris, "The effect of leaf size on the microwave backscattering by corn," Remote Sensing Environ., vol. 19, pp. 81-95, 1986.

[11] F. T. Ulaby, "Radar response to vegetation," IEEE Trans. Antennas Propagat., vol. AP-23, no. 1, pp. 36-45, Jan. 1975.

[12] F. T. Ulaby, C. T. Allen, G. Eger III, and E. T. Kanemasu,

"Relating the microwave backscattering coefficient to leaf area index," Remote Sensing Environ., vol. 14, pp. 113-133, 1984.

[13] F. T. Ulaby, G. A. Bradley, and M. C. Dobson, "Microwave backscatter dependence on surface roughness, soil moisture, and soil texture: part II - vegetation-covered soil," IEEE Trans. Geosci. Electron., vol. GE-17, no. 2, pp. 33-40, April 1979.

[14] F. T. Ulaby and T. F. Bush, "Corn growth as monitored by radar," IEEE Trans. Antennas Propagat., vol. AP-24, no. 6, pp. 819-828, Nov. 1976.

[15] F. T. Ulaby, T. F. Bush, and P. P. Batlivala, "Radar response to vegetation II: 8-18 GHz band," IEEE Trans. Antennas Propagat., vol. AP-23, no. 5, pp. 608-618, Sept. 1975.

[16] T. J. Jackson, A. Chang, and T. J. Schmugge, "Aircraft active microwave measurements for estimating soil moisture," Photogramm. Eng. Remote Sens., vol. 47, No. 6, pp. 801-805, June 1981.

[17] T. J. Jackson and P. E. O'Neil, "Aircraft scatterometer observations of soil moisture on rangeland watersheds," Int. J. Remote Sens., vol. 6, no. 7, pp. 1135-1152, 1985.

[18] G. L. Ajtay, P. Ketner, and P. Durigneaud, "Terrestrial primary production and phytomass," in The Global Carbon Cycle, B. Bolin, E. T. Degens, S. Kempe, and P. Ketner Eds. New York: Wiley, 1977, pp. 129-181.

[19] R. G. Bailey, "Description of the ecoregions of the United States," U.S. Dept. of Agriculture, Intermtn. Forest Service, Ogden, UT, 1978.

[20] The Tallgrass Laboratory, Konza Prairie, Division of Biology, Kansas State University, Manhattan, KS, 20 pp., 1984.

[21] Klute, A. Water retention: laboratory methods. Methods of soil analysis, 2nd ed., part I, physical and mineralogical methods. A. Klute, ed. No. 9, part 1 in the series Agronomy. Amer. Soc. Agron, Inc. and Soil Sci. Soc. Amer., Inc., Madison, WI. pp.635-662. 1986.

[22] B. A. Kimball, "Smoothing data with cubic splines," Agron. J., vol. 63, pp. 126-129, Jan.-Feb. 1976.

[23] A. Retta, Personal communication and unpublished data, E. T. Lab, KSU, Manhattan, KS, Sept. 1986.

[24] G. Asrar, R. L. Weiser, D. E. Johnson, E. T. Kanemasu and J. M. Killeen, "Distinguishing among tallgrass prairie cover types from measurements of multispectral reflectance," Remote Sensing Environ., vol. 19, pp. 159-169, 1986.

[25] T. J. Schmugge, "Effect of texture on microwave emission from soils," IEEE Trans. Geosci. Remote Sensing, vol. GE-18, no. 4, pp. 353-361, Oct. 1980.

Table 1. Polarization-view angle combinations and measurement labels.

Polarization Transmit	Polarization Receive	View Angle (degrees from nadir)	Measurement Label
H	H	15	HH15
H	H	30	HH30
H	H	45	HH45
H	V	15	HV15
H	V	30	HV30
H	V	45	HV45
V	V	15	VV15
V	V	30	VV30
V	V	45	VV45

H - horizontal
V - vertical

Table 2. Soil type and properties for each year and treatment.

Soil Property	SITE 1984 B	1984 U	1985 B	1985 U	1986 B	1986 U
Sand (%)	22	23	27	31	22	20
Silt (%)	50	48	50	46	54	58
Clay (%)	28	29	23	23	24	22
Soil Type	clay loam	clay loam	loam or silt loam	loam	silt loam	silt loam
Bulk Density ($x\ 10^3$ kg/m^3)	1.04	1.03	0.79	0.69	0.83	0.77
Organic Matter (%)	4.5	4.4	5.0	4.7	7.8	7.2

B - burned site
U - unburned site

Table 3. Summary statistics of the agronomic parameters for all years and treatments.

AGRONOMIC PARAMETER	STATISTIC	SITE 1984 B	1984 U	1985 B	1985 U	1986 B	1986 U
Moisture Content on Dry Weight Basis (%)	MEAN	116	96	97	110	197	124
	STD. DEV.	56	32	11	1	12	5
	MINIMUM	60	42	74	109	174	114
	MAXIMUM	263	161	120	114	216	131
Moisture Content on Wet Weight Basis (%)	MEAN	50	46	49	51	62	52
	STD. DEV.	10	7	3	0	3	4
	MINIMUM	36	34	42	51	60	49
	MAXIMUM	71	60	54	52	66	62
Live, Dry Weight Biomass (kg/ha)	MEAN	2919	3318	2433	2749	2789	2869
	STD. DEV.	694	919	180	99	320	569
	MINIMUM	941	901	2181	2464	219	1812
	MAXIMUM	3548	4226	2783	2862	3371	3824
Moisture Content Normalized for Canopy Height (kg/m^3)	MEAN	N.A.	N.A.	0.52	0.49	1.27	0.65
	STD. DEV.	N.A.	N.A.	0.09	0.09	0.04	0.07
	MINIMUM	N.A.	N.A.	0.23	0.41	1.22	0.59
	MAXIMUM	N.A.	N.A.	0.63	0.71	1.30	0.78
LAI	MEAN	1.29	1.20	1.07	0.95	1.73	1.31
	STD. DEV.	0.42	0.43	0.11	0.16	0.11	0.22
	MINIMUM	0.57	0.47	0.71	0.81	1.46	0.89
	MAXIMUM	1.85	1.82	1.15	1.33	1.79	1.67
LITTER (kg/ha)	MEAN	1130	6945	888	8986	919	6524
	STD. DEV.	768	1618	535	1965	378	1771
	MINIMUM	2215	4462	0	5880	496	3671
	MAXIMUM	2215	11809	1849	12098	1427	8245
GREEN CANOPY HEIGHT (m)	MEAN	N.A.	N.A.	0.39	0.52	0.53	0.53
	STD. DEV.	N.A.	N.A.	0.23	0.04	0.08	0.05
	MINIMUM	N.A.	N.A.	0.14	0.44	0.33	0.48
	MAXIMUM	N.A.	N.A.	0.93	0.58	0.53	0.61
LITTER HEIGHT (m)	MEAN	N.A.	N.A.	0.00	0.12	0.00	0.11
	STD. DEV.	N.A.	N.A.	0.00	0.01	0.00	0.01
	MINIMUM	N.A.	N.A.	0.00	0.11	0.00	0.10
	MAXIMUM	N.A.	N.A.	0.00	0.14	0.00	0.12

N.A. - Not Available
B - burned site
U - unburned site

Table 4. Correlation coefficients for σ° versus various vegetation parameters for all polarization-view angle combinations for the Burned treatment, 1984.

Polarization-View Angle Combination	LAI	Dry Weight of Green Biomass	Moisture Content on Dry Weight Basis	Moisture Content on Wet Weight Basis	Moisture Content Normalized for Canopy Height
HH15	0.09	-0.56**	0.63**	0.56**	N.A.
HH30	0.18	-0.52**	0.62**	0.57**	N.A.
HH45	0.31*	-0.42**	0.63**	0.61**	N.A.
HV15	0.29*	-0.45**	0.69**	0.67**	N.A.
HV30	0.35*	-0.40**	0.72**	0.71**	N.A.
HV45	0.46**	-0.32*	0.73**	0.75**	N.A.
VV15	0.15	-0.51**	0.65**	0.60**	N.A.
VV30	0.13	-0.64**	0.74**	0.66**	N.A.
VV45	0.31	-0.50**	0.78**	0.75**	N.A.

* - significant at the α=0.05 level
** - significant at the α=0.01 level
N.A. - Not Available

Table 5. Correlation coefficients for σ° versus various vegetation parameters for all polarization-view angle combinations for the Unburned treatment, 1984.

Polarization-View Angle Combination	LAI	Dry Weight of Green Biomass	Moisture Content on Dry Weight Basis	Moisture Content on Wet Weight Basis	Moisture Content Normalized for Canopy Height
HH15	-0.07	-0.62**	0.70**	0.70**	N.A.
HH30	-0.07	-0.55**	0.62**	0.62**	N.A.
HH45	-0.09	-0.58**	0.55**	0.55**	N.A.
HV15	-0.06	-0.37**	0.58**	0.58**	N.A.
HV30	-0.08	-0.44**	0.70**	0.69**	N.A.
HV45	0.30*	-0.24	0.79**	0.79**	N.A.
VV15	-0.11	-0.60**	0.65**	0.65**	N.A.
VV30	-0.02	-0.58**	0.74**	0.74**	N.A.
VV45	-0.00	-0.55**	0.75**	0.75**	N.A.

• - significant at the α=0.05 level
** - significant at the α=0.01 level
N.A. - Not Available

Table 6. Correlation coefficients for σ° versus various vegetation parameters for all polarization-view angle combinations for the Burned treatment, 1985.

Polarization-View Angle Combination	LAI	Dry Weight of Green Biomass	Moisture Content on Dry Weight Basis	Moisture Content on Wet Weight Basis	Moisture Content Normalized for Canopy Height
HH15	0.04	0.48	0.45	0.38	0.36
HH30	0.21	0.29	0.62*	0.57*	0.48
HH45	0.33	0.18	0.64*	0.61*	0.62*
HV15	0.09	0.32	0.43	0.38	0.32
HV30	0.23	0.20	0.46	0.45	0.37
HV45	-0.06	0.36	0.44	0.33	0.18
VV15	0.03	0.42	0.52	0.42	0.34
VV30	0.25	0.21	0.66*	0.61*	0.51
VV45	0.45	0.08	0.72*	0.71*	0.65*

* - significant at the α=0.05 level
** - significant at the α=0.01 level

Table 7. Correlation coefficients for σ° versus various vegetation parameters for all polarization-view angle combinations for the Unburned treatment, 1985.

Polarization-View Angle Combination	LAI	Dry Weight of Green Biomass	Moisture Content on Dry Weight Basis	Moisture Content on Wet Weight Basis	Moisture Content Normalized for Canopy Height
HH15	0.72**	0.71**	0.01	0.22	0.69**
HH30	0.64*	0.59*	0.06	0.21	0.62*
HH45	0.03	0.19	0.05	-0.13	0.00
HV15	0.48	0.44	0.14	0.16	0.46
HV30	0.47	0.38	0.24	0.22	0.45
HV45	0.24	-0.02	0.47	0.26	0.25
VV15	0.71**	0.68**	0.10	0.23	0.69**
VV30	0.73**	0.79**	-0.14	0.12	0.72**
VV45	0.02	-0.26	0.44	0.26	0.02

* - significant at the α=0.05 level
** - significant at the α=0.01 level

Table 8. Correlation coefficients for σ° versus various vegetation parameters for all polarization-view angle combinations for the Burned treatment, 1986.

Polarization-View Angle Combination	LAI	Dry Weight of Green Biomass	Moisture Content on Dry Weight Basis	Moisture Content on Wet Weight Basis	Moisture Content Normalized for Canopy Height
HH15	-0.30	-0.14	0.07	0.21	0.93**
HH30	-0.34	-0.39	0.34	0.09	0.79*
HH45	-0.05	-0.24	0.23	-0.17	0.61
HV15	-0.45	-0.16	0.07	0.37	0.75
HV30	-0.74*	-0.16	0.03	0.75*	0.74
HV45	-0.31	-0.05	-0.02	0.27	0.73
VV15	-0.33	-0.38	0.34	0.09	0.79*
VV30	-0.26	-0.45	0.42	-0.05	0.70
VV45	-0.16	-0.32	0.29	-0.08	0.75

* - significant at the α=0.05 level
** - significant at the α=0.01 level

Table 9. Correlation coefficients for σ° versus various vegetation parameters for all polarization-view angle combinations for the Unburned treatment, 1986.

Polarization-View Angle Combination	LAI	Dry Weight of Green Biomass	Moisture Content on Dry Weight Basis	Moisture Content on Wet Weight Basis	Moisture Content Normalized for Canopy Height
HH15	-0.52	-0.45	0.52	0.34	0.01
HH30	-0.35	-0.30	0.40	0.11	-0.02
HH45	-0.35	-0.30	0.38	0.16	-0.01
HV15	-0.35	-0.28	0.32	0.37	0.26
HV30	-0.55	-0.49	0.46	0.71*	0.44
HV45	-0.12	-0.06	0.02	0.57	0.63
VV15	-0.25	-0.17	0.23	0.36	0.44
VV30	-0.29	-0.21	0.29	0.32	0.33
VV45	-0.45	-0.41	0.41	0.38	0.02

* - significant at the α=0.05 level
** - significant at the α=0.01 level

Table 10. Correlation coefficients for σ° versus leaf water potential and partial correlation coefficients for σ° versus leaf water potential given volumetric soil moisture for 1985 and 1986 data combined.

	Burned		Unburned	
Measurement Label	Correlation Coefficient	Partial Correlation Coefficient	Correlation Coefficient	Partial Correlation Coefficient
HH15	0.82**	0.66*	0.59*	0.40
HH30	0.77**	0.36	0.53	0.32
HH45	0.82**	0.56	0.61*	0.44
HV15	0.79**	0.52	0.70*	0.59
HV30	0.69*	0.39	0.45	0.16
HV45	0.79**	0.51	0.63*	0.50
VV15	0.80**	0.49	0.47	0.07
VV30	0.83**	0.57	0.51	0.24
VV45	0.85**	0.69*	0.75**	0.68*

* - significant at the α=0.05 level
** - significant at the α=0.01 level

Table 11. Correlation coefficients for σ° versus volumetric soil moisture for all polarization-view angle combinations, years and treatments.

Polarization-View Angle Combination	1984 B	1984 U	1985 B	1985 U	1986 B	1986 U
HH15	0.93**	0.92**	0.88**	0.86**	0.97**	0.81*
HH30	0.94**	0.94**	0.82**	0.76**	0.97**	0.75*
HH45	0.94**	0.92**	0.71**	0.45	0.80*	0.74*
HV15	0.96**	0.90**	0.68**	0.76**	0.71*	0.69
HV30	0.96**	0.93**	0.70**	0.76**	0.59	0.86**
HV45	0.93**	0.81**	0.69**	0.60**	0.74*	0.67
VV15	0.90**	0.87**	0.84**	0.93**	0.97**	0.93**
VV30	0.92**	0.83**	0.79**	0.79**	0.96**	0.89**
VV45	0.94**	0.85**	0.75**	0.23	0.94**	0.73*

B - burned site
U - unburned site
* - significant at the $\alpha=0.05$ level
** - significant at the $\alpha=0.01$ level

Table 12. Slope values for the linear regression equations of σ° versus each expression of soil moisture (independent variable). The y-intercept, r^2 and root mean square error (RMSE) for the regression equations are listed at the bottom of the table.

	Slope Values					
	1984		1985		1986	
Independent Variable	B	U	B	U	B	U
1) Gravimetric Soil Moisture (m_g)	0.307	0.222	0.304	0.163	0.373	0.174
2) Volumetric Soil Moisture (m_v)	29.52	21.56	38.50	23.53	44.75	22.52
3) Percentage of -32.5 KPa m_v	0.106	0.076	0.107	0.060	0.136	0.068
4) Percentage of -1500 KPa m_v	0.045	0.037	0.045	0.026	0.056	0.031
5) Logarithm of Soil Water Potential	-3.711	-2.412	-3.732	-2.082	-4.819	-2.222
6) Percentage of -32.5 to -1500 KPa m_v Difference	0.061	0.039	0.062	0.035	0.081	0.038
Y-intercept (1-4)	-16.00	-15.73	-13.82	-13.83	-15.07	-14.26
Y-intercept (5)	-0.31	-4.75	2.07	-4.93	5.28	-4.33
Y-intercept (6)	-11.54	-12.04	-9.28	-11.25	-9.47	-11.17
r^2	0.87	0.85	0.78	0.74	0.93	0.65
RMSE	1.10	0.86	1.43	0.8	0.95	1.18

Table 13. Regression coefficients and statistics for the combined data sets of all three years for those expressions of soil moisture which exhibited groupings of the sensitivity of σ° to soil moisture into burned and unburned classes.

	Gravimetric Soil Moisture (m_g)		Logarithm of Soil Water Potential		Percentage of -32.5 to -1500 KPa m_v Difference	
Statistic	B	U	B	U	B	U
Slope	0.337	0.214	-4.067	-2.447	0.067	0.040
Y-intercept	-15.88	-15.46	1.41	-4.46	-10.92	-11.87
r^2	0.80	0.83	0.77	0.82	0.78	0.82
RMSE	1.52	0.91	1.63	0.93	1.61	0.92

B - burned site
U - unburned site
RMSE - root mean square error

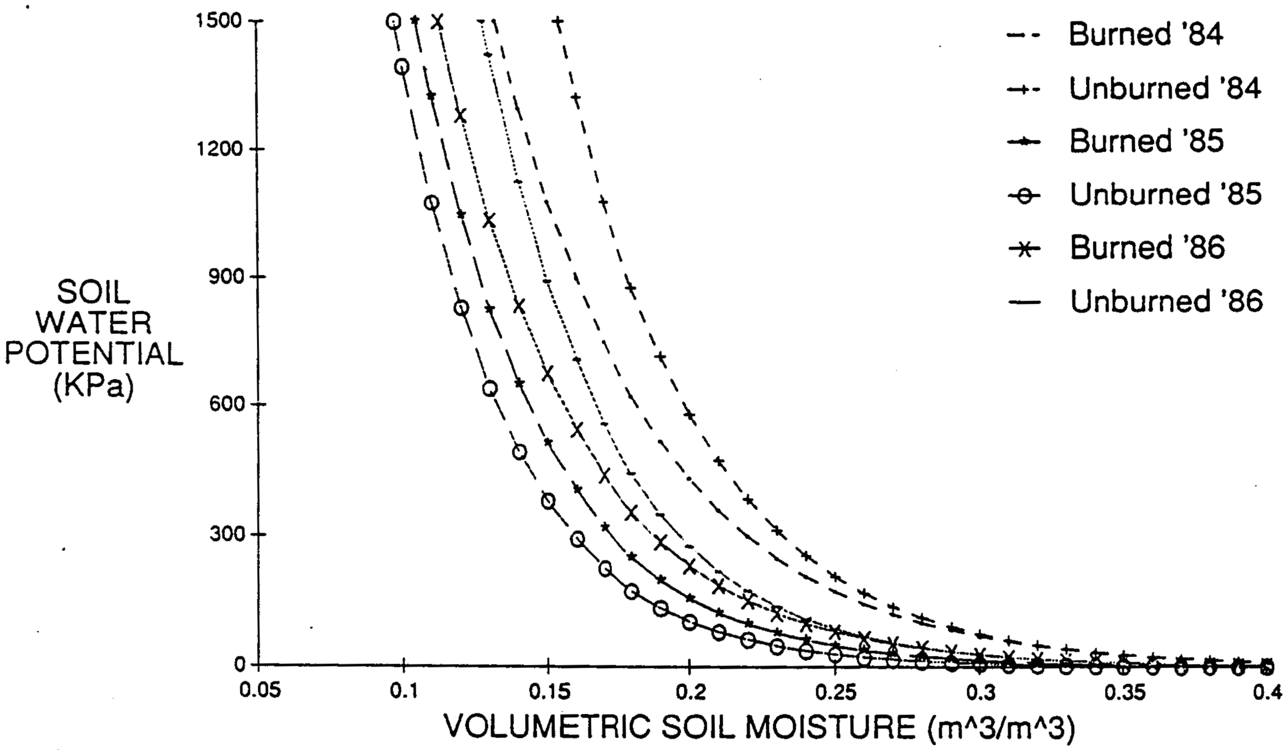

Fig. 1. Soil moisture release curves for all years and treatments. Points on the lines are not measured values, but are shown to aid line identification.

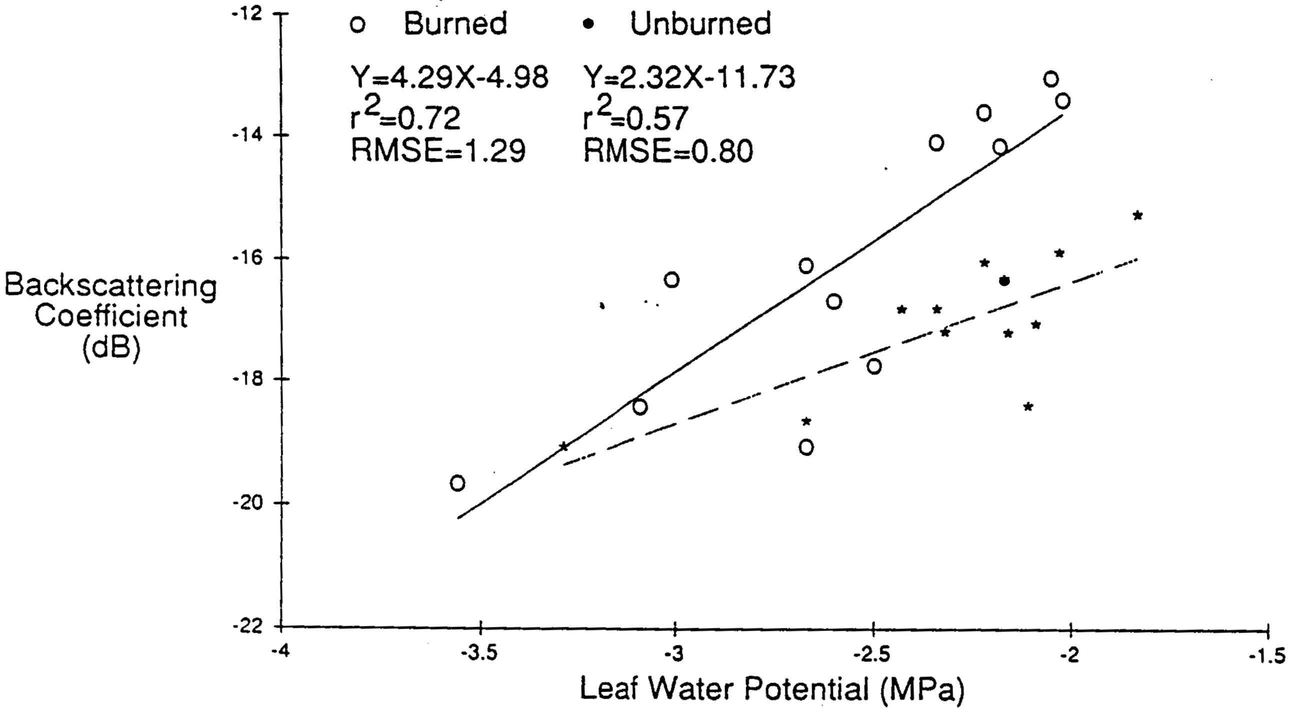

Fig. 2. Backscattering coefficient (VV45) versus leaf water potential for the burned and unburned treatments.

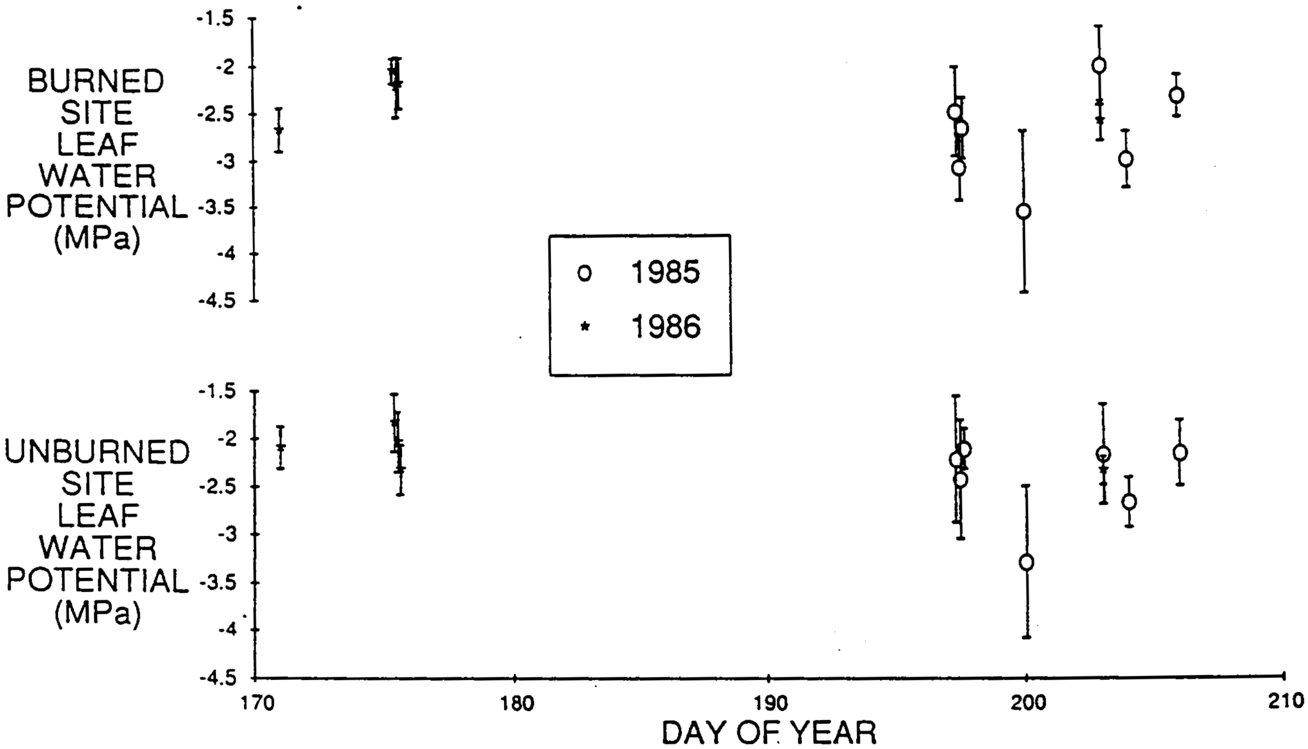

Fig. 3. Mean leaf water potential versus day of year for the burned and unburned sites. Standard error bars indicate one standard deviation about the mean.

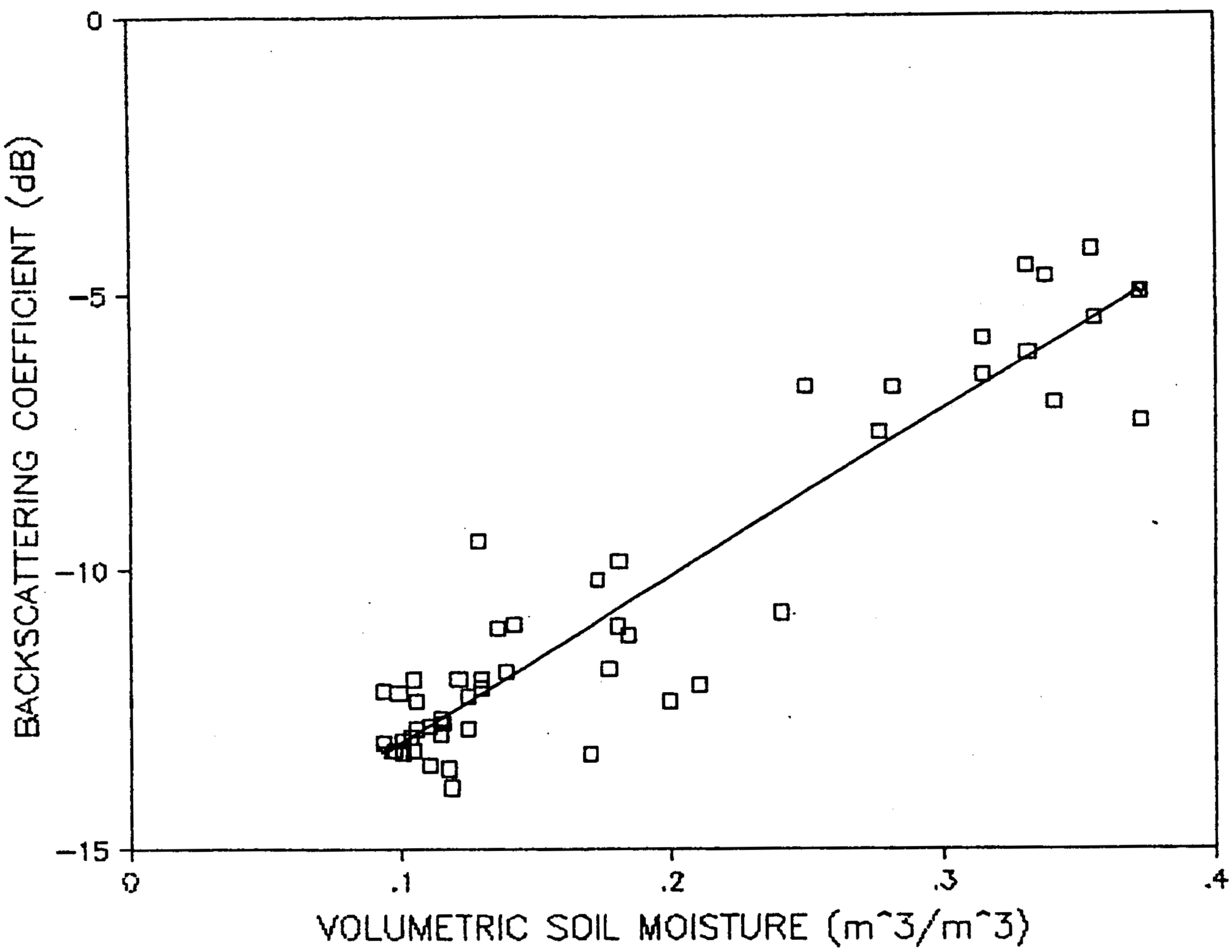

Fig. 4. Scatter plot of the backscattering coefficient (HH15) versus volumetric soil moisture for the burned, 1984 site shown along with the line-of-best-fit. See Table 12 for the linear regression equation.

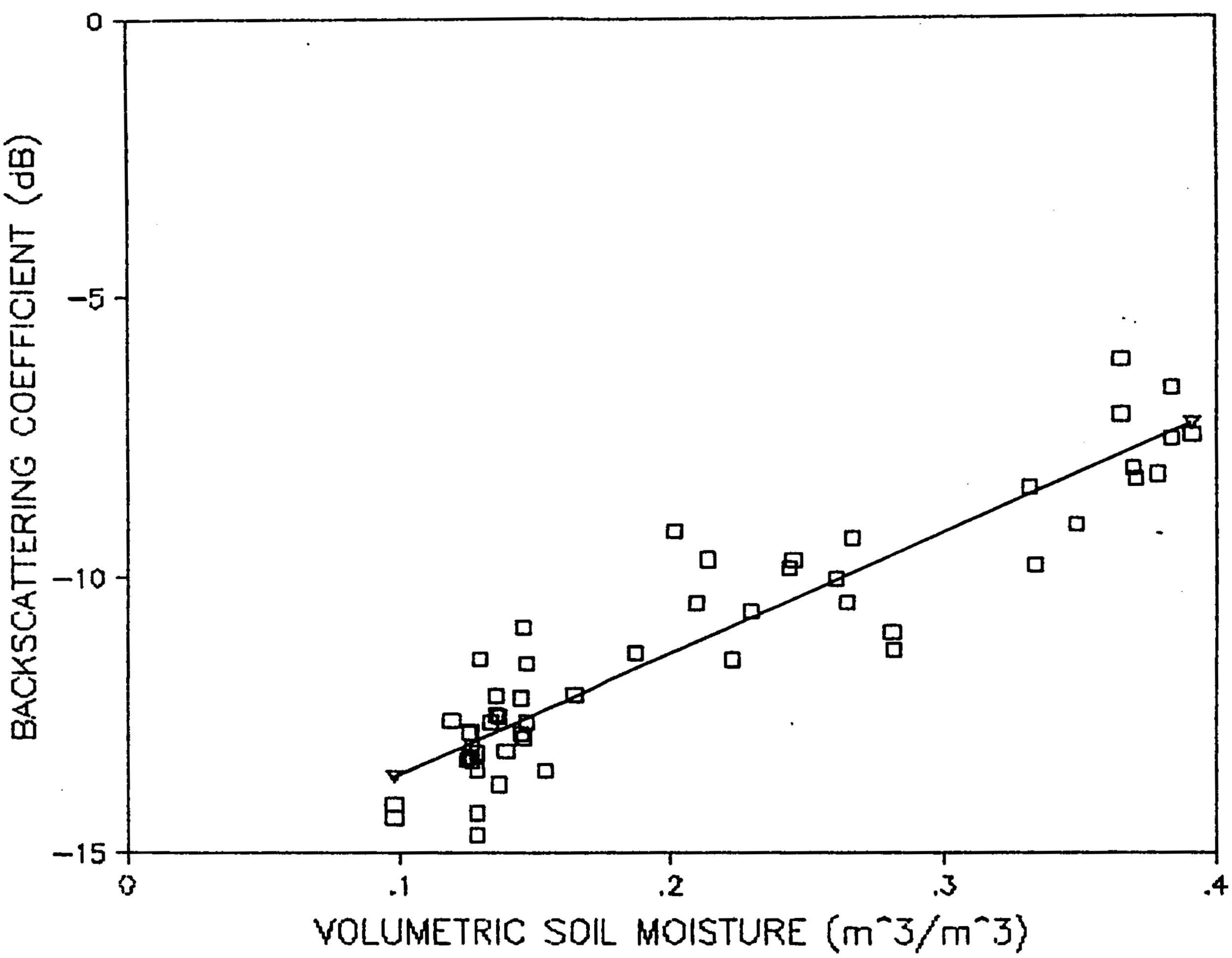

Fig. 5. Scatter plot of the backscattering coefficient (HH15) versus volumetric soil moisture for the unburned, 1984 site shown along with the line-of-best-fit. See Table 12 for the linear regression equation.

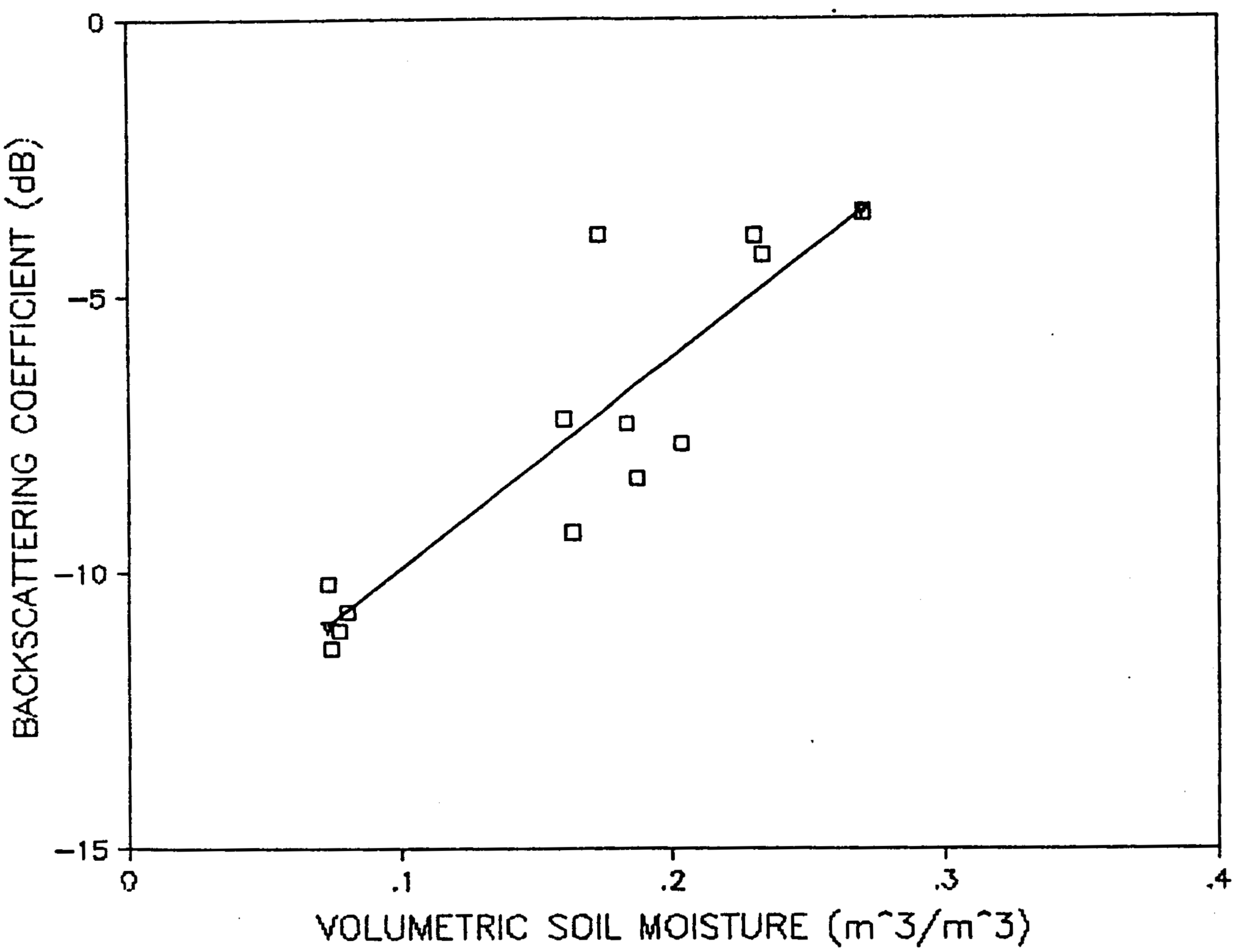

Fig. 6. Scatter plot of the backscattering coefficient (HH15) versus volumetric soil moisture for the burned, 1985 site shown along with the line-of-best-fit. See Table 12 for the linear regression equation.

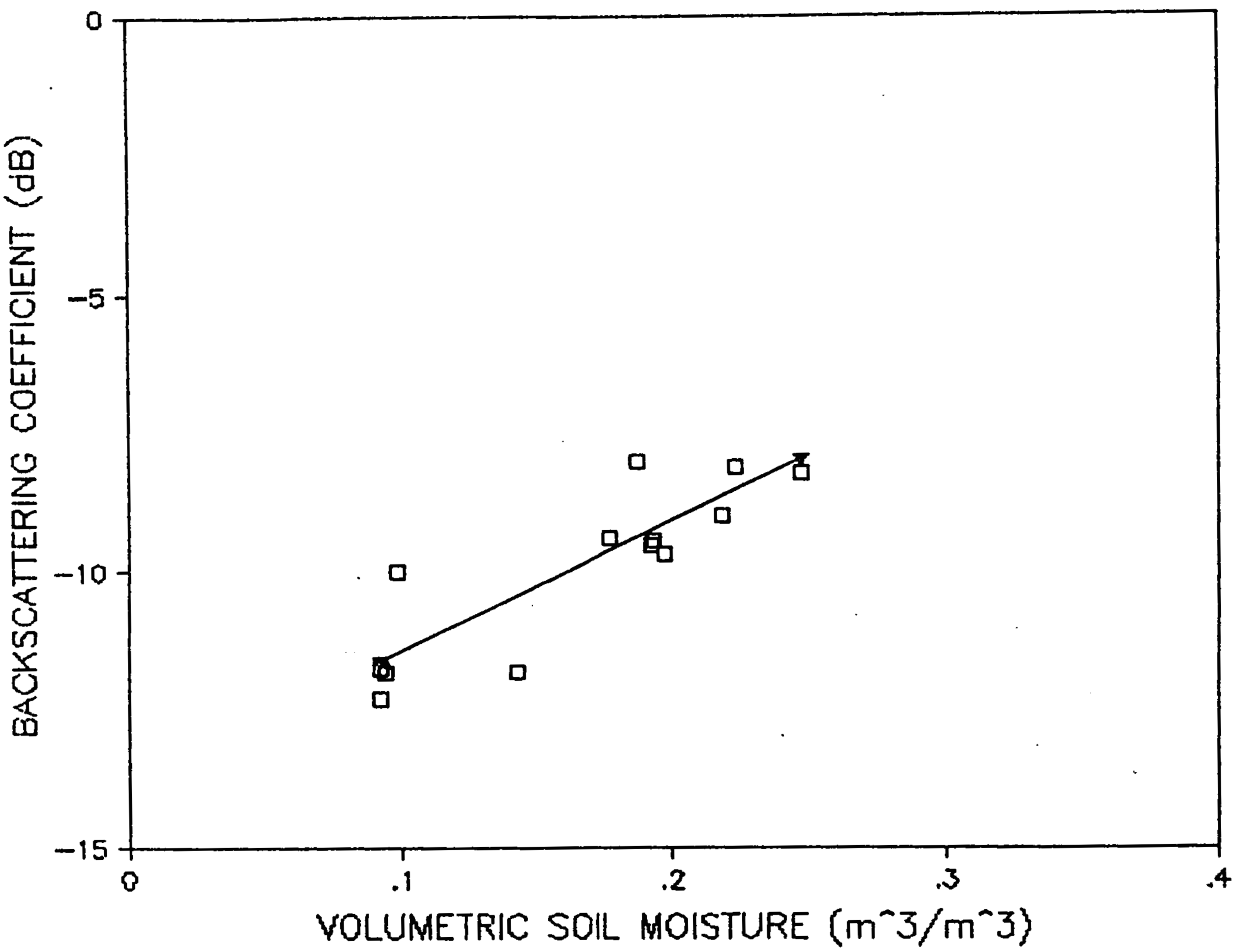

Fig. 7. Scatter plot of the backscattering coefficient (HH15) versus volumetric soil moisture for the unburned, 1985 site shown along with the line-of-best-fit. See Table 12 for the linear regression equation.

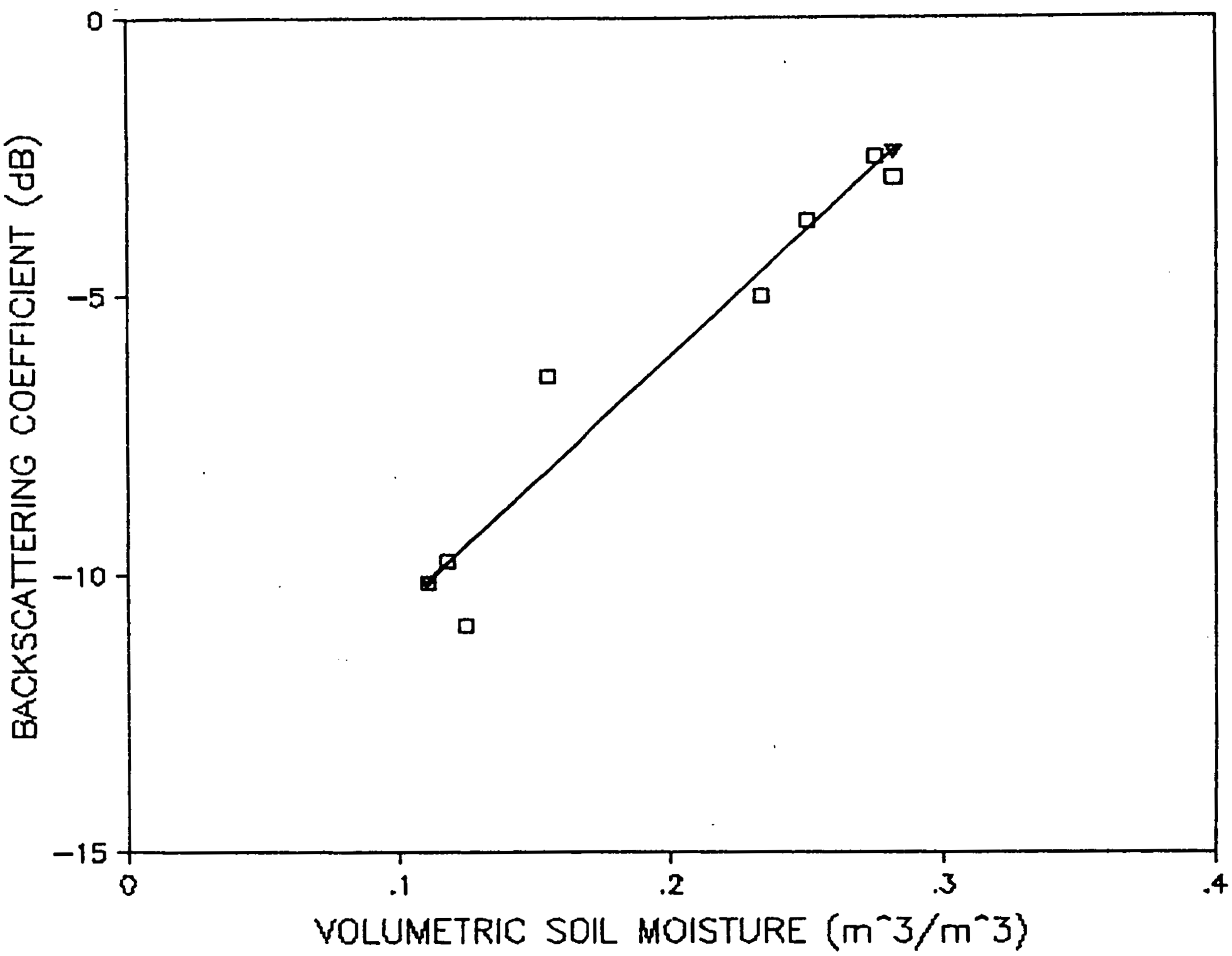

Fig. 8. Scatter plot of the backscattering coefficient (HH15) versus volumetric soil moisture for the burned, 1986 site shown along with the line-of-best-fit. See Table 12 for the linear regression equation.

C-2

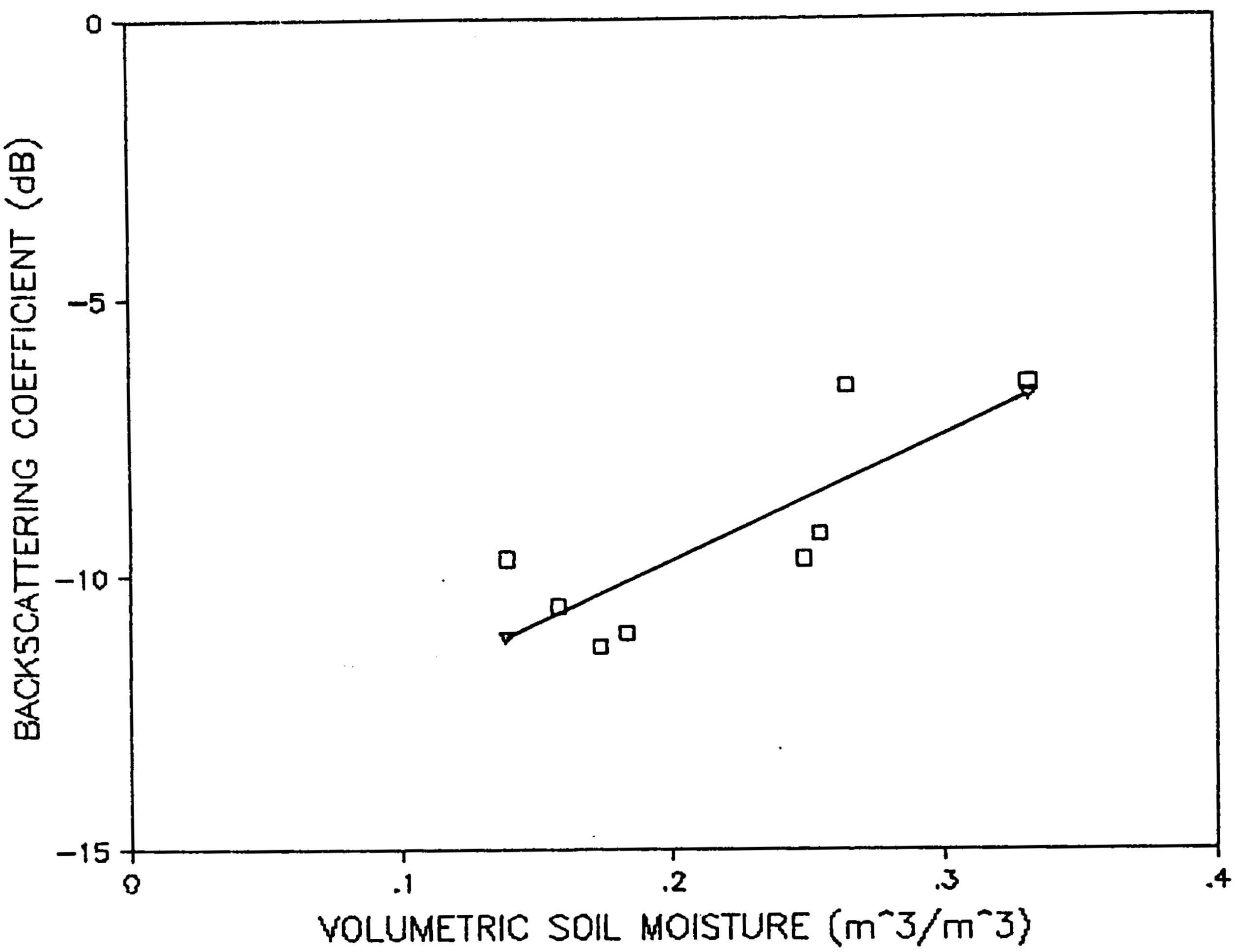

Fig. 9. Scatter plot of the backscattering coefficient (HH15) versus volumetric soil moisture for the unburned, 1986 site shown along with the line-of-best-fit. See Table 12 for the linear regression equation.